ARTICLE

Unsymmetrical Benzothiazole-Based Dithienylethene Photoswitches

Received 00th January 20xx,
Accepted 00th January 20xx

DOI: 10.1039/x0xx00000x

Michelangelo Bovoloni[a], Juraj Filo[b], Ivica Sigmundová[b], Peter Magdolen[b], Šimon Budzák[c], Eliška Procházková[d], Matteo Tommasini[e], Marek Cigáň[b,*] and Andrea Bianco[a,*]

Herein, we investigate structure-property relationships in a new series of benzothiazole based unsymmetrical hexafluorocyclopentene dithienylethenes (DTEs) and compare the results with the known facts for symmetric diarylethenes (DAEs). We reveal high photocyclization efficiency resulted from significant shift of ground state equilibrium to antiparallel conformer and barrierless excited state pathway to conical intersection, which remains unperturbed even in polar solvent for most of prepared DTEs. Furthermore, we uncover that rate of back thermal cycloreversion correlates clearly more with the central C-C bond-length in the transition state than with the central C-C bond-length in the ground state of the cyclic form. Finally, our detailed vibrational spectral analysis of studied DTEs points out significant changes in Raman and infrared spectrum during photoswitching cycle which pave a way for a non-destructive readout of stored information.

* - corresponding authors

Supporting Information (SI)

NMR data including 2D spectra are available from the authors.

[a] *INAF- Osservatorio Astronomico di Brera, Via Bianchi 46, 23807, Merate, Italy, email: andrea.bianco@inaf.it*
[b] *Department of Organic Chemistry, Faculty of Natural Sciences, Comenius University, Ilkovičova 6, 842 15 Bratislava, Slovakia, email: marek.cigan@uniba.sk*
[c] *Department of Chemistry, Faculty of Natural Sciences, Matej Bel University, Tajovského 40, 974 01 Banská Bystrica, Slovakia*
[d] *NMR Spectroscopy Department, Institute of Organic Chemistry and Biochemistry, Czech Academy of Sciences, Flemingovo nám. 2, 160 00 Prague 6, Czech Republic*
[e] *Dipartimento di Chimica, Materiali e Ingegneria Chimica "G. Natta", Politecnico di Milano, Piazza Leonardo Da Vinci 32, 20133 Milano, Italy*

Table of contents

1. Synthesis

1.1. General information

All solvents were purified by standard operating methods; 1,2-dimetoxyoethane (DME) was distilled from calcium hydride. All commercial reagents were used without additional purification. Thin-layer chromatography (TLC) was performed on gel 60 F254 plates, visualized by ultraviolet light (254 nm). Product purifications were performed using column chromatography on silica gel (0.040−0.063 mm).**^{1}H NMR**, **^{13}C NMR** and **^{19}F NMR** spectra were recorded in $CDCl_3$ solution (^{1}H δ 7.26, ^{13}C δ 77.0 ppm) on Varian NMR System 400 and 600 instruments and Bruker Avance III spectrometer operating at 500 MHz for ^{1}H and 125 MHz for ^{13}C. Chemical shift (δ) is expressed in ppm relative to tetramethylsilane, multiplicities are as indicated: s = singlet, d = doublet, t = triplet, q = quartet, quint = quintet, dd = doublet of doublets, tt = triplet of triplets, m = multiplet, br = broad, *J*-couplings are expressed in Hz. Melting points were determined on the Büchi Melting Point M-565 apparatus. High-resolution mass spectral analysis (**HRMS**) data were measured on Thermo Scientifc Orbitrap Fusion Tribrid® mass spectrometer (Thermo Fisher Scientific, Waltham, MA, USA) equipped with Dionex Ultimate 3000RS HPLC pump and Dionex Ultimate 3000RS autosampler.

1.2. Preparation of starting diiododithienylethene **11**

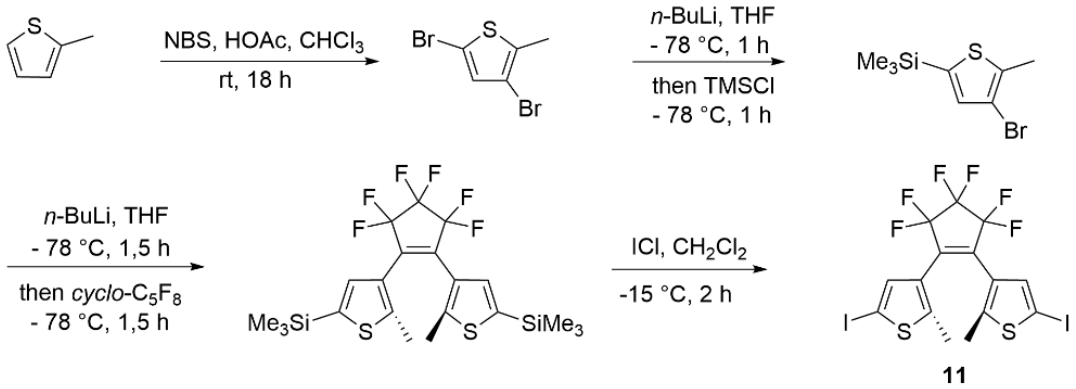

11

Diiodo compound was synthesized over 4 steps according to the literature procedure[1,2].

[1] S.,Yagai, K. Ohta, M. Gushiken, K. Iwai, A. Asano, S. Seki, Y. Kikkawa, M. Morimoto, A. Kitamura, ,T. Karatsu. *Chem.Eur.J.,* **2012**, *18*, 2244-2253.

[2] D. Becker, N. Konnertz, M. Böhning, J. Schmidt, A. Thomas, *Chemistry of Materials,* **2016**, *28*, 8523 – 8529.

1.3. Preparation of 2-methylbenzothiazole-6-boronic acid pinacol ester

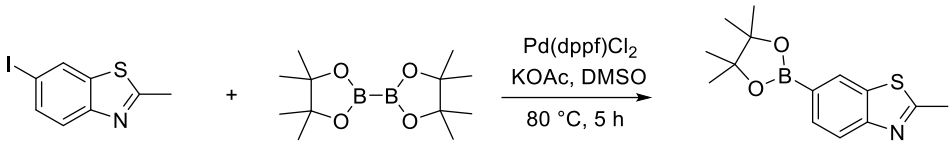

A mixture of 2.00 g (7.35 mmol) 6-iodo-2-methylbenzothiazole, 2.05 g (8.08 mmol) bis(pinacolato)diboron, 0.60 g (0.76 mmol) (1,1´-bis(diphenylphosphino)ferrocene)palladium(II) dichloride and 1.08 g (11.02 mmol) potassium acetate in dimethyl sulfoxide (35 mL) under argon atmosphere was heated to 80 °C for 5 h. The reaction mixture was then cooled to ambient temperature, quenched with water (100 mL), and extracted with ethyl acetate (3 × 50 mL). The combined organic phase was dried over Na_2SO_4, filtered, and concentrated in vacuo. The residue was purified by flash column chromatography (hexane: ethyl acetate = 7:1) to afford title boronic acid pinacol ester (2.9 g, 73%yield) as a pale yellow solid.
Lit[3]: T.t. = 50–52 °C; exp.t.t = 62.5–64.0 °C.

^{1}H NMR (600 MHz $CDCl_3$) δ 8.31 (s, 1H); 7.93 (d, *J* = 8.4 Hz, 1H); 7.86 (d, *J* = 8.4 Hz, 1H); 2.84 (s, 3H); 1.37 (s, 12 H).

1.4. Preparation of benzothiazolyl(iodo)dithienylethene **12**

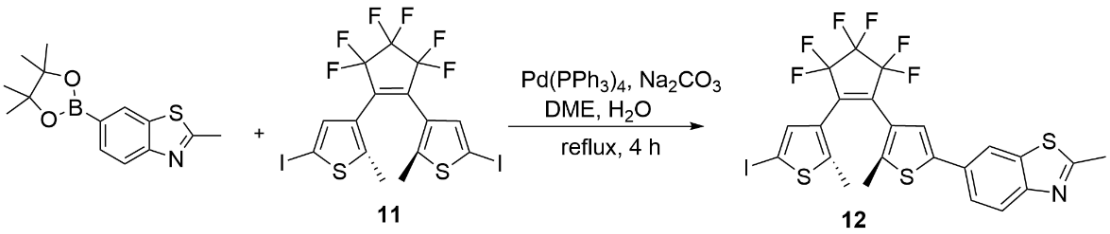

To a mixture of 1.50 g (2.42 mmol) diiodo compound **11**, 0.67 g (2.42 mmol) 2-methylbenzothiazole-6-boronic acid pinacol ester, 0.14 g (0.12 mmol) tetrakis(triphenylphosphine)palladium(II) and 0.51 g (4.84 mmol) sodium carbonate in degassed DME (50 mL) under argon atmosphere was added degassed water (12 mL). The mixture was refluxed 4 h until TLC indicated that the starting compound **11** disappeared and then cooled to ambient temperature. DME was removed under reduced pressure, and the residue was extracted with ether (3x). The combined organic layers were dried over Na_2SO_4 and the solvent was evaporated in vacuum. The residue was purified by flash column chromatography (hexane: ethyl acetate = 5:1) to afford the title compound **12** (0.98 g, 63% yield) as a violet solid. Unreacted starting compound **11** (0.33 g, 22 % yield) together with bis-coupling product **5** (0.19 g, 12% yield) were isolated simultaneously.

[3] S. Jin, H. T. Dang, G. C. Haug, R. He, V. D. Nguyen, V. T. Nguyen, H. D. Arman, K. S. Schanze, O. V. Larionov, *JACS*, **2020,** *142*, 1603-1613.

M.p.: 175–176 °C. **^{1}H NMR** (600 MHz, CDCl3) δ 7.97 (d, *J* = 1.5 Hz, 1H), 7.93 (d, *J* = 8.5 Hz, 1H), 7.61 (dd, *J* = 8.5, 1.5 Hz, 1H), 7.27 (s, 1H), 7.23 (s, 1H), 2.85 (s, 3H), 1.96 (s, 3H), 1.94 (s, 3H). **^{13}C NMR** (151 MHz, CDCl3) δ 167.72, 153.03, 147.65, 141.85, 141.57, 136.66, 136.15, 134.71, 130.10, 127.87, 126.85, 125.68, 124.09, 122.70, 122.57, 118.19, 115.96, 110.91, 70.60, 20.22, 14.55, 14.33, one signal for CF_2 was not recorded. **^{19}F NMR** (564 MHz, $CDCl_3$) δ: -136.63 (quint, *J* = 5.0 Hz, 2F), -114.92 (2F), -114.87 (2F). **HRMS (ESI):** $[M+H]^+$ calcd for $C_{23}H_{15}F_6INS_3$: 641.9315, found: 641.9319.

1.5. Preparation of bis(benzothiazolyl)dithienylethene **5**

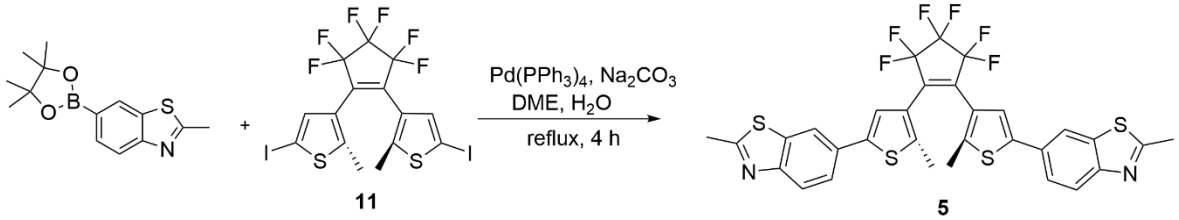

11 **5**

To a mixture of 1.00 g (1.63 mmol) diiodo compound **11**, 0.96 g (3.55 mmol) 2-methylbenzothiazole-6-boronic acid pinacol ester, 0.187 g (0.16 mmol) tetrakis(triphenylphosphine)palladium(II) and 0.69 g (6.50 mmol) sodium carbonate in degassed DME (50 mL) under argon atmosphere was added degassed water (12 mL) and the mixture was refluxed for 5 h. The reaction mixture was then cooled to ambient temperature, DME was removed under reduced pressure, water (20 mL) and diethyether (30 mL) were added to the residue. Aqueous layer was extracted with diethylether (2 × 30 mL), combined organic layers were washed with water and brine, dried over Na_2SO_4, filtered and concentrated in vacuo. The blue crude product was purified by flash column chromatography on silica gel (hexane : ethyl acetate = 3:1) to afford compound **5** (0.85 g, 79% yield) as a dark blue solid. The monocoupling violet product **12** (0.105 g, 10% yield) was also isolated.

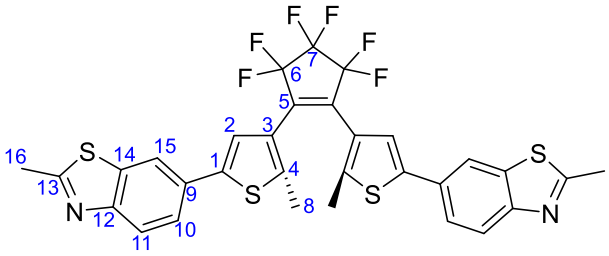

M.p.: 203–204 °C. **^{1}H NMR** (600 MHz, CDCl3) δ 7.98 (d, $J_{H,H}$ = 1.7 Hz, 2H, H15), 7.93 (d, $J_{H,H}$ = 8.5 Hz, 2H, H11), 7.62 (dd, $J_{H,H}$ = 8.5, 1.7 Hz, 2H, H10), 7.32 (s, 2H, H2), 2.85 (s, 6H, H16), 2.00 (s, 6H, H8). **^{13}C NMR** (151 MHz, CDCl3) δ 167.68 (C13), 152.99 (C12), 141.72 (C1), 141.56 (C4), 136.65 (C14), 136.13 (C5), 130.17 (C9), 125.97 (C3), 124.09 (C10), 122.74 (C2), 122.68 (C11), 118.17 (C15), 116.14 (tt, *J* = 256.9 Hz, 23.5 Hz, C6), 111.02 (t, quint, *J* = 270.7 Hz, 24.9 Hz, C7), 20.20 (C16), 14.59 (C8). **^{19}F NMR** (564 MHz, $CDCl_3$) δ -131.85 (quint, *J* = 4.8 Hz, 2F), -110.01 (*J* = 4.9 Hz, 4F). **HRMS (ESI)**: $[M+H]^+$ calcd for $C_{31}H_{21}F_6N_2S_4$: 663.0492, found: 663.0492.

1.6. Synthesis of aryl(benzothiazolyl) dithienylethenes **1**–**4** and **6**–**10**

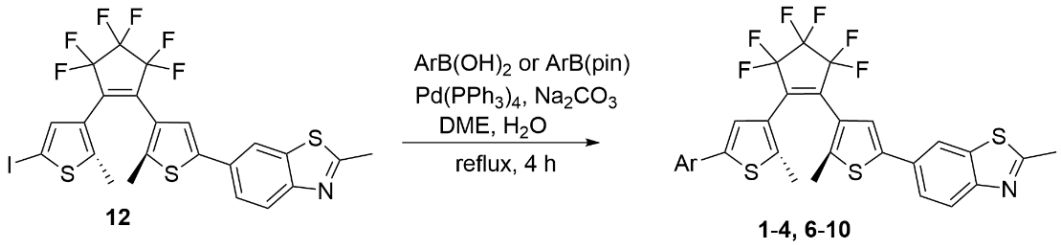

General procedure

To a mixture of 0.45 g (0.70 mmol) iodo compound **12**, 1,4 eq. (0.98 mmol) arylboronic acid or its pinacol ester, 0.061 g (0.05 mmol) tetrakis(triphenylphosphine)palladium(II) and 0.149 g (1.41 mmol) sodium carbonate in degassed DME (20 mL) under argon atmosphere was added degassed water (4 mL). The mixture was refluxed until TLC indicated that the starting compound **12** disappeared (0.5–3 h) and then cooled to ambient temperature. DME was removed under reduced pressure, water (10 mL) and dichloromethane (30 mL) were added to the residue. Aqueous layer was extracted with DCM (15 mL), combined organic layers were washed with water and brine, dried over Na_2SO_4, filtered and concentrated in vacuo. The crude product was purified by flash column chromatography on silica gel using hexane–ethyl acetate (5:1) to afford the desired compounds (**1**–**4, 6**–**10**). If further purification was required, the resulting solid was recrystallized from petrolether.

6-(4-(3,3,4,4,5,5-hexafluoro-2-(2-methyl-5-(4-nitrophenyl)thiophen-3-yl)cyclopent-1-en-1-yl)-5-methylthiophen-2-yl)-2-methylbenzo[d]thiazole (1)

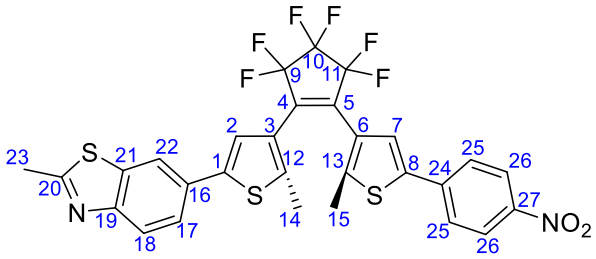

Compound **1** (0.30 g, 74%) was obtained from **12** and 4-nitrophenylboronic acid pinacol ester as a bluish solid following the general procedure. **M.p.:** 194–196.5 °C. **^{1}H NMR** (600 MHz, CDCl3) δ 8.25 (d, $J_{H,H}$ = 8.8 Hz, 2H, H24), 7.98 (d, $J_{H,H}$ = 1.6 Hz, 1H, H22), 7.94 (d, $J_{H,H}$ = 8.5 Hz, 1H, H18), 7.68 (d, $J_{H,H}$ = 8.8 Hz, 2H, H25), 7.62 (dd, $J_{H,H}$ = 8.5, 1.6 Hz, 1H, H17), 7.45 (s, 1H, H7), 7.31 (s, 1H, H2), 2.86 (s, 3H, H23), 2.04 (s, 3H, H15), 2.00 (s, 3H, H14). **^{13}C NMR** (151 MHz, CDCl3) δ 167.80 (C20), 153.07 (C19), 146.90 (C27), 144.09 (C13), 142.01 (C1), 141.52 (C12), 139.47 (C8), 139.29 (C24), 136.89 (C4), 136.69 (C21), 135.7 (C5), 130.04 (C16), 126.60 (C6), 126.09 (C7), 125.82 (C25), 125.78 (C3), 124.50 (C26), 124.08 (C17), 122.73 (C18), 122.59 (C2), 118.21 (C22), 20.23 (C1), 14.76 (C15), 14.61 (C14); due to complicated splitting from fluorine atoms, signals for carbon atoms C9, C10 and C11 of cyclopentene ring were not assigned. **^{19}F NMR** δ -131.83 (quint, J = 4.9 Hz, 2F, F10), -110.13 (4F, F9 and F11). **HRMS (ESI):** $[M+H]^+$ calcd for $C_{29}H_{19}F_6N_2O_2S_3$: 637.0513, found: 637.0508.

4-(4-(3,3,4,4,5,5-hexafluoro-2-(2-methyl-5-(2-methylbenzo[d]thiazol-6-yl)thiophen-3-yl)cyclopent-1-en-1-yl)-5-methylthiophen-2-yl)benzonitrile (2)

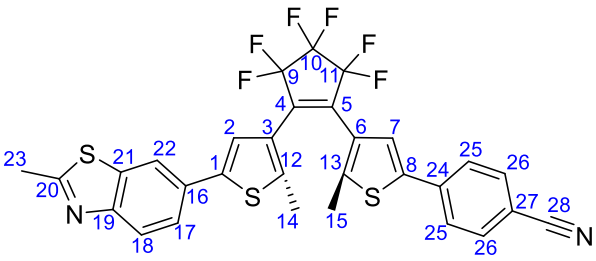

Compound **2** (0.285 g, 74%) was obtained from **12** and 4-cyanophenylboronic acid as a blue solid following general procedure. **M.p.:** 188 – 188.6 °C**. ^{1}H NMR** (600 MHz, CDCl3) δ 7.98 (d, $J_{H,H}$ = 1.5 Hz, 1H, H22), 7.93 (d, $J_{H,H}$ = 8.5 Hz, 1H, H18), 7.66 (d, $J_{H,H}$ = 8.3 Hz, 2H, H26), 7.63 (d, $J_{H,H}$ = 8.3 Hz, 2H, H25), 7.62 (dd, $J_{H,H}$ = 8.5, 1.5 Hz, 1H, H17), 7.40 (s, 1H, H7), 7.31 (s, 1H, H2), 2.85 (s, 3H, H23), 2.02 (s, 3H, H15), 1.99 (s, 3H, H14). **^{13}C NMR** (151 MHz, CDCl3) δ 167.81 (C20), 153.03 (C19), 143.50 (C6), 141.94 (C1), 141.52 (C12), 139.93 (C8), 137.43 (C13), 136.67 (2C, C21 and C4), 135.63 (C5), 132.83 (C26), 130.07 (C16), 126.42 (C24), 125.82 (C25), 125.82 (C3), 124.51 (C7), 124.09 (C17), 122.71 (C18), 122.61 (C2), 118.58 (C28), 118.20 (C22), 111.10 (C27), 20.22 (C23), 14.72 (C15), 14.59 (C14); due to complicated splitting from fluorine atoms, signals for carbon atoms C9, C10 and C11 of cyclopentene ring were not assigned. **^{19}F NMR** (564 MHz, $CDCl_3$**)** δ: -131.85 (2F), -110.12 (2F), -109.98 (2F). **HRMS (ESI):** $[M+H]^+$ calcd for $C_{30}H_{19}F_6N_2S_3$: 617.0514, found: 617.0511.

6-(4-(2-(5-(3,5-bis(trifluoromethyl)phenyl)-2-methylthiophen-3-yl)-3,3,4,4,5,5-hexafluorocyclopent-1-en-1-yl)-5-methylthiophen-2-yl)-2-methylbenzo[d]thiazole (3)

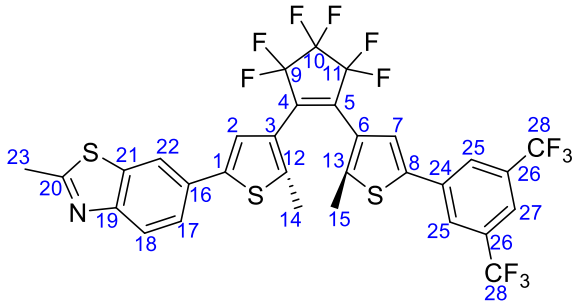

Compound **3** (0.390 g, 86%) was obtained from **12** and 3.5-bis(trifluoromethyl)phenylboronic acid as a bluish solid following general procedure. **M.p.:** 189 – 189.5 °C. **^{1}H NMR** (600 MHz, CDCl3) δ 7.98 (d, $J_{H,H}$ = 1.5 Hz, 1H, H22), 7.94 (d, $J_{H,H}$ = 8.5 Hz, 1H, H18), 7.92 (s, 2H, H25), 7.79 (s, 1H, H27), 7.62 (dd, $J_{H,H}$ = 8.5, 1.5 Hz, 1H, H17), 7.41 (s, 1H, H7), 7.31 (s, 1H, H2), 2.85 (s, 3H, H23), 2.04 (s, 3H, H15), 2.00 (s, 3H, H14). **^{13}C NMR** (151 MHz, CDCl3) δ 167.78 (C20), 153.09 (C19), 143.49 (C6), 142.04 (C1), 141.51 (C12), 138.76 (C8), 136.69 (C21), 136.89 (C4), 135.52 (2C, C5 and C13), 132.53 (q, J = 33.5 Hz, C26), 130.04 (C16), 126.46 (C6), 125.77 (C3), 125.38 (q, J = 2.7 Hz, C25), 124.67 (C7), 124.10 (C17), 123.05 (q, J = 273.4 Hz, C28), 122.73 (C18), 122.59 (C2), 121.18 (m, J = 3.7 Hz, C27), 118.23 (C22), 116.02 (m, 2C, C9 and C11), 111.00 (m, C10), 20.22 (C23), 14.69 (C15), 14.62 (C14). **^{19}F NMR** (564 MHz, $CDCl_3$**)** δ: -131.86 (quint, J = 4.5 Hz, 2F), -110.09 (2F), -110.01 (2F), -62.65 (6F). **HRMS (ESI):** $[M+H]^+$ calcd for $C_{31}H_{18}F_{12}NS_3$: 728.0410, found: 728.0402.

6-(4-(3,3,4,4,5,5-hexafluoro-2-(2-methyl-5-(4-(trifluoromethyl)phenyl)thiophen-3-yl)cyclopent-1-en-1-yl)-5-methylthiophen-2-yl)-2-methylbenzo[d]thiazole (4)

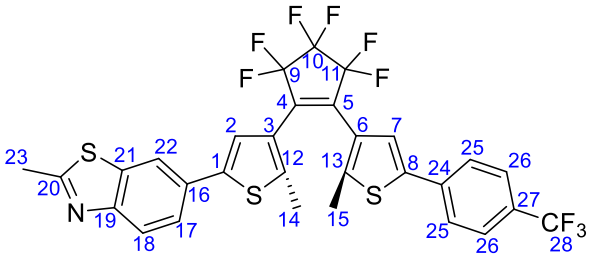

Compound **4** (0.233 g, 51%) was obtained from **12** and 4-(trifluoromethyl)phenylboronic acid as a dark blue solid following general procedure. **M.p.:** 159 – 161 °C. **^{1}H NMR** (600 MHz, CDCl3) δ 7.98 (d, $J_{H,H}$ = 1.6 Hz, 1H, H22), 7.93 (d, $J_{H,H}$ = 8.5 Hz, 1H, H18), 7.64 (s, 4H, H25 and H26), 7.62 (dd, $J_{H,H}$ = 8.5, 1.6 Hz, 1H, H17), 7.37 (s, 1H, H7), 7.31 (s, 1H, H2), 2.85 (s, 3H, H23), 2.01 (s, 3H, H15), 1.99 (s, 3H, H14). **^{13}C NMR** (151 MHz, CDCl3) δ 167.73 (C20), 153.05 (C19), 142.67 (C6), 141.86 (C1), 141.54 (C12), 140.48 (C8), 136.69 (C21), 136.59 (C13), 130.12 (C16), 129.71 (q, J = 32.7 Hz, C27)), 126.17 (C3), 126.03 (q, J = 3.7 Hz, C26),, 125.88 (C25), 124.09 (C17), 123.98 (q, J = 271.9 Hz, C28), 123.84 (C7), 122.72 (C18), 122.67 (C2), 118.20 (C22), 116.11 (m, 2C), 110.99 (m), 20.24 (C23), 14.65 (C15), 14.58 (C14); due to complicated splitting from fluorine atoms, signals for carbon atoms of cyclopentene ring were not assigned. **^{19}F NMR** (564 MHz, $CDCl_3$**)** δ: -131.86 (quint, J = 5.0 Hz, 2F), -110.18 (2F), -109.95 (2F), -63.06 (6F). **HRMS (ESI):** $[M+H]^+$ calcd for $C_{30}H_{19}F_9NS_3$: 660.0536, found: 660.0532.

6-(4-(3,3,4,4,5,5-hexafluoro-2-(2-methyl-5-phenylthiophen-3-yl)cyclopent-1-en-1-yl)-5-methylthiophen-2-yl)-2-methylbenzo[d]thiazole (6)

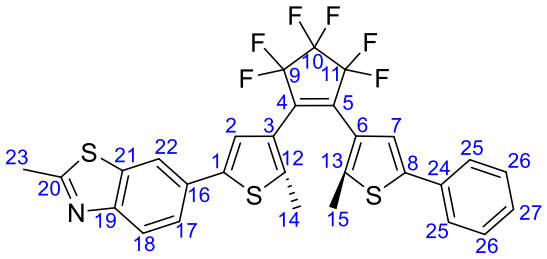

Compound **6** (0.137 g, 75%) was obtained from **12** and phenylboronic acid pinacol ester as a bluish solid following general procedure. **M.p.:** 181,3-183,8°C. **^{1}H NMR** (600 MHz, CDCl3) δ 7.98 (d, $J_{H,H}$ = 1.5 Hz, 1H, H22), 7.93 (d, $J_{H,H}$ = 8.5 Hz, 1H, H18), 7.62 (dd, $J_{H,H}$ = 8.5, 1.5 Hz, 1H, H17), 7.55 (d, $J_{H,H}$ = 7.4 Hz, 2H, H25), 7.39 (t, $J_{H,H}$ = 7.4 Hz, 2H, H26), 7.32 (s, 1H, H2), 7.30 (t, $J_{H,H}$ = 7.4 Hz, 1H, H27),7.29 (s, 1H, H7), 2.85 (s, 3H, H23), 1.98 (s, 6 H, H14 and H15). **^{13}C NMR** (151 MHz, CDCl3) δ 167.67 (C20), 153.01 (C19), 142.31 (C8), 141.67 (C1), 141.60 (C12), 141.26 (C13), 136.67 (C21), 136.10 (C4 and C5), 133.23 (C24), 130.23 (C16), 129.01 (C26), 127.93 (C27), 126.02 (C3), 125.80 (C6), 125.61 (C25), 124.11 (C17), 122.77 (C2), 122.70 (C18), 122.38 (C7), 118.19 (C22), 20.23 (C23), 14.57 (C14 and C15); due to complicated splitting from fluorine atoms, signals for carbon atoms C9, C10 and C11 of cyclopentene ring were not assigned. **^{19}F NMR** (564 MHz, $CDCl_3$) δ: -131.87 (J = 4.9 Hz, 2F), -110.07 (2F), -110.01 (2F). **HRMS (ESI):** $[M+H]^+$ calcd for $C_{29}H_{20}F_6NS_3$: 592.0662, found: 592.0659

6-(4-(3,3,4,4,5,5-hexafluoro-2-(2-methyl-5-(2-methylbenzo[d]thiazol-6-yl)thiophen-3-yl)cyclopent-1-en-1-yl)-5-methylthiophen-2-yl)phenol (7)

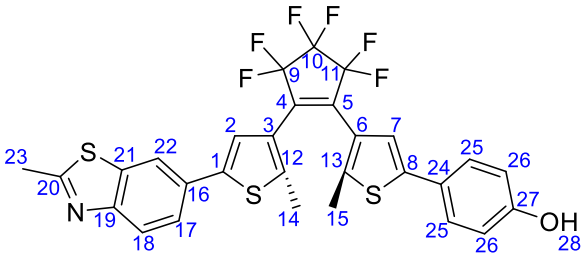

Compound **7** (0.151 g, 53%) was obtained from **12** and 4-hydroxyphenylboronic acid as a bluish solid following the general procedure. **M.p.:** 224,7-225,3 °C. **^{1}H NMR** (600 MHz, CDCl3) δ 7.98 (d, $J_{H,H}$ = 1.5 Hz, 1H, H22), 7.93 (d, $J_{H,H}$ = 8.5 Hz, 1H, H18), 7.62 (dd, $J_{H,H}$ = 8.5, 1.5 Hz, 1H, H17), 7.42 (d, $J_{H,H}$ = 8.8 Hz, 2H, H25), 7.32 (s, 1H, H2), 7.15 (s, 1H, H7), 6.85 (d, $J_{H,H}$ = 8.8 Hz, 2H, H26), 5.20 (br s, 1H, H28), 2.85 (s, 3H, H23), 1.99 (s, 3H, H14), 1.96 (s, 3H, H15). **^{13}C NMR** (151 MHz, CDCl3) δ 167.83 (C20), 155.66 (C27), 152.82 (C19), 142.16 (C1), 141.62 (C6), 141.54 (C12), 140.27 (C8), 136.58 (C21), 136.36 (C5), 135.76 (C4), 130.32 (C16), 127.15 (C25), 126.29 (C24), 126.07 (C3), 125.66 (C13), 124.16 (C17), 122.85 (C2), 122.63 (C18), 121.25 (C7), 118.19 (C22), 115.88 (C26), 20.19 (C23), 14.59 (C14), 14.51 (C15); due to complicated splitting from fluorine atoms, signals for carbon atoms C9, C10 and C11 of cyclopentene ring were not assigned. **^{19}F NMR** (564 MHz, $CDCl_3$**)** δ: -131.88 (2F), -110.08 (2F), -109.97 (2F). **HRMS (ESI):** $[M+H]^+$ calcd for $C_{29}H_{20}F_6NOS_3$: 608.0601, found: 608.0605.

6-(4-(3,3,4,4,5,5-hexafluoro-2-(5-(4-methoxyphenyl)-2-methylthiophen-3-yl)cyclopent-1-en-1-yl)-5-methylthiophen-2-yl)-2-methylbenzo[d]thiazole (8)

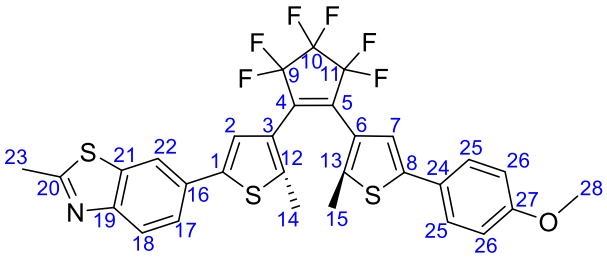

Compound **8** (0.146 g, 64%) was obtained from **12** and 4-methoxyphenylboronic acid as a bluish solid following general procedure. **M.p.:** 81.5 – 83 °C. **^{1}H NMR** (600 MHz, CDCl3) δ 7.98 (d, $J_{H,H}$ = 1.5 Hz, 1H, H22), 7.93 (d, $J_{H,H}$ = 8.5 Hz, 1H, H18), 7.62 (dd, $J_{H,H}$ = 8.5, 1.5 Hz, 1H, H17), 7.47 (d, $J_{H,H}$ = 8.7 Hz, 2H, H25), 7.32 (s, 1H, H2), 7.16 (s, 1H, H7), 6.91 (d, $J_{H,H}$ = 8.7 Hz, 2H, H26), 3.83 (s, 3H, H28), 2.85 (s, 3H, H23), 1.99 (s, 3H, H14), 1.97 (s, 3H, H15). **^{13}C NMR** (151 MHz, CDCl3) δ 167.67 (C20), 159.50 (C27), 152.98 (C19), 142.22 (C1), 141.58 (C12), 140.26 (C8), 136.65 (C21), 136.36 (C5), 135.74 (C4), 130.25 (C16), 126.91 (C25), 126.14 (C24), 126.06 (C3), 125.67 (C13), 124.10 (C17), 122.81 (C2), 122.68 (C18), 121.23 (C7), 118.17 (C22), 114.38 (C26), 55.39 (C28), 20.21 (C23), 14.57 (C14), 14.50 (C15), due to complicated splitting from fluorine atoms, signals for carbon atoms C9, C10 and C11 of cyclopentene ring were not assigned. **^{19}F NMR** (564 MHz, $CDCl_3$**)** δ: -131.88 (2F), -110.07 (2F), -109.97 (2F**). HRMS (ESI):** $[M+H]^+$ calcd for $C_{30}H_{22}F_6NOS_3$: 622.0767, found: 622.0761.

4-(4-(3,3,4,4,5,5-hexafluoro-2-(2-methyl-5-(2-methylbenzo[d]thiazol-6-yl)thiophen-3-yl)cyclopent-1-en-1-yl)-5-methylthiophen-2-yl)-*N,N*-diphenylaniline (9)

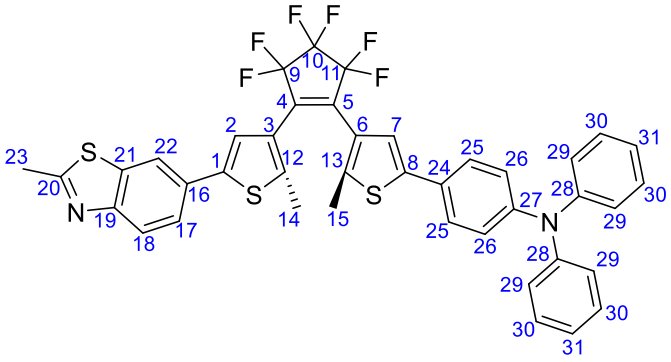

Compound **9** (0.365 g, 81%) was obtained from **12** and 4-(*N,N*-diphenylamino)phenylboronic acid pinacol ester as a greenish solid following the general procedure. **M.p.:** 117 – 118.5 °C. **^{1}H NMR** (600 MHz, $CDCl_3$) δ 7.98 (d, $J_{H,H}$ = 1.5 Hz, 1H, H22), 7.93 (d, $J_{H,H}$ = 8.5 Hz, 1H, H18), 7.62 (dd, $J_{H,H}$ = 8.5, 1.5 Hz, 1H, H17), 7.37 (d, $J_{H,H}$ = 8.6 Hz, 2H, H25), 7.31 (s, 1H, H2), 7.27 (t, $J_{H,H}$ = 8.1 Hz, 4H, H30), 7.18 (s, 1H, H2), 7.11 (d, $J_{H,H}$ = 7.9 Hz, 4H, H29), 7.06 (d, $J_{H,H}$ = 8.6 Hz, 2Hm H26), 7.05 (t, $J_{H,H}$ = 7.9 Hz, 2H, H31), 2.85 (s, 3H, H2), 1.99 (s, 3H, H14), 1.96 (s, 3H, H15). **^{13}C NMR** (151 MHz, CDCl3) δ 167.65 (C20), 152.99 (C20), 147.68 (C27), 147.33 (C28), 142.21 (C1), 141.59 (2C, C8 and C12)), 140.37 (C13), 136.66 (C21), 136.33 (C5), 135.77 (C4), 130.24 (C16), 129.34 (C30), 127.15 (C24), 126.39 (C25), 126.07 (C3), 125.76 (C6), 124.59 (C29), 124.11 (C17), 123.48 (C26), 123.27 (C31), 122.81 (C2), 122.69 (C18), 121.33 (C7), 118.18 (C22), 20.23 (C23), 14.61 (C14), 14.56 (C15); due to complicated splitting from fluorine atoms, signals for carbon atoms C9, C10 and C11 of cyclopentene ring were not assigned. **^{19}F NMR** (564 MHz, $CDCl_3$**)** δ: -131.87 (2F), -110.06 (2F), -109.69 (2F). **HRMS (ESI):** $[M+H]^+$calcd for $C_{41}H_{29}F_6N_2S_3$: 759.1397, found: 759.1390.

4-(4-(3,3,4,4,5,5-hexafluoro-2-(2-methyl-5-(2-methylbenzo[d]thiazol-6-yl)thiophen-3-yl)cyclopent-1-en-1-yl)-5-methylthiophen-2-yl)-N,N-dimethylaniline (10)

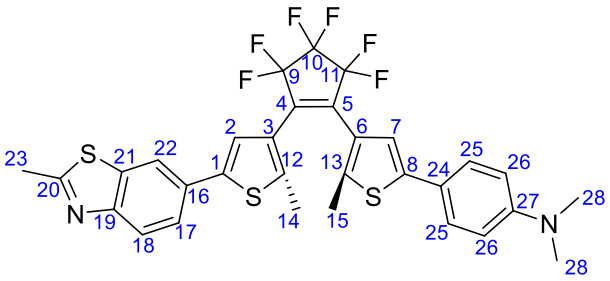

Compound **10** (0.119 g, 55 %) was obtained from **12** and 4-(*N,N*-dimethylamino)phenylboronic acid as a greenish solid following the general procedure. **M.p.:** 142.7 – 143.5 °C. **^{1}H NMR** (600 MHz, $CDCl_3$) δ 8.00 (d, $J_{H,H}$ = 1.5 Hz, 1H, H22), 7.94 (d, $J_{H,H}$ = 8,5 Hz, 1H, H18), 7.63 (dd, $J_{H,H}$ = 8.5, 1.5 Hz, 1H, H17), 7.42 (d, $J_{H,H}$ = 8.8 Hz, 2H, H25), 7.33 (s, 1H, H2), 7.11 (s, 1H, H7), 6.72 (d, $J_{H,H}$ = 8.8 Hz, 2H, H26), 3.00 (s, 6H, H28), 2.86 (s, 3H, H23), 1.99 (s, 3H, H14), 1.96 (s, 3H, H15). **^{13}C NMR** (151 MHz, CDCl3) δ 167.62 (C20), 152.93 (C19), 150.21 (C27), 143.13 (C6), 141.64 (C12), 141.45 (C1), 139.12 (C8), 136.64 (2C, C5 and C21), 135.43 (C5), 130.32 (C16), 126.55 (C25), 126.15 (C3), 125.54 (C13), 124.11 (C17), 122.87 (C2), 122.67 (C18), 121.65 (C24), 119.86 (C7), 118.16 (C22), 112.46 (C26), 40.43 (C28), 20.22 (C23), 14.58 (C14), 14.48 (C15); due to complicated splitting from fluorine atoms, signals for carbon atoms C9, C10 and C11 of cyclopentene ring were not assigned. **^{19}F NMR** (564 MHz, $CDCl_3$**)** δ: -131.88 (2F), -110.08 (2F), -109.92 (2F). **HRMS (ESI):** $[M+H]^+$ calcd for $C_{31}H_{25}F_6N_2S_3$: 635.1084, found: 635.1081.

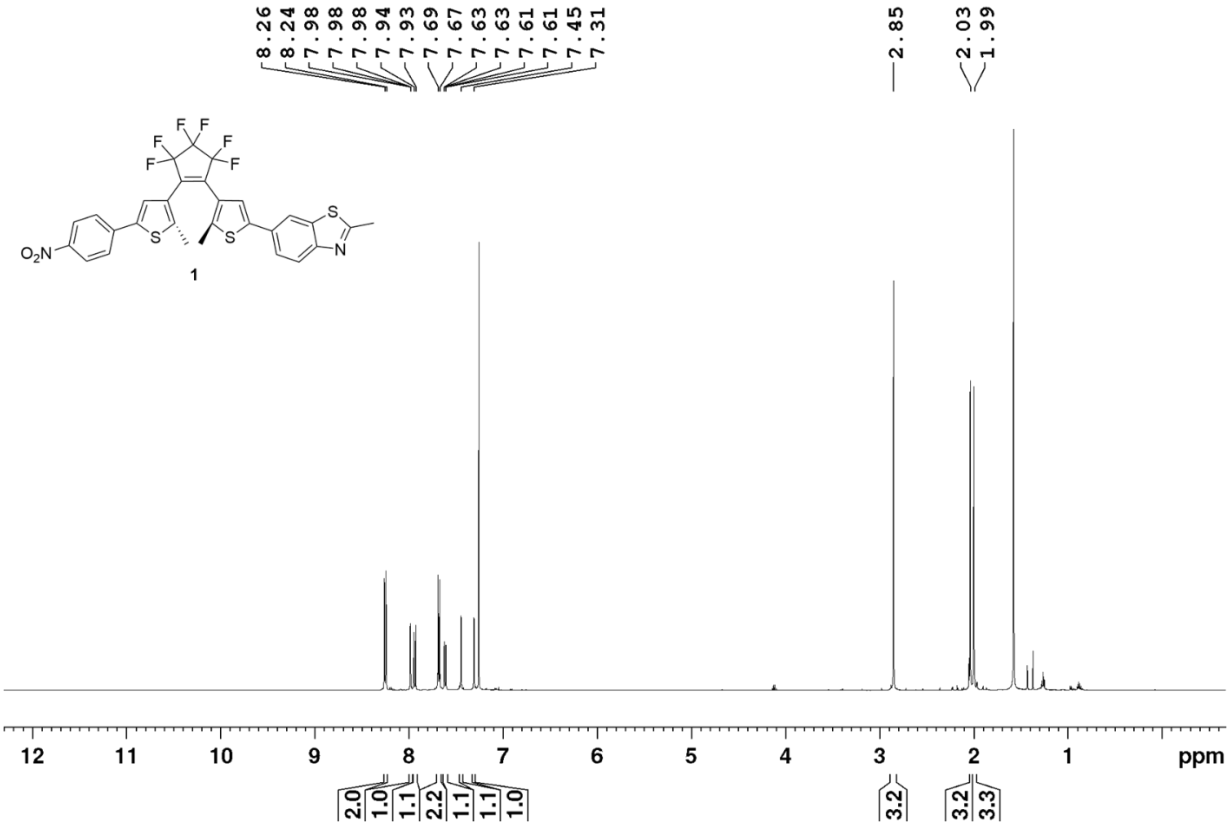

Figure S1. ^{1}H NMR spectrum of compound **1** in $CDCl_3$.

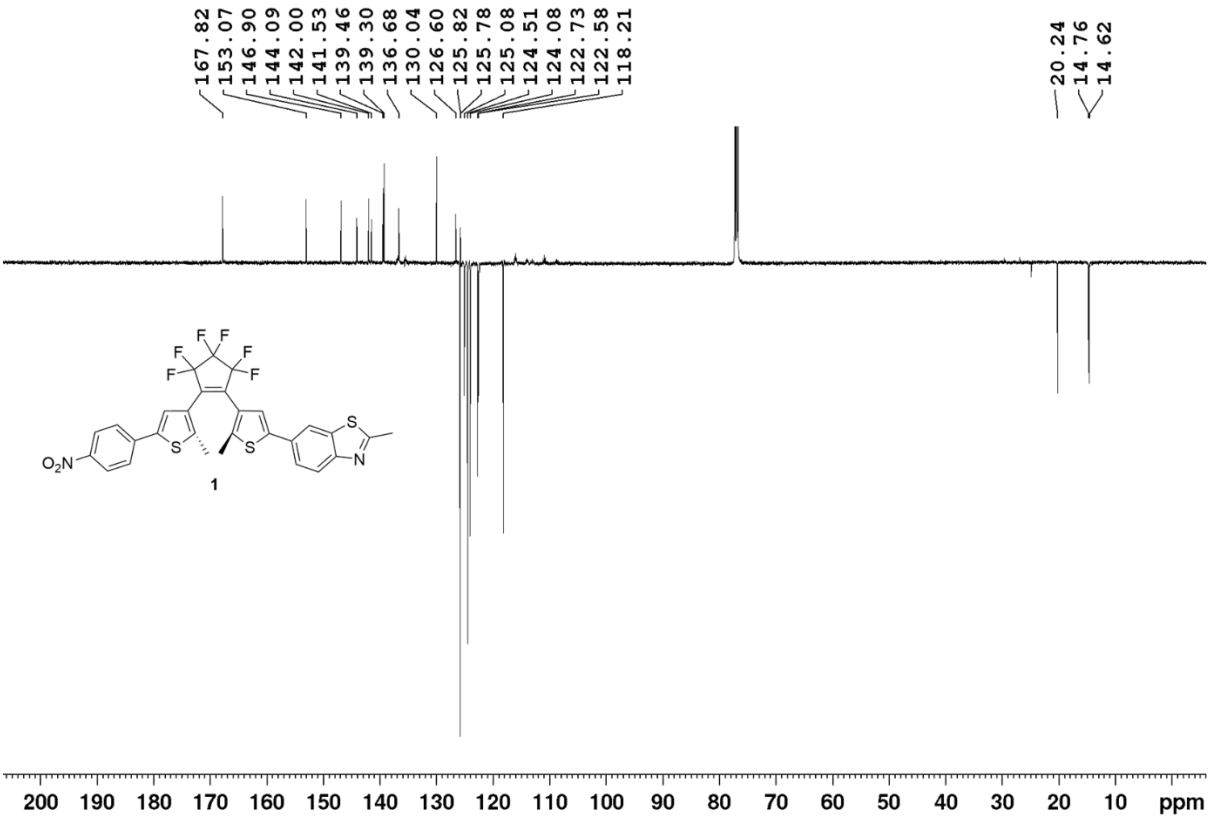

Figure S2. ^{13}C APT spectrum of compound **1** in $CDCl_3$.

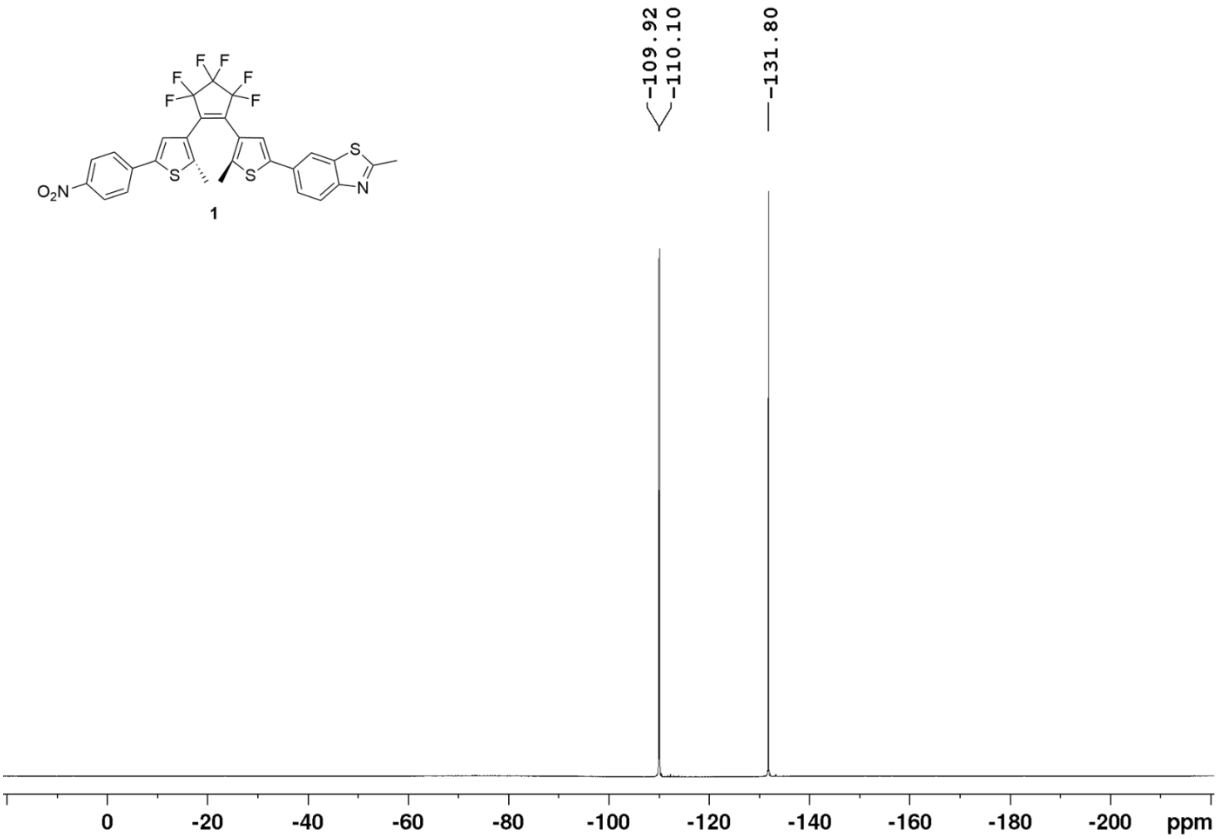

Figure S3. ^{19}F NMR spectrum of compound **1** in $CDCl_3$.

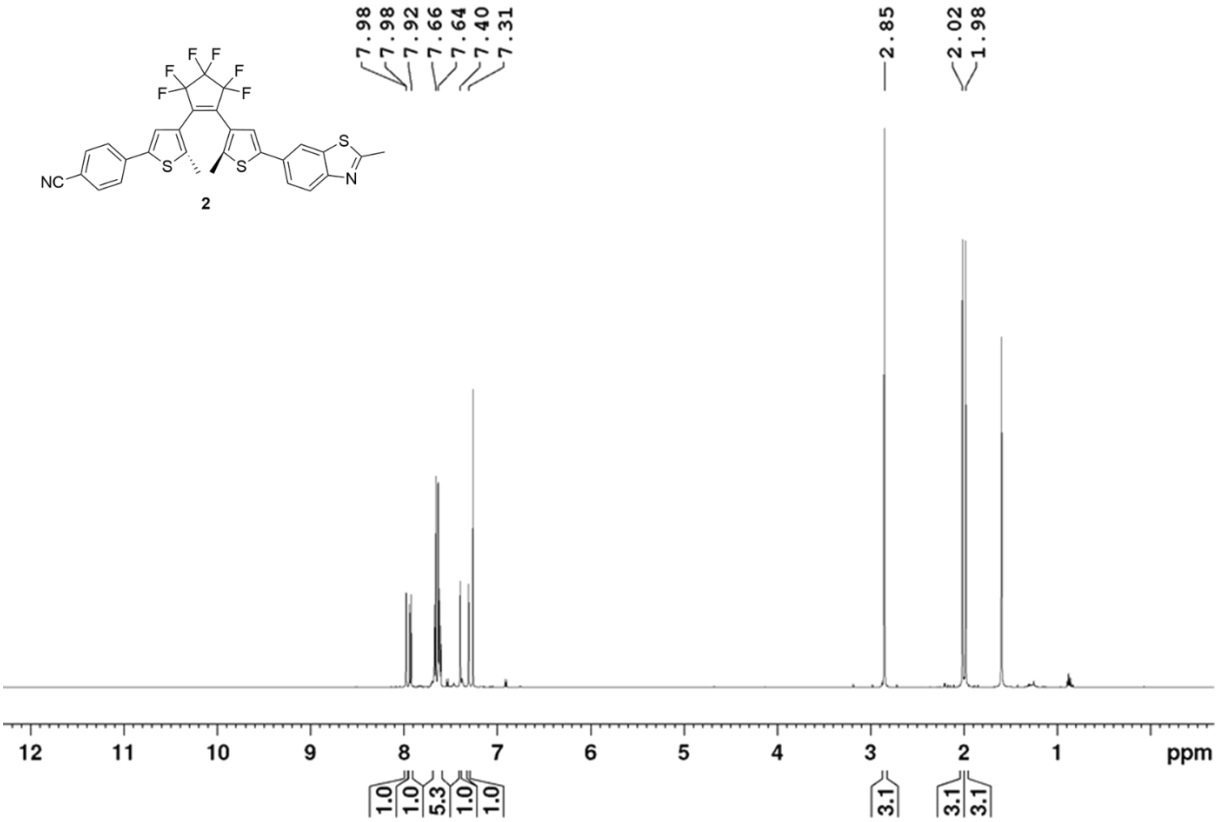

Figure S4. ^{1}H NMR spectrum of compound **2** in $CDCl_3$.

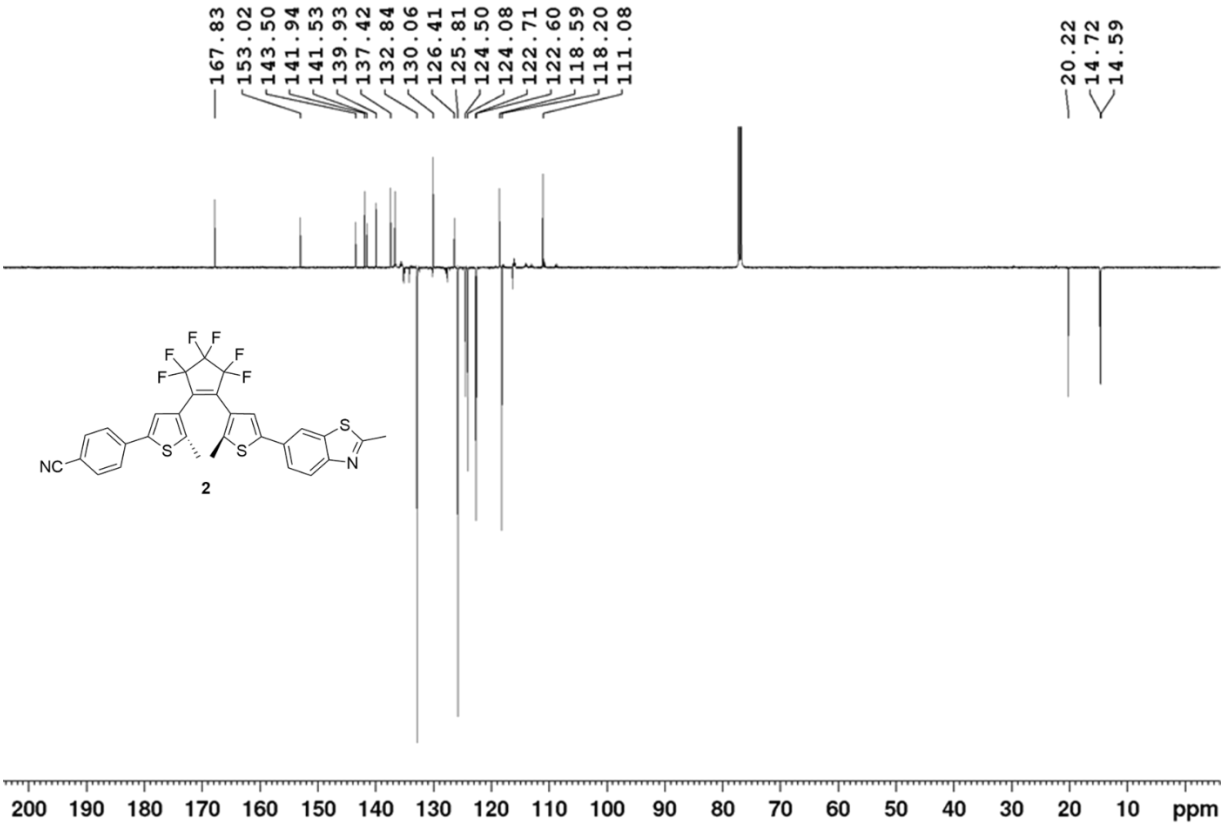

Figure S5. ^{13}C APT spectrum of compound **2** in $CDCl_3$.

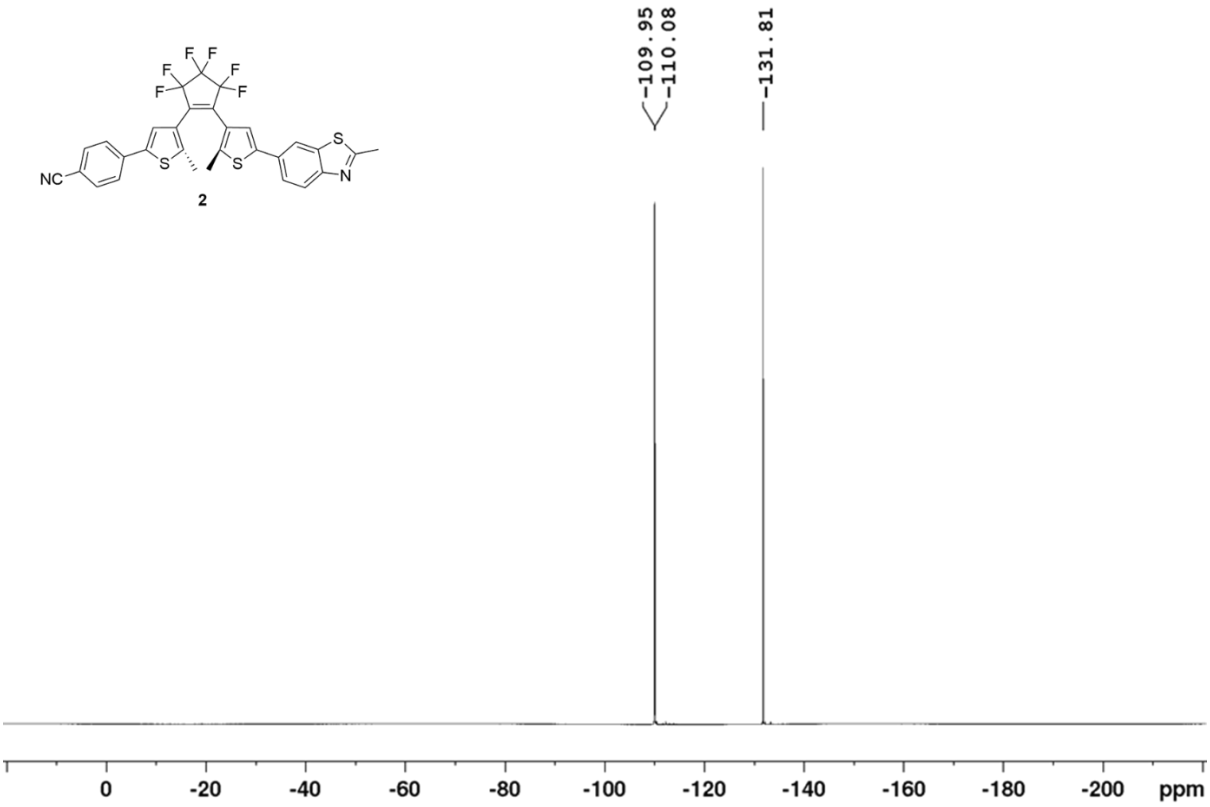

Figure S6. ^{19}F NMR spectrum of compound **2** in $CDCl_3$.

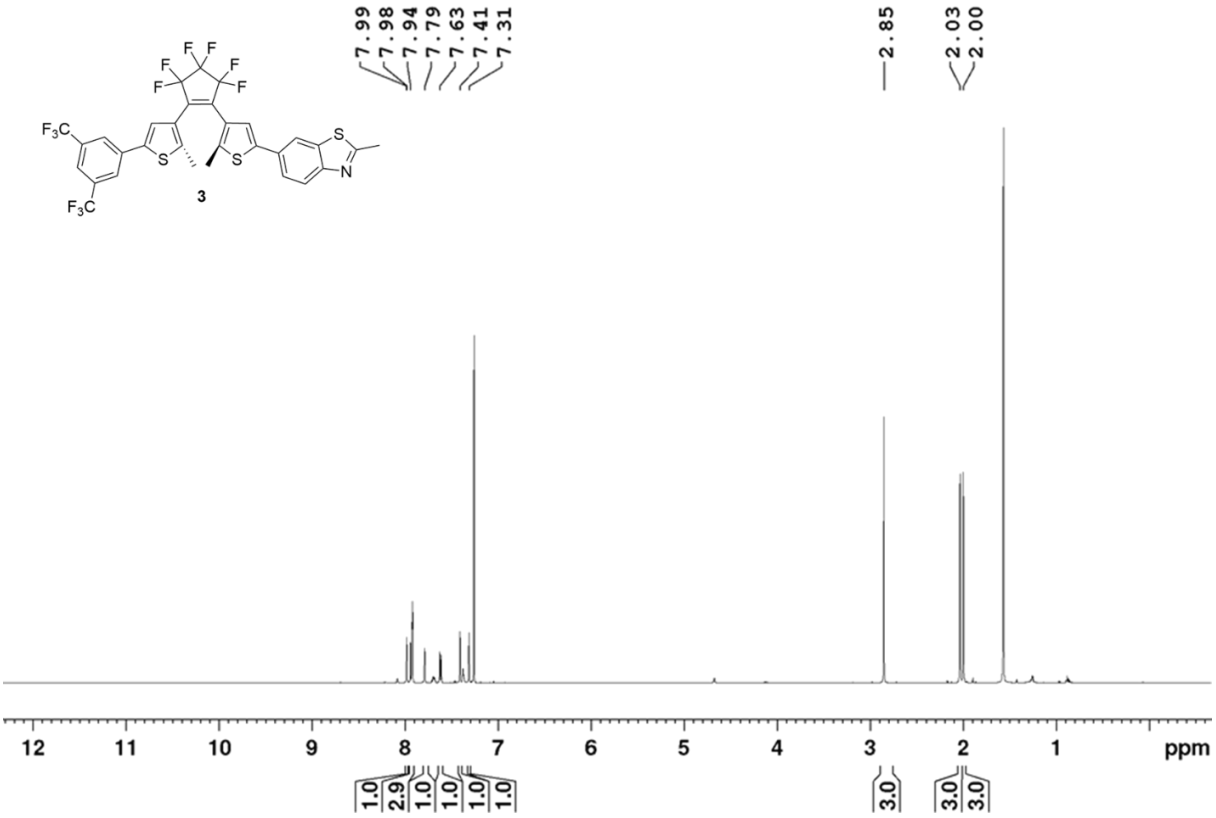

Figure S7. ^{1}H NMR spectrum of compound **3** in $CDCl_3$.

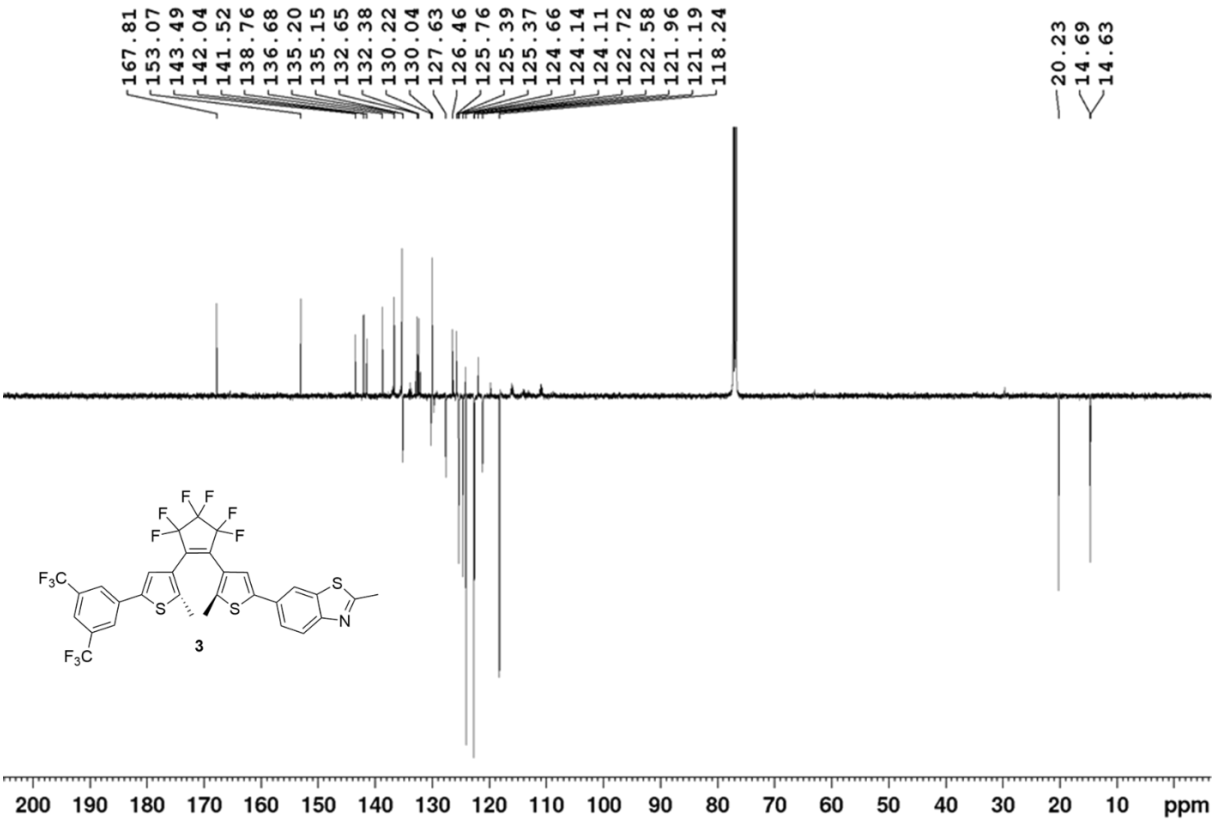

Figure S8. ^{13}C ATP spectrum of compound **3** in $CDCl_3$.

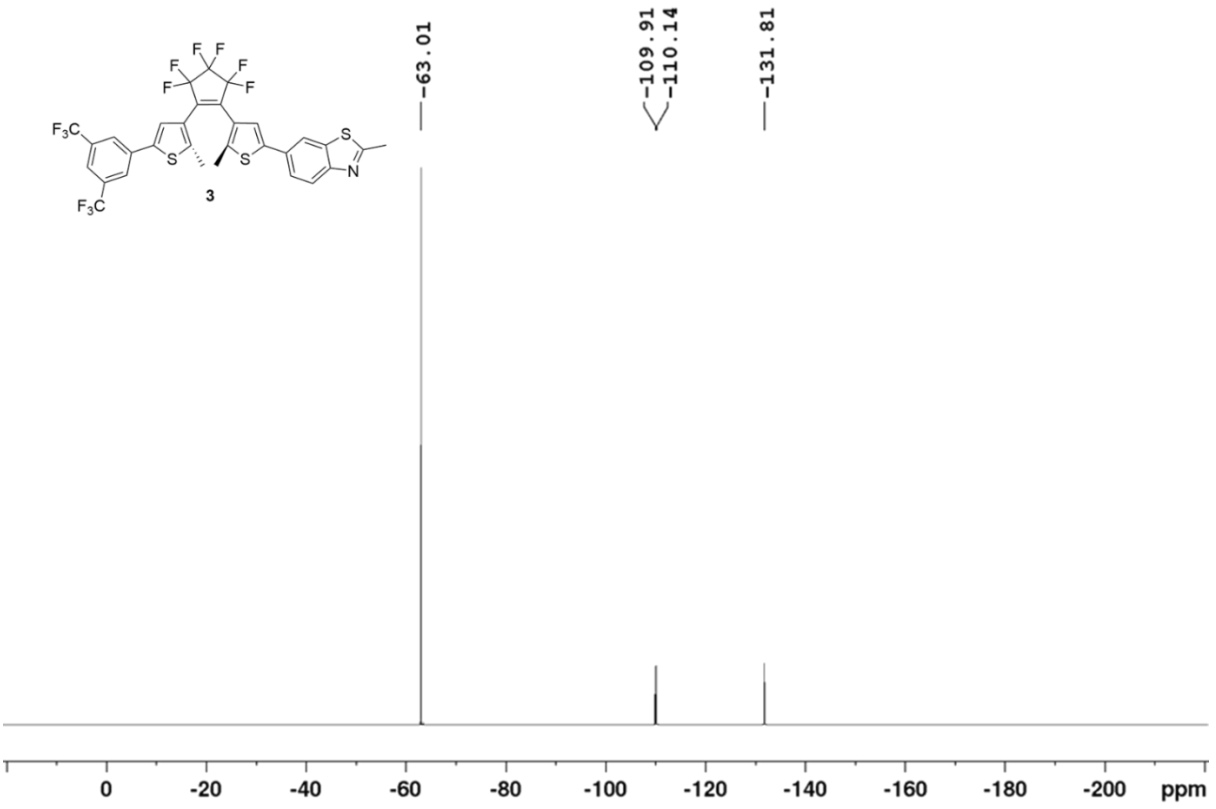

Figure S9. ^{19}F NMR spectrum of compound **3** in $CDCl_3$.

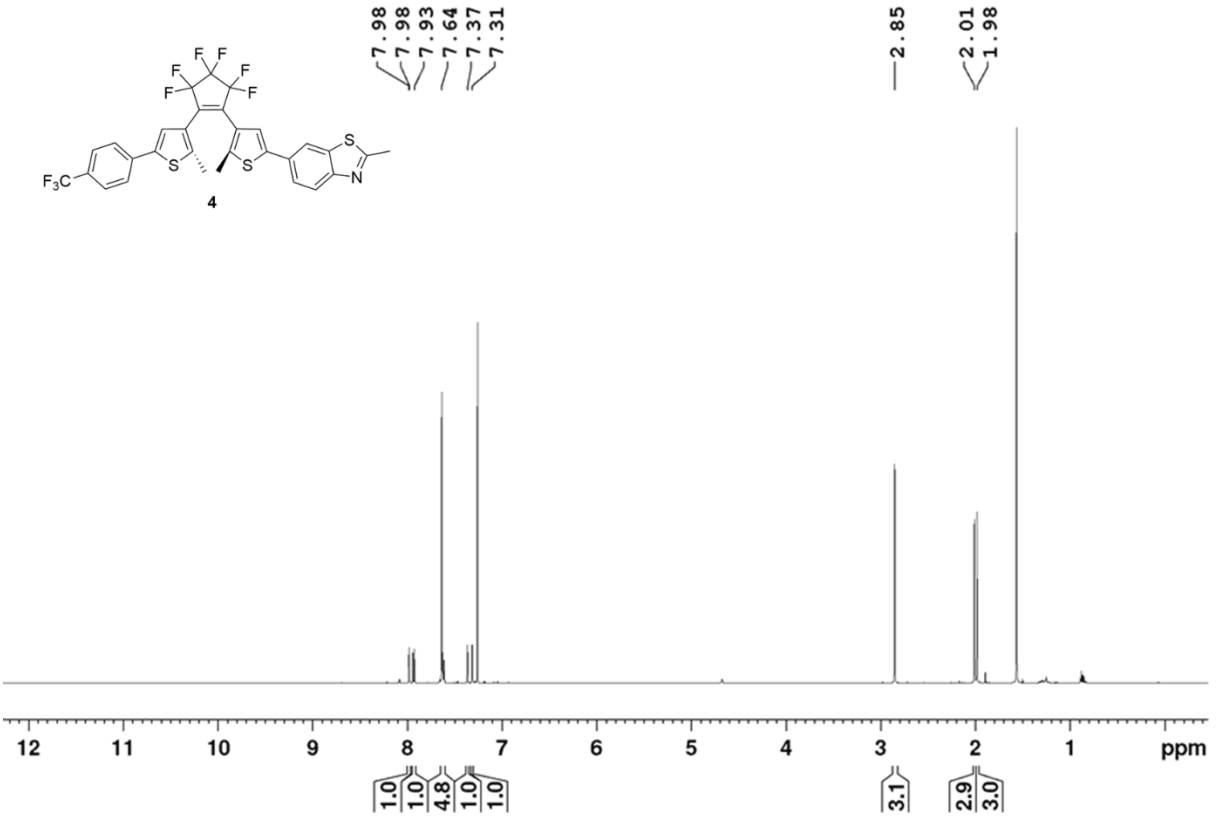

Figure S10. ^{1}H NMR spectrum of compound **4** in $CDCl_3$.

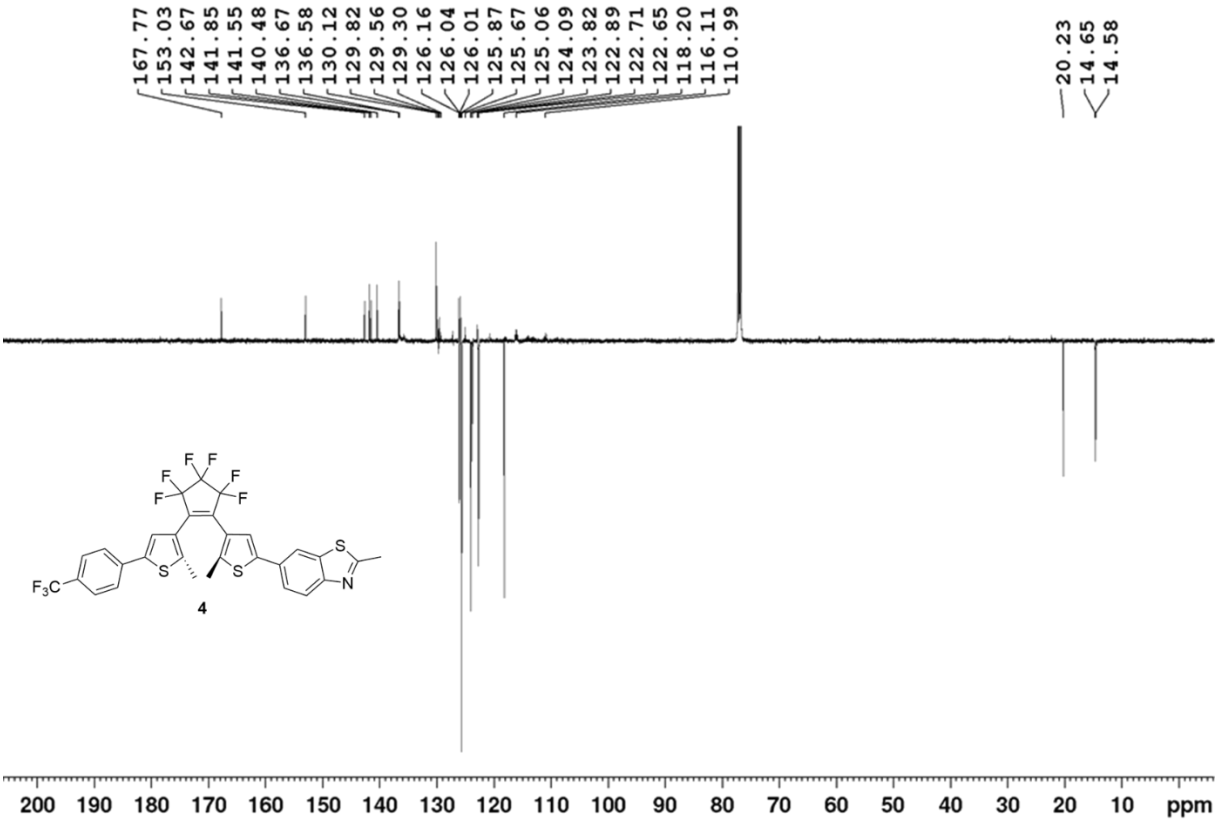

Figure S11. ^{13}C NMR spectrum of compound **4** in $CDCl_3$.

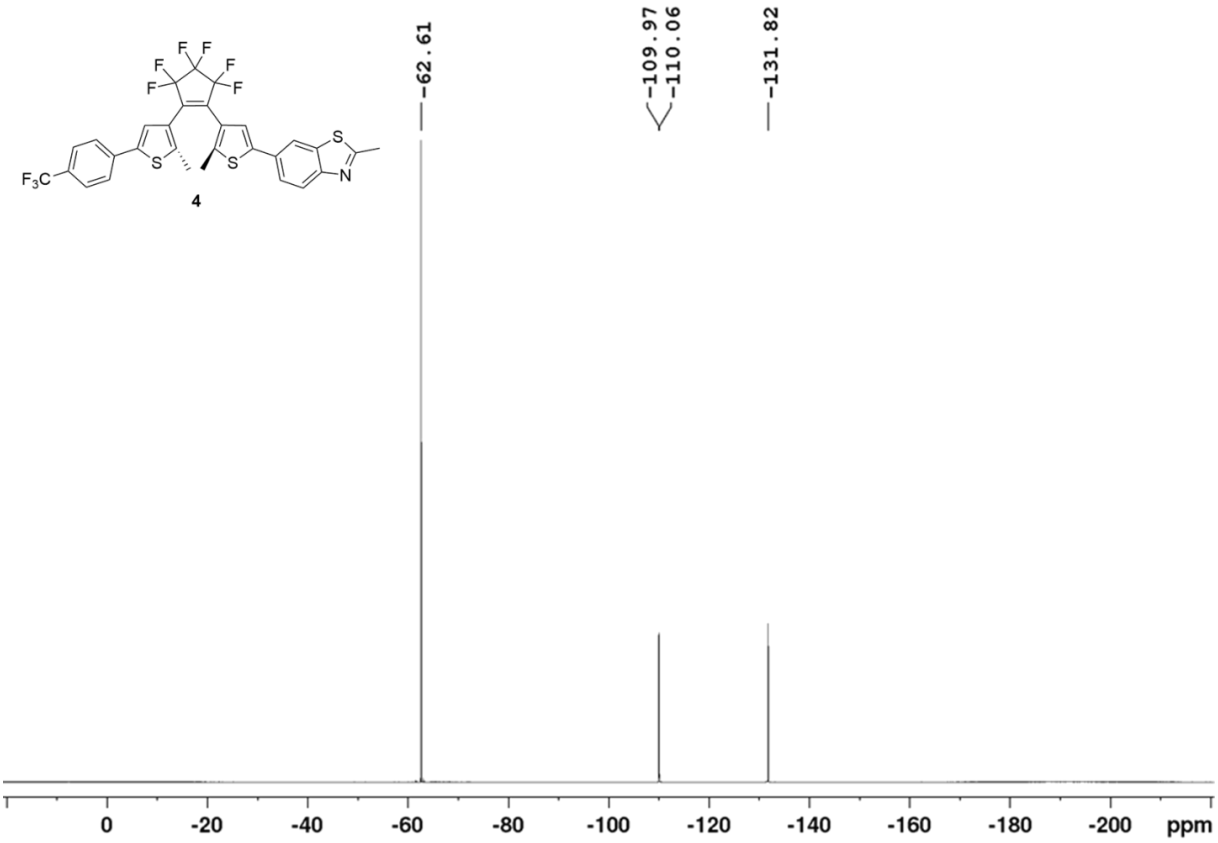

Figure S12. ^{19}F NMR spectrum of compound **4** in $CDCl_3$.

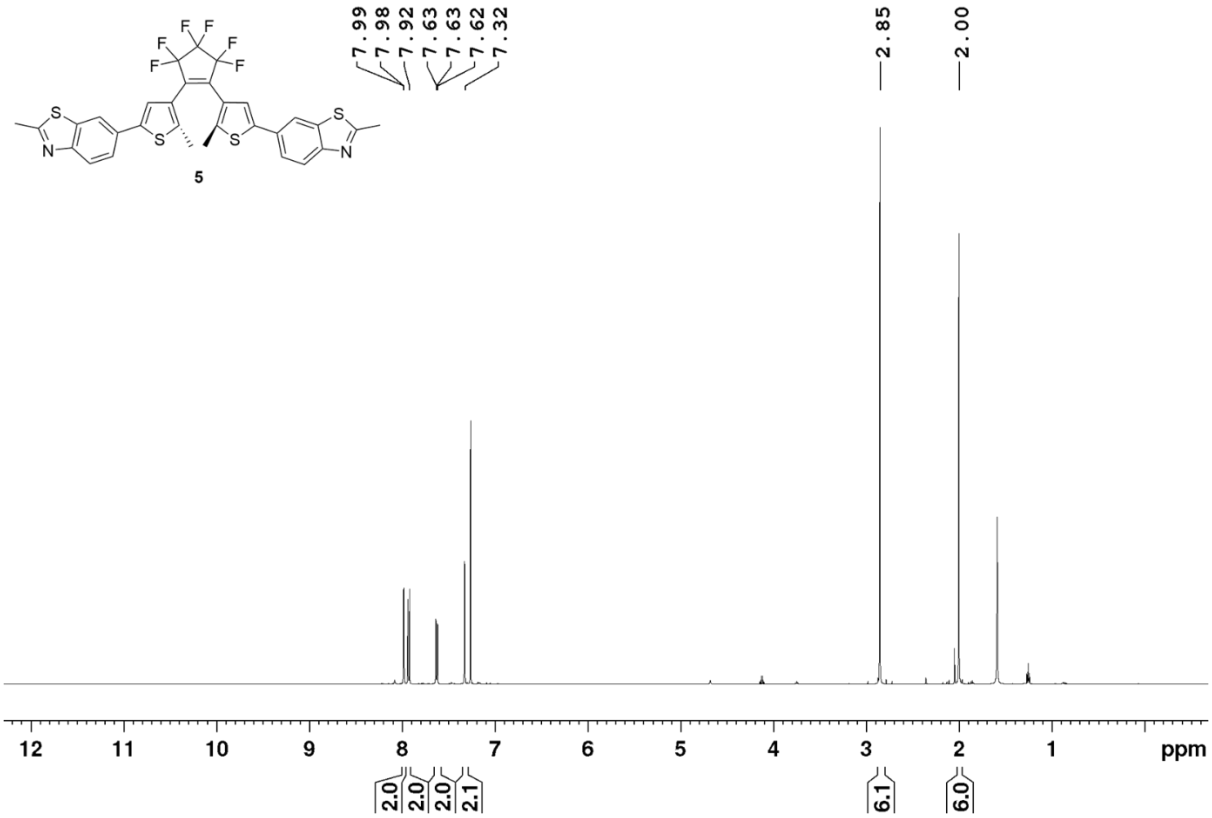

Figure S13. ^{1}H NMR spectrum of compound **5** in $CDCl_3$.

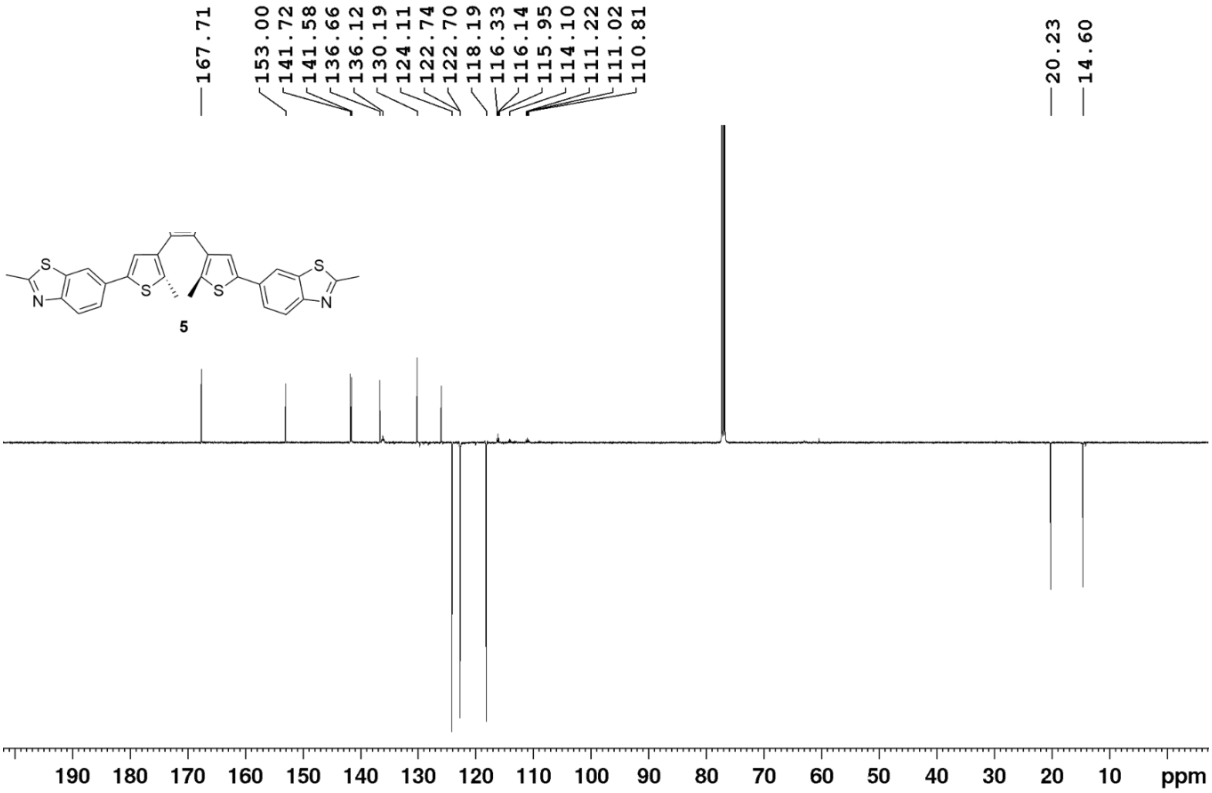

Figure S14. ^{13}C APT NMR spectrum of compound **5** in $CDCl_3$.

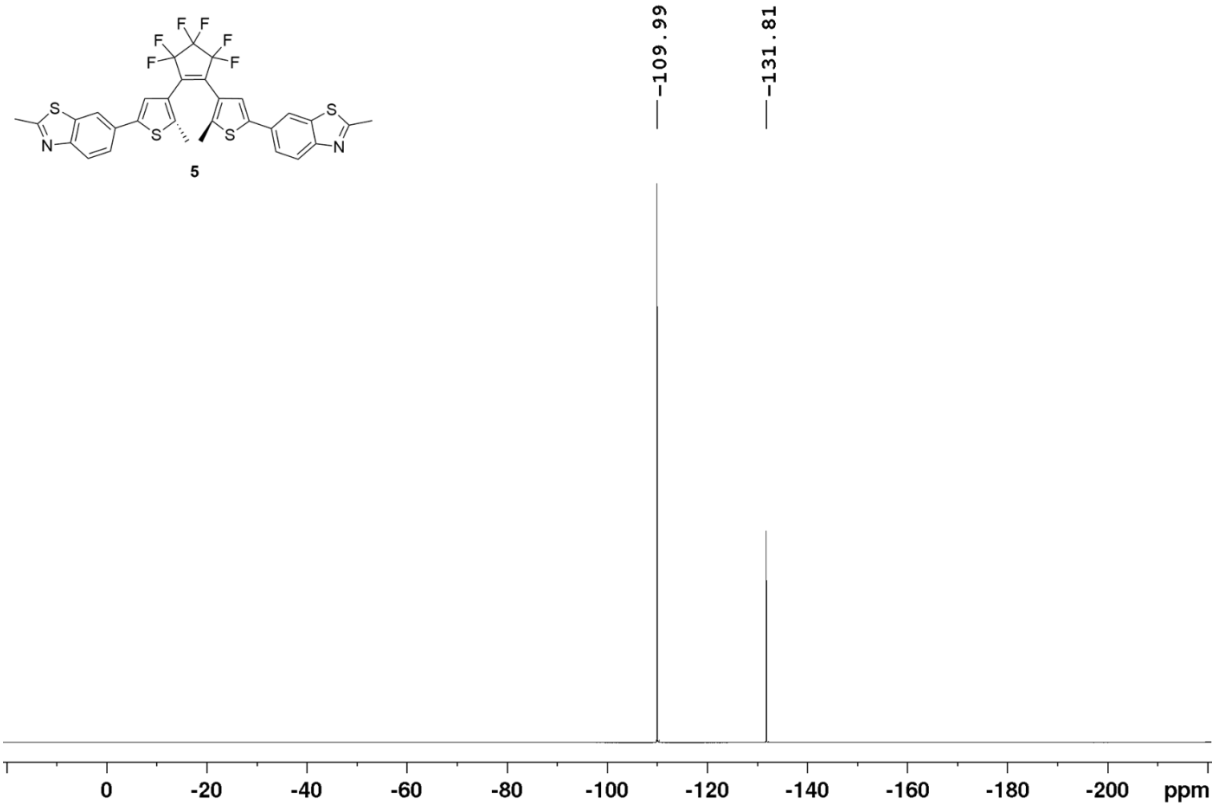

Figure S15. ^{19}F NMR spectrum of compound **5** in $CDCl_3$.

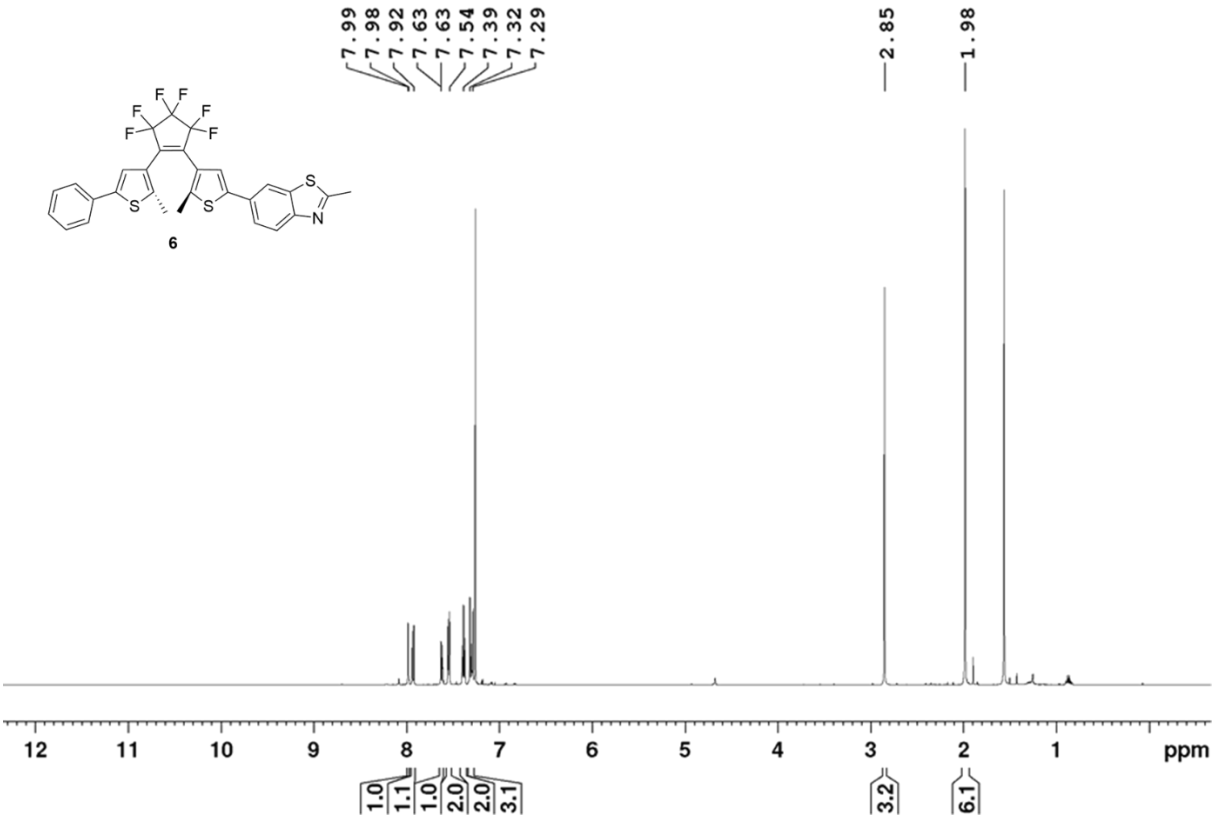

Figure S16. ^{1}H NMR spectrum of compound **6** in $CDCl_3$.

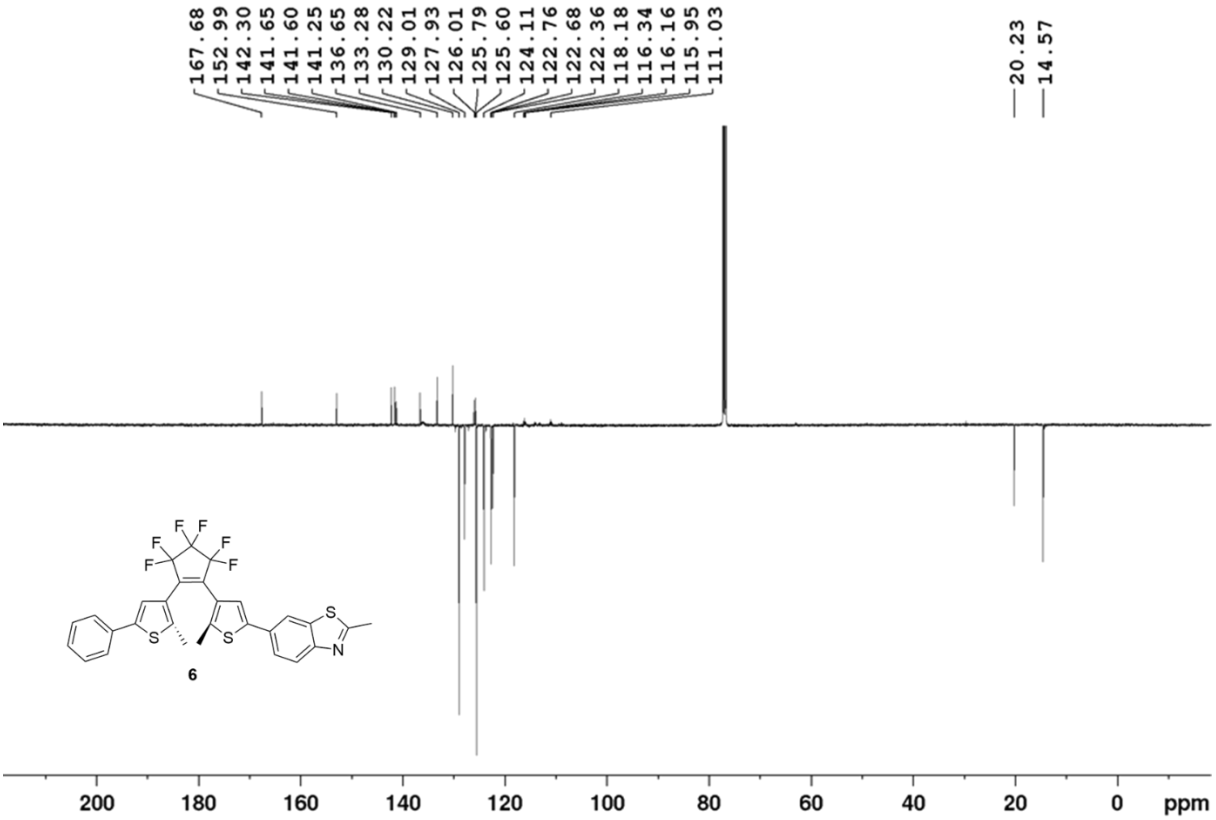

Figure S17. ^{13}C APT spectrum of compound **6** in $CDCl_3$.

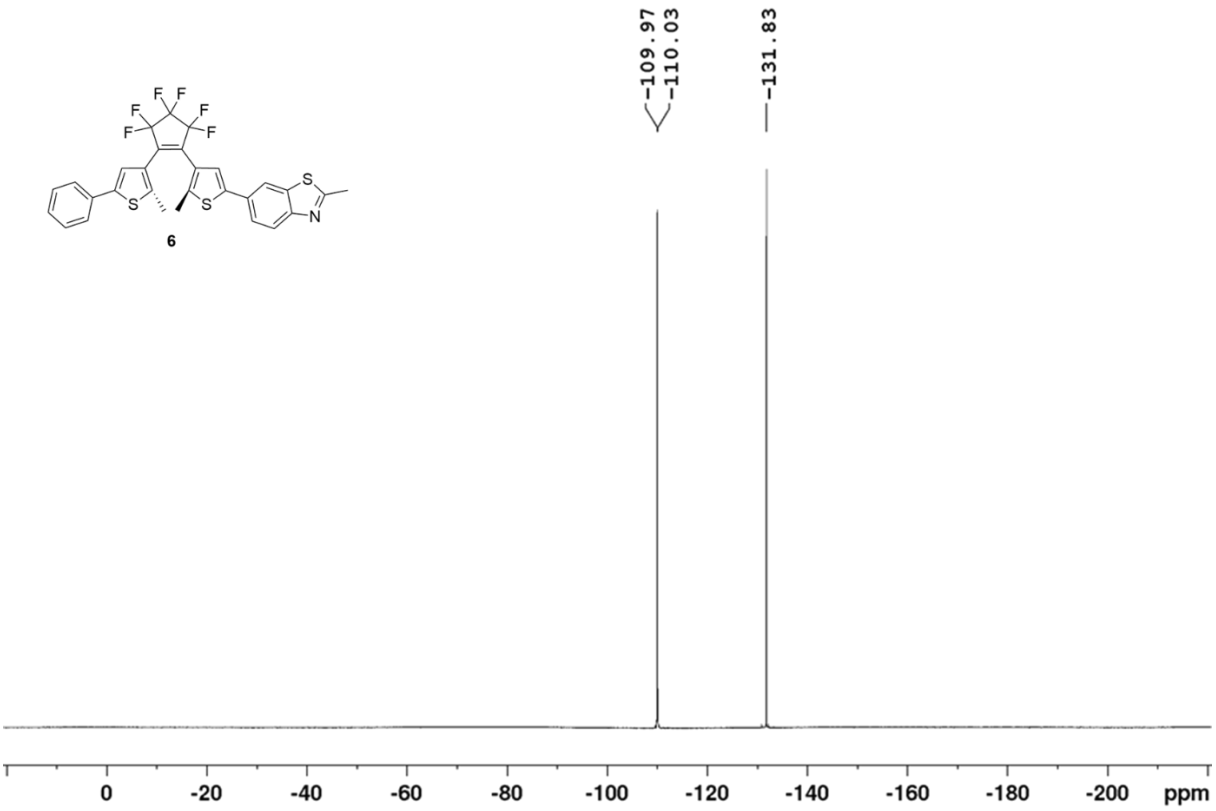

Figure S18. ^{19}F NMR spectrum of compound **6** in $CDCl_3$.

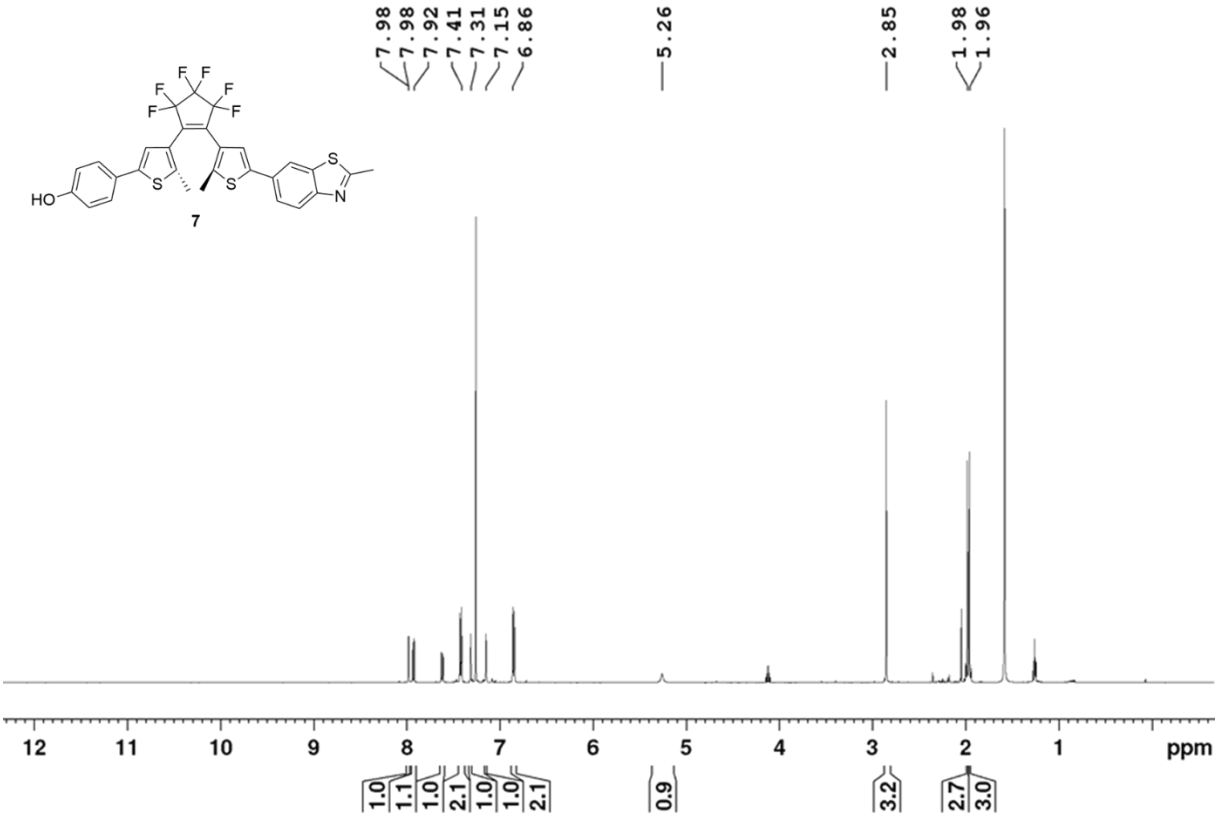

Figure S19. ^{1}H NMR spectrum of compound **7** in $CDCl_3$.

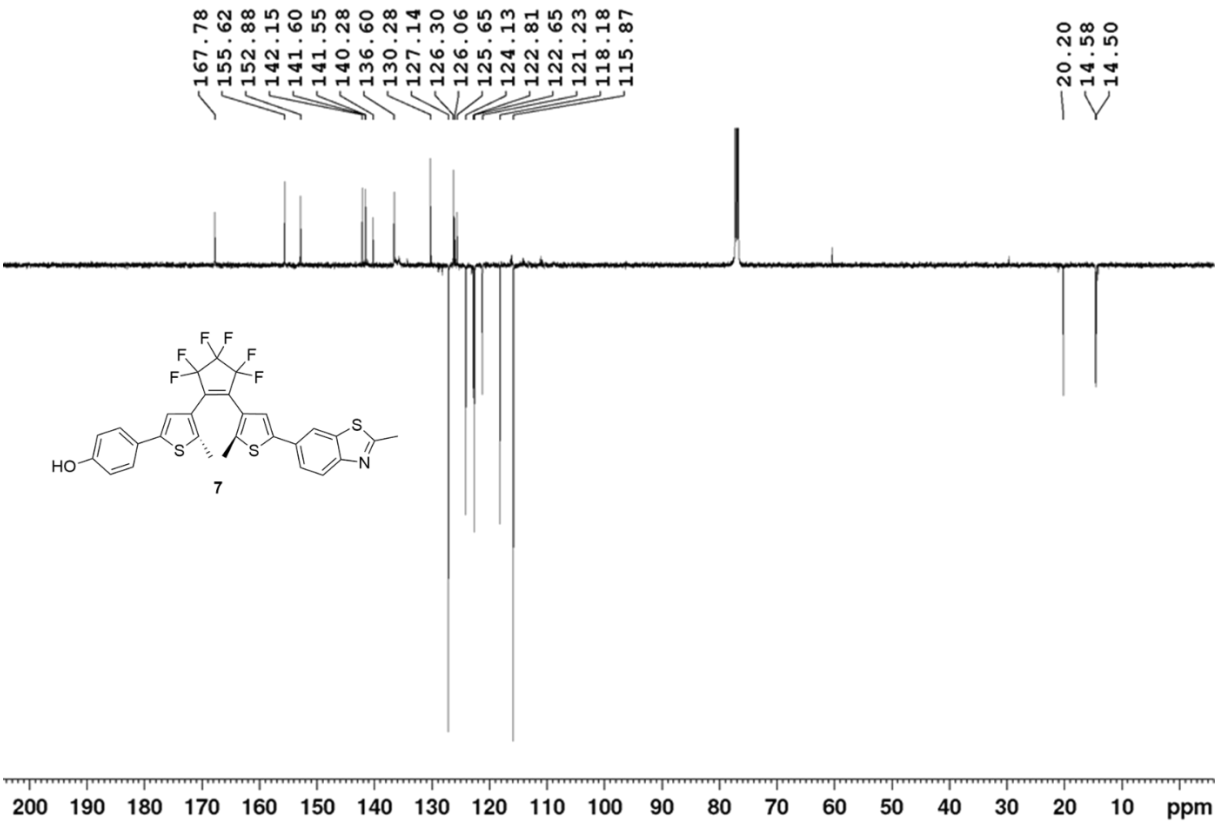

Figure S20. ^{13}C APT spectrum of compound **7** in $CDCl_3$.

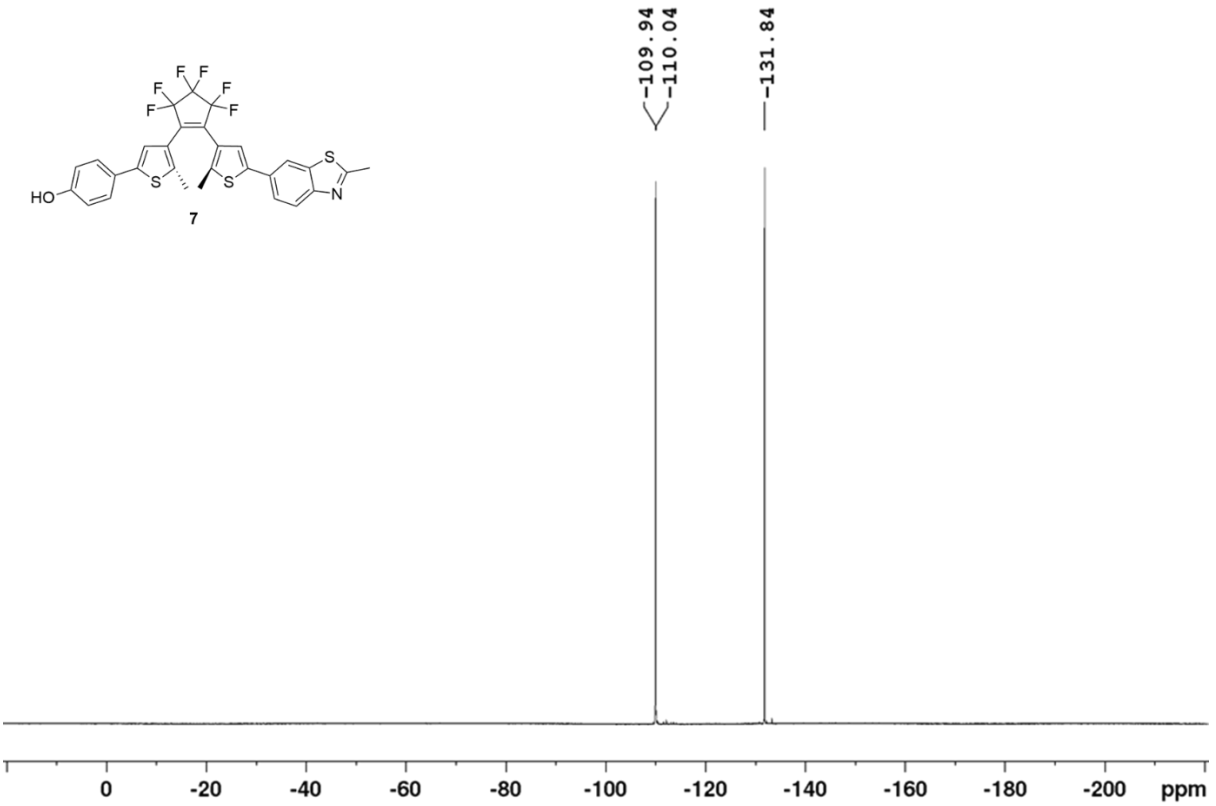

Figure S21. ^{19}F NMR spectrum of compound **7** in $CDCl_3$.

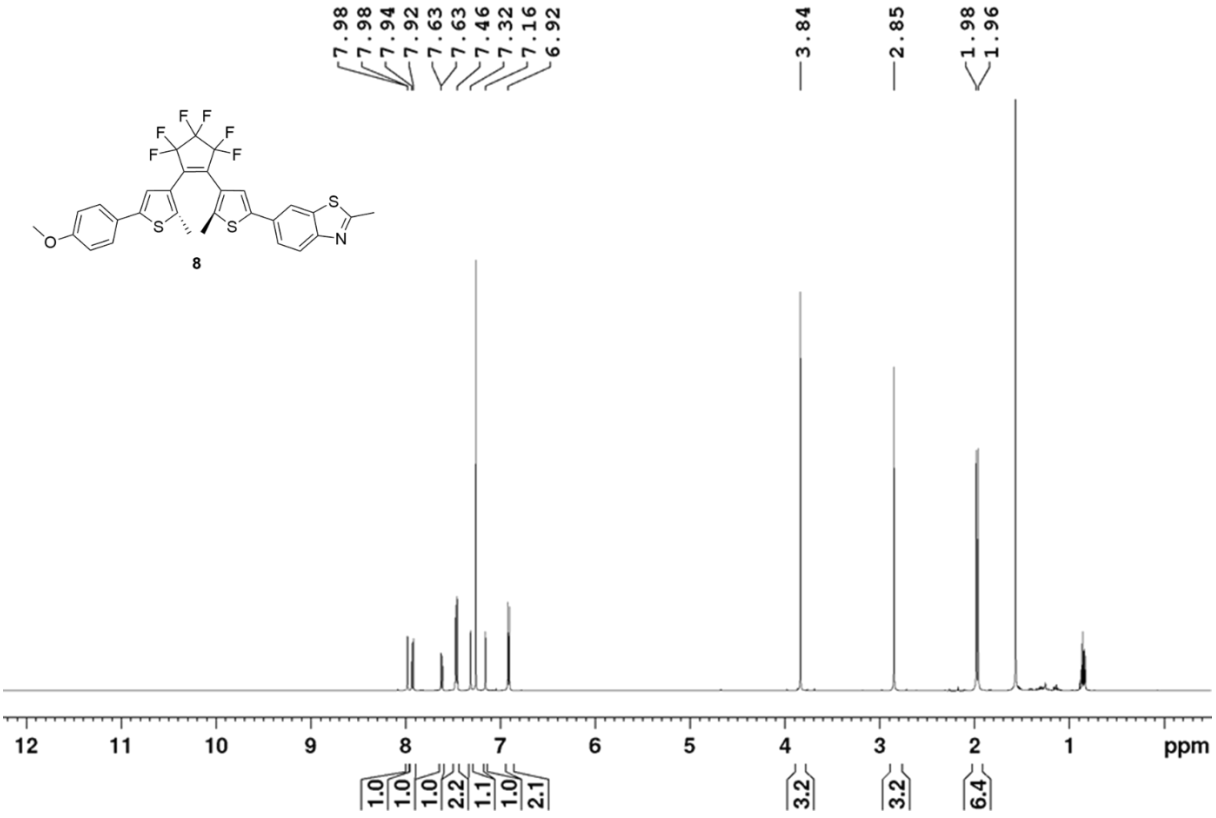

Figure S22. ^{1}H NMR spectrum of compound **8** in $CDCl_3$.

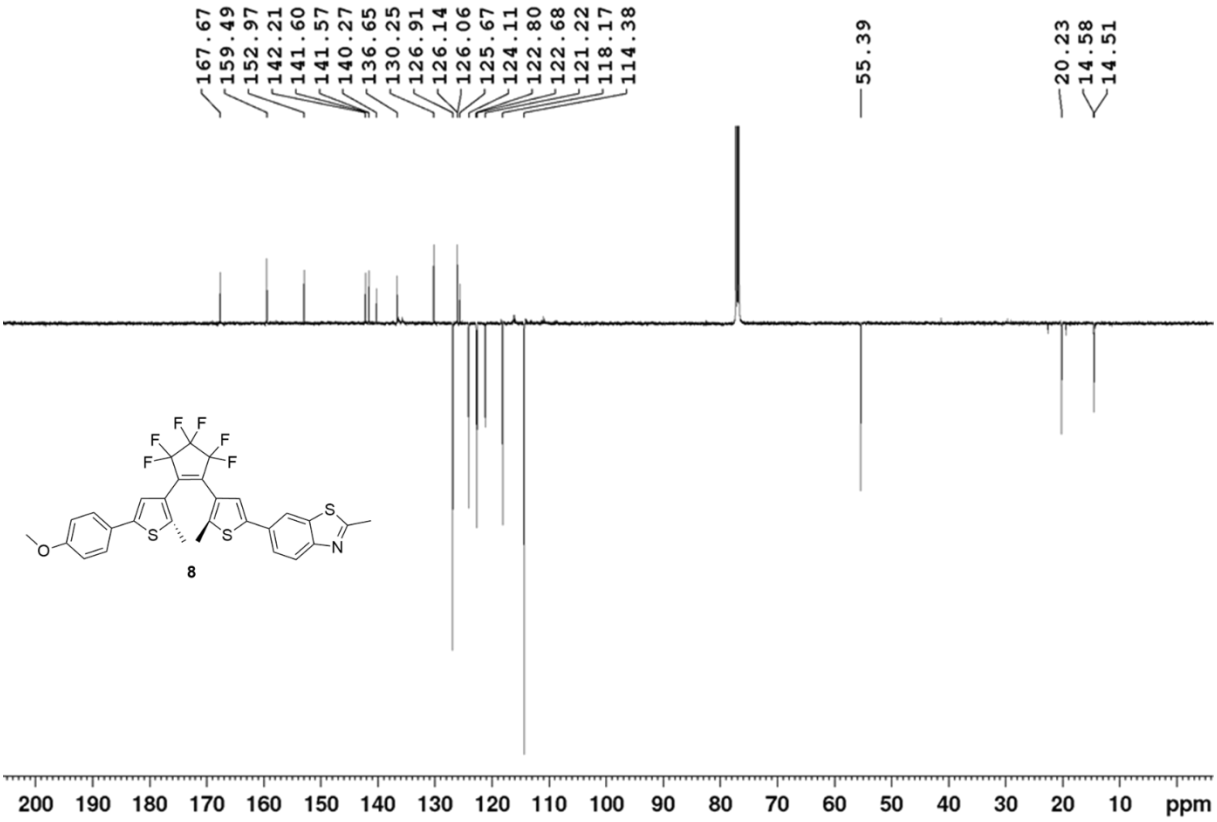

Figure S23. ^{13}C APT spectrum of compound **8** in $CDCl_3$.

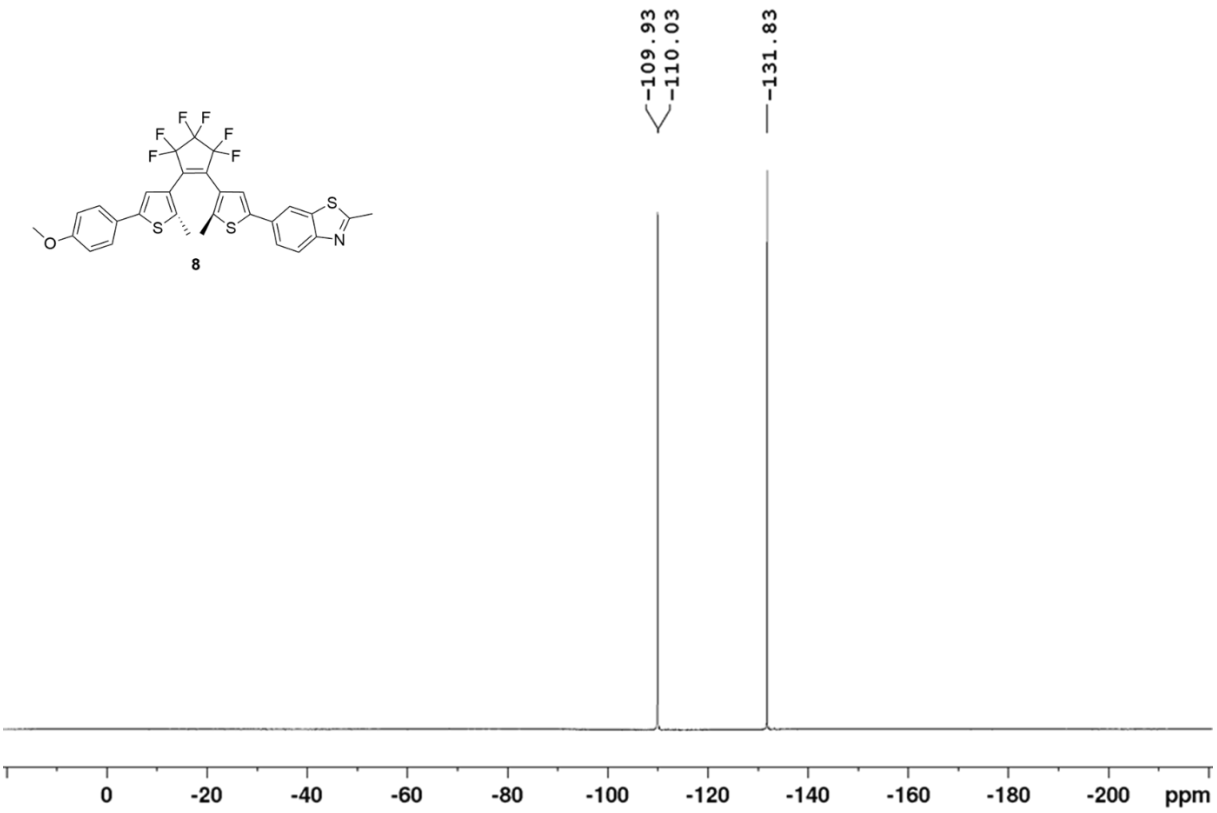

Figure S24. ^{19}F NMR spectrum of compound **8** in $CDCl_3$.

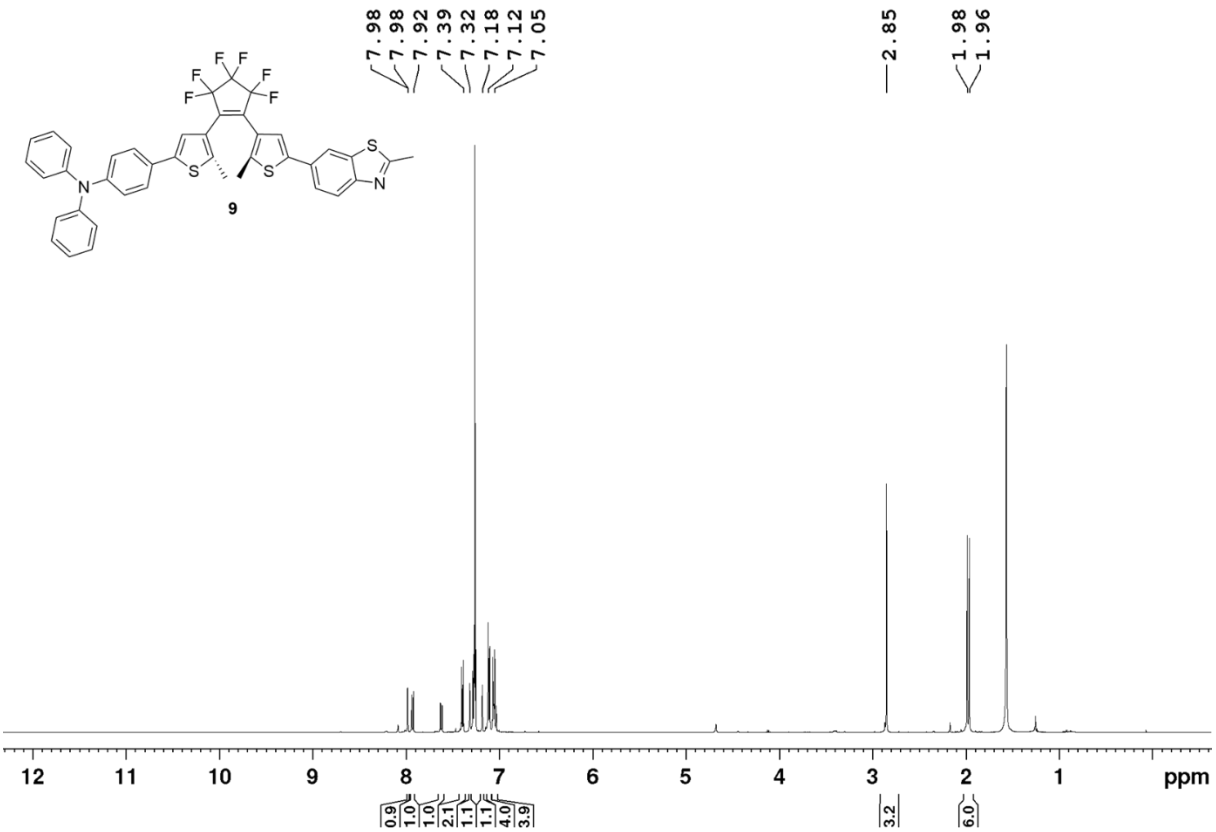

Figure S25. ^{1}H NMR spectrum of compound **9** in $CDCl_3$.

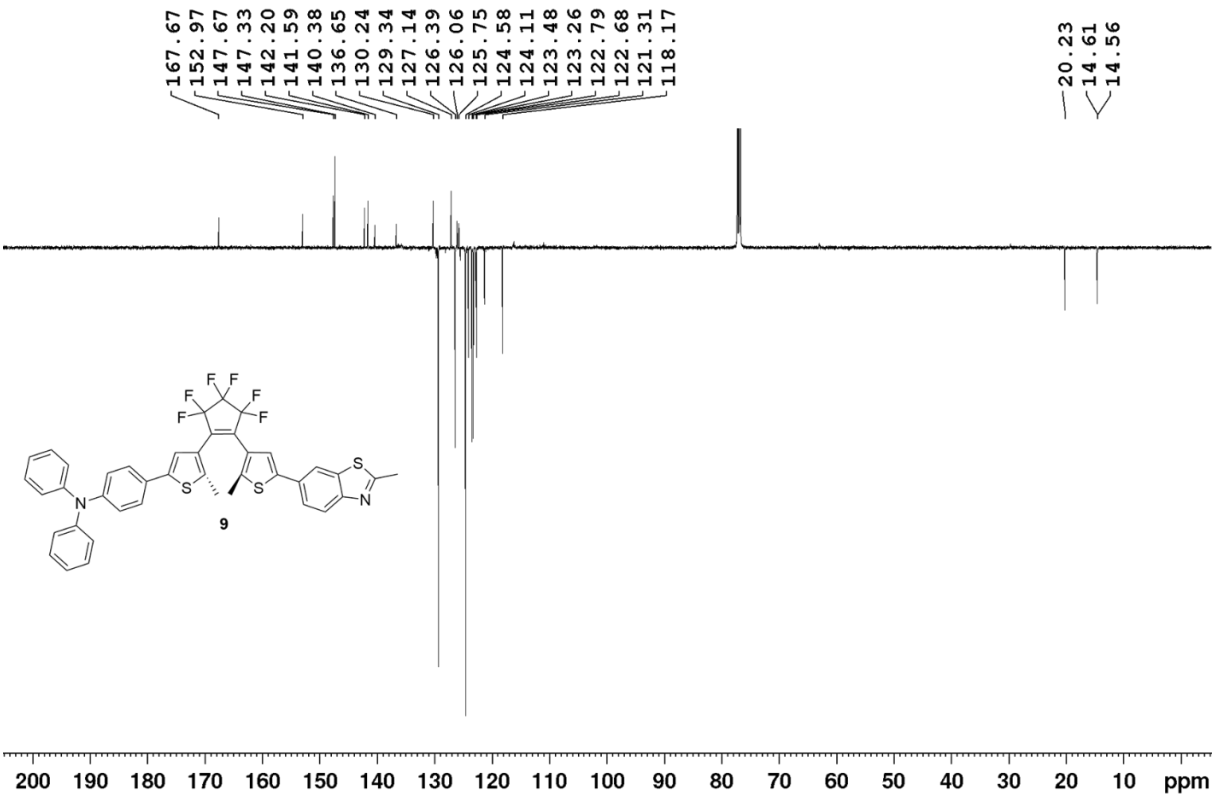

Figure S26. ^{13}C APT NMR spectrum of compound **9** in $CDCl_3$.

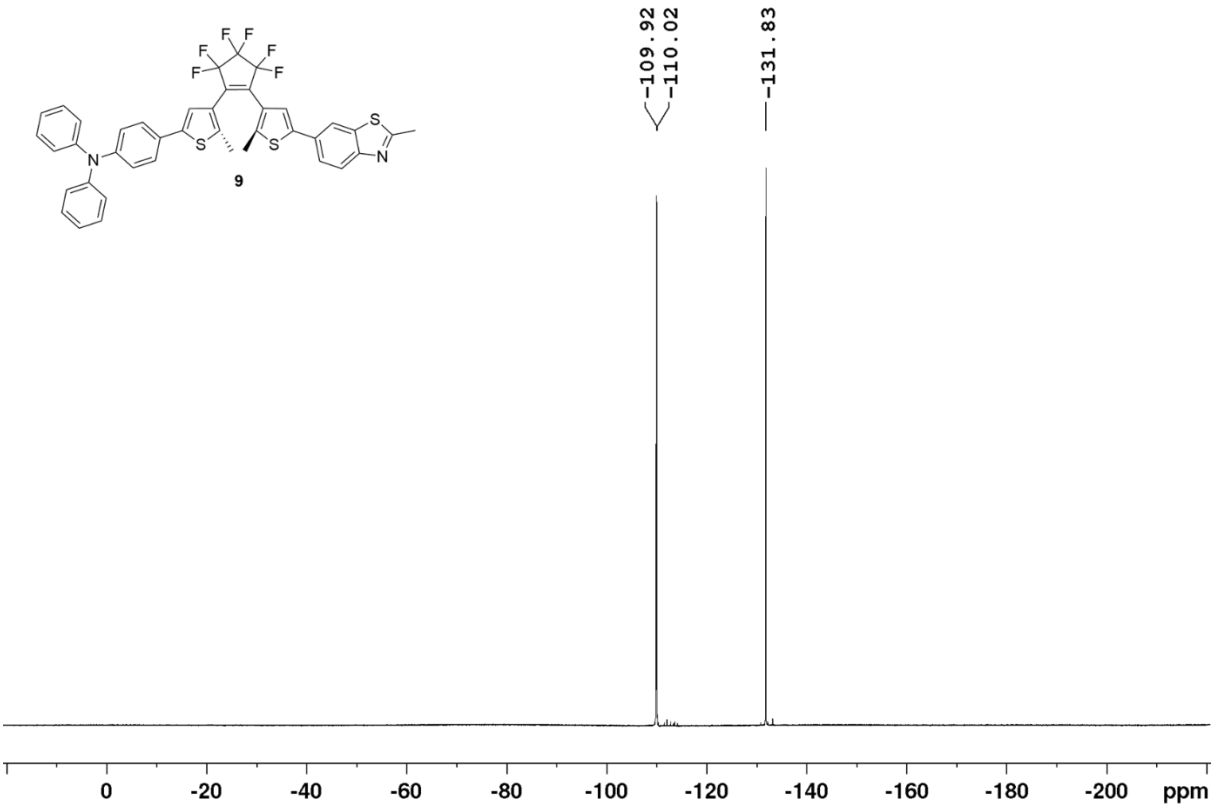

Figure S27. ^{19}F NMR spectrum of compound **9** in $CDCl_3$.

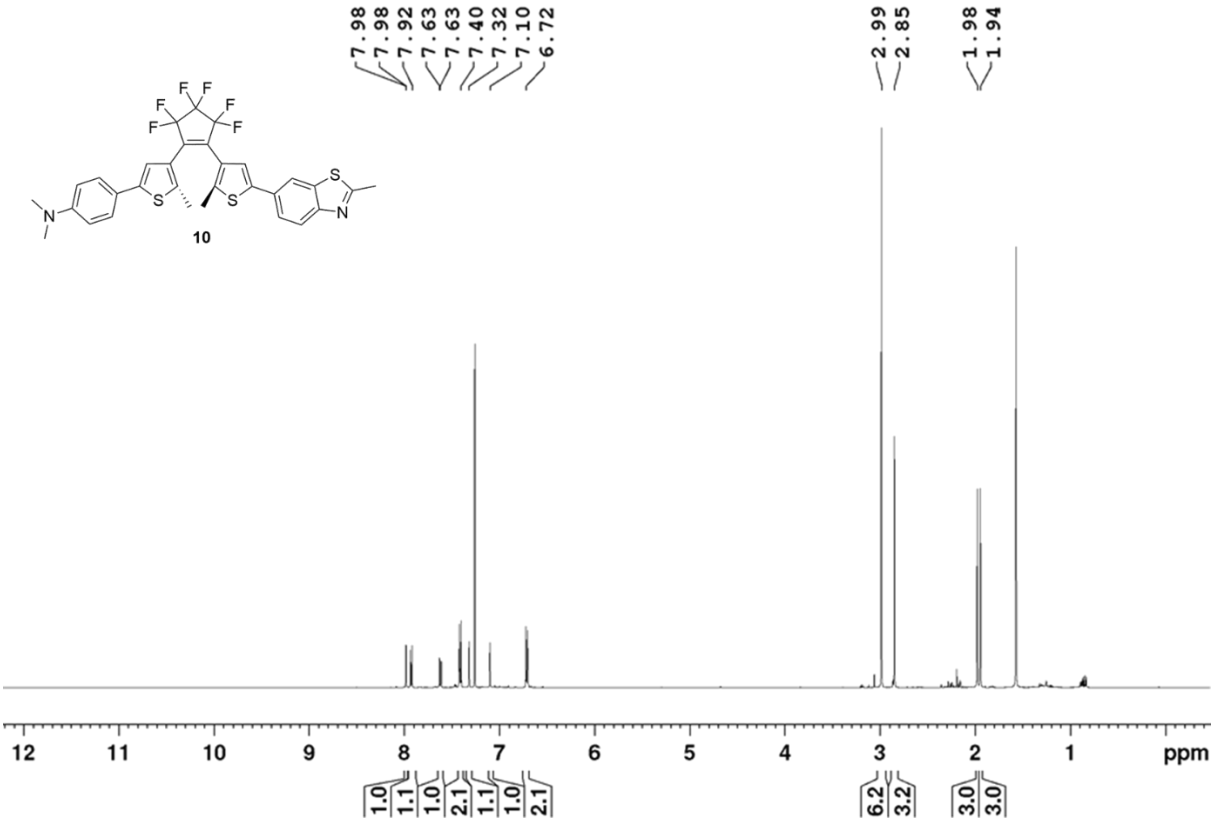

Figure S28. ^{1}H NMR spectrum of compound **10** in $CDCl_3$.

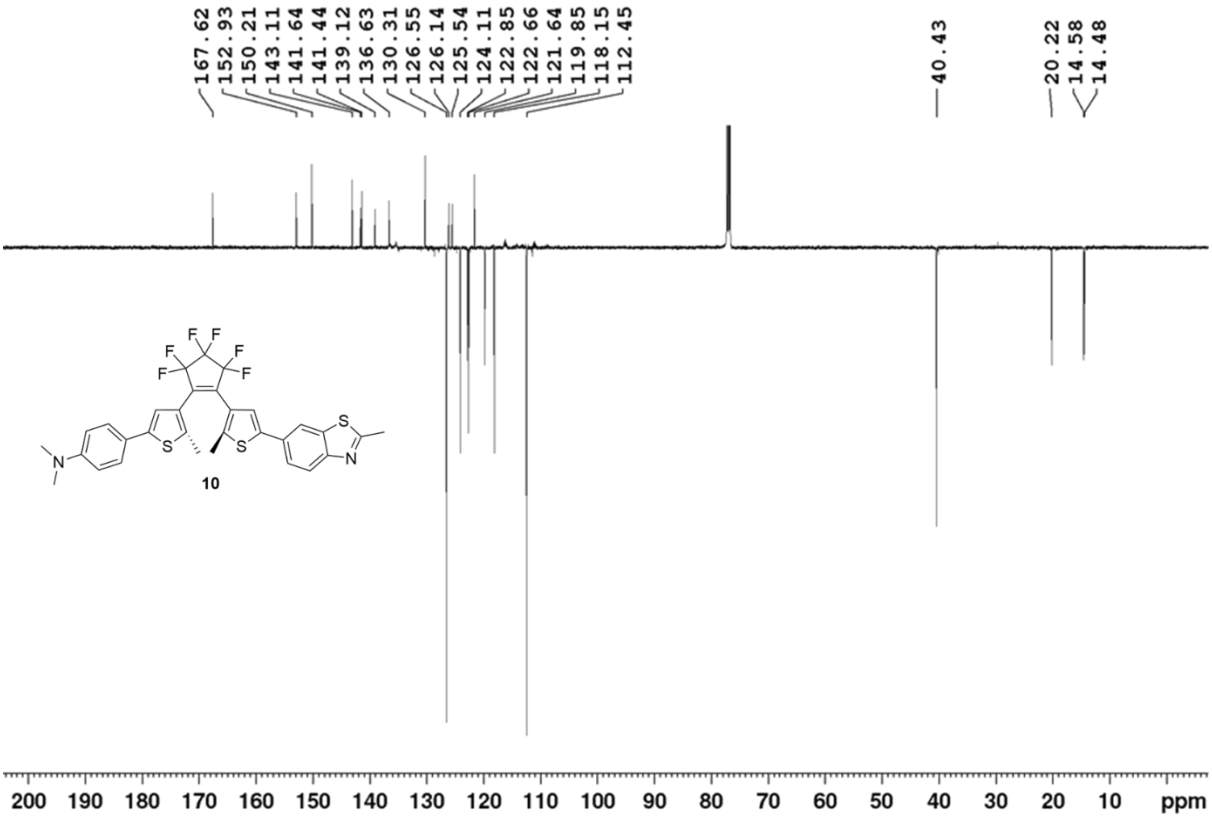

Figure S29. ^{13}C APT spectrum of compound **10** in $CDCl_3$.

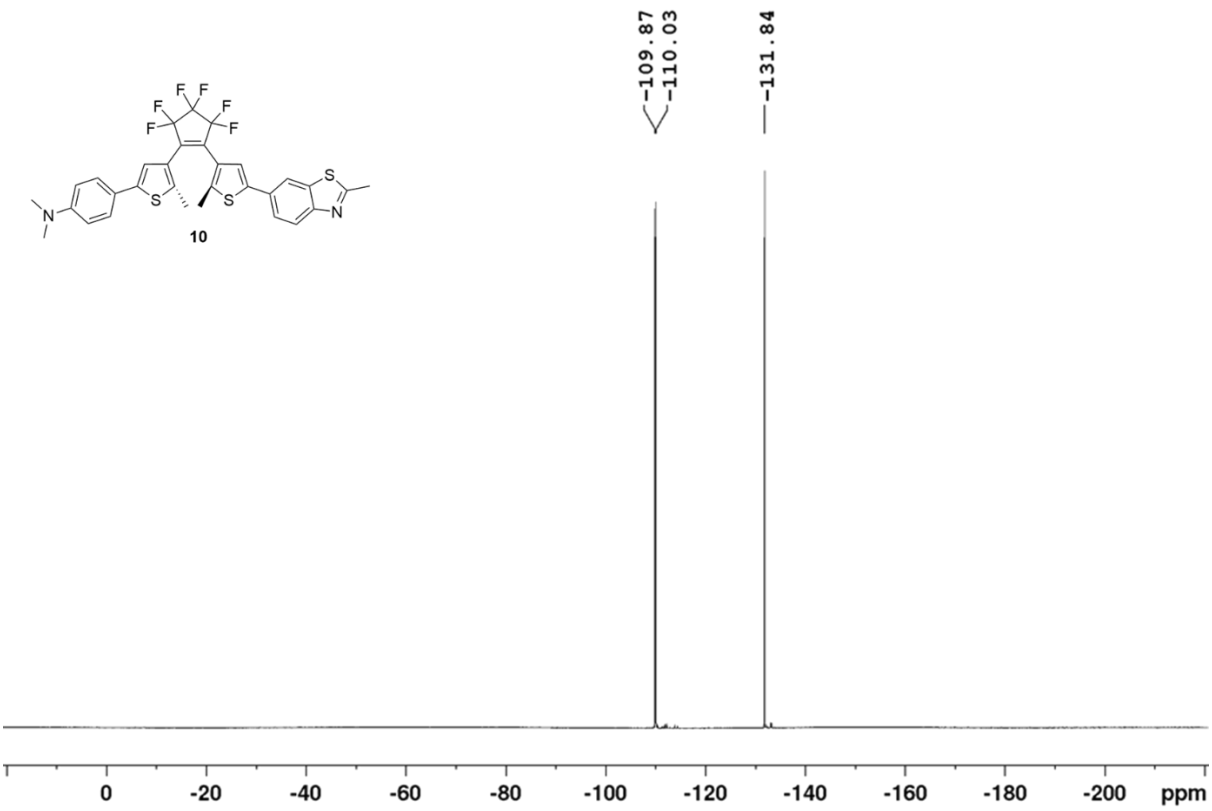

Figure S30. ^{19}F NMR spectrum of compound **10** in $CDCl_3$.

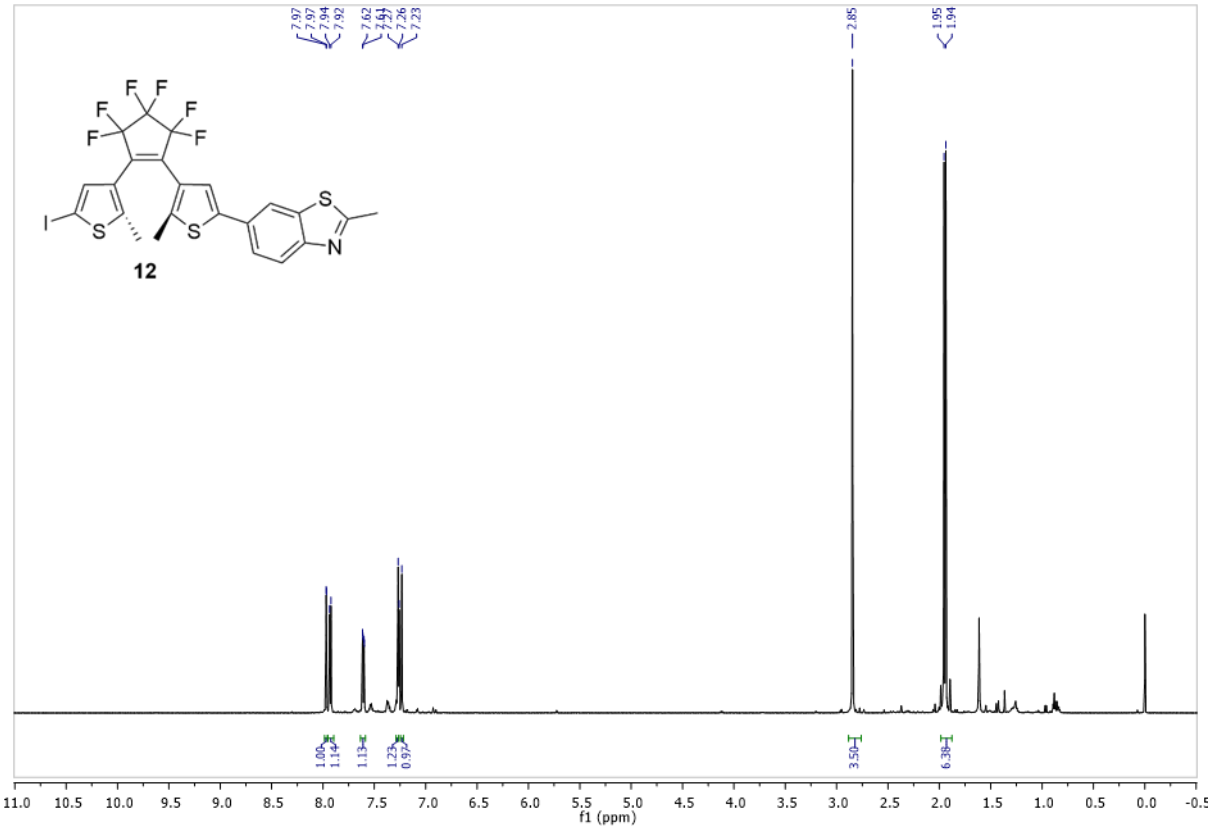

Figure S31. ^{1}H NMR spectrum of compound **12** in $CDCl_3$.

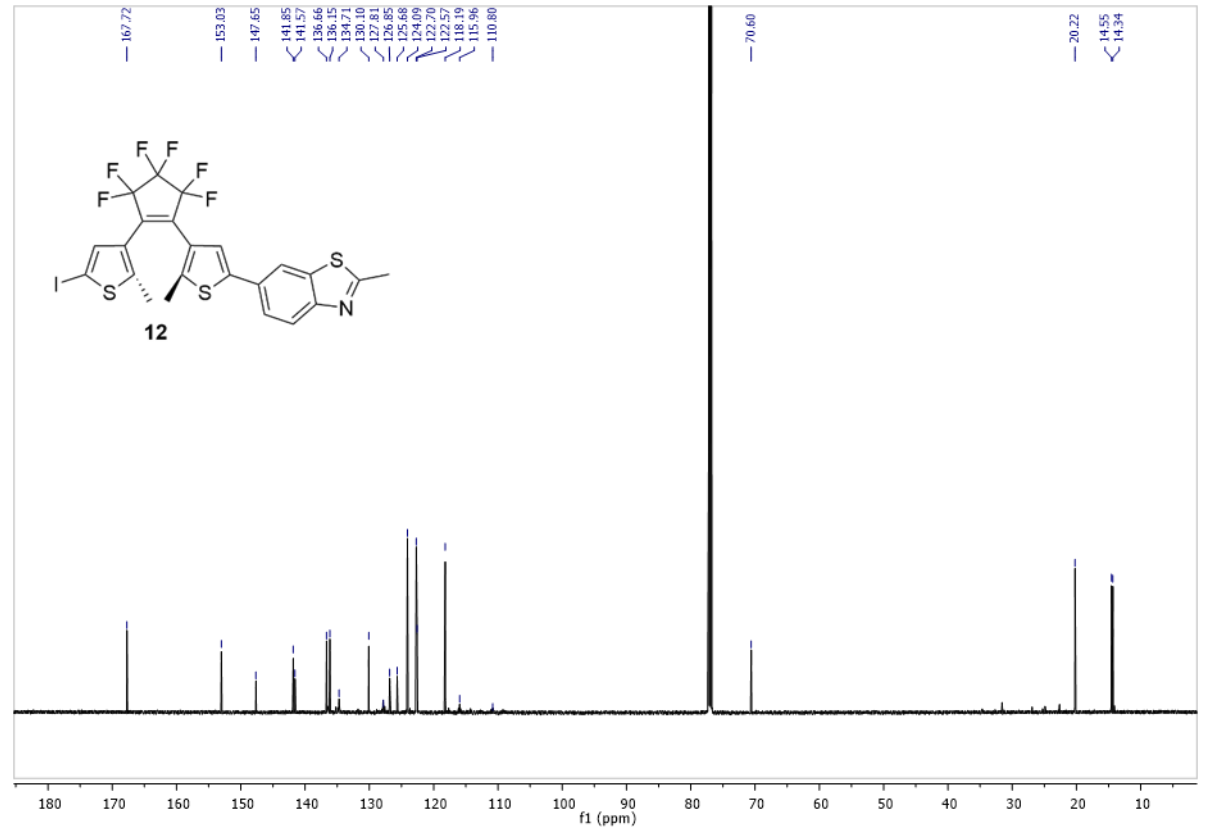

Figure S32. ^{13}C NMR spectrum of compound **12** in $CDCl_3$.

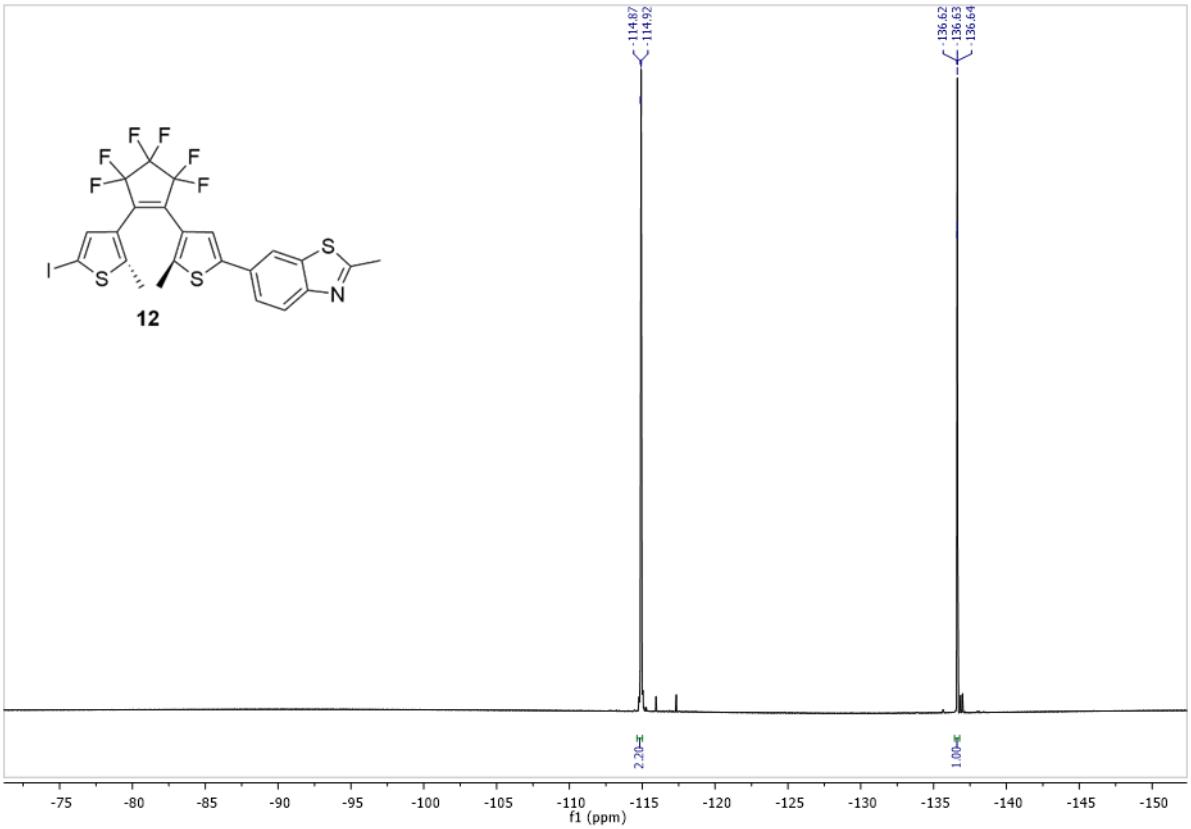

Figure S33. ^{19}F NMR spectrum of compound **12** in $CDCl_3$.

2. Molecular structure

2.1. Substituent parameters

Table S1. Substituent electronic parameters (Bond Length Alternation parameters BLA BT and BLA Full, Hammett σ_p constant and Benzene chemical shift increment I_p) used in this study.

Cpd	substituent	BLA BT	BLA Full	Hammett σ_p [4]	Hammett σ_p calc.*[,5]	Benzene chemical shift I_p [6]
1	***p*-NO$_2$**	0.075	0.063	0.78	0.372	0.39
2	***p*-CN**	0.076	0.063	0.66	0.187	0.28
3	**di-*m*-CF$_3$**	0.076	0.065	-	0.386	-0.14
4	***p*-CF$_3$**	0.077	0.065	0.54	0.205	0
5	**BTZ**	0.078	0.065	-	0.066	-
6	**H**	0.078	0.065	0	0.012	0
7	***p*-OH**	0.079	0.064	-0.37	-0.047	-0.44
8	***p*-OMe**	0.079	0.064	-0.27	-0.037	-0.44
9	***p*-N(Ph)$_2$**	0.079	0.063	-	-0.013	-0.34
10	***p*-NMe$_2$**	0.080	0.062	-0.83	-0.147	-0.66

* Calculated for the whole Ar arm (see Scheme 1 in the main text).

Asymmetrical substitution of DTE core leads to a shift of electron density toward one of the DTE arms. Such a shifts are visible on the shape of HOMO/LUMO orbitals. Shift in electron density relates to small change of bond lengths, as the contributing bonding orbitals lose small part of their electron density – one arm being slightly electron deficient. In the BLA-Full the changes compensate each other: double bond length on one arm of the molecule shortens (with respect to symmetrical molecule **5**), on the other arm the corresponding double bond becomes longer. This prevents correlation of observed/calculated values with BLA-Full parameter. Choosing only one arm of the molecule as a source of bond lengths, the BLA-BT parameter becomes free of compensations and thus could better describe substituent electronic effects.

[4] E. V. Anslyn, D. A. Dougherty, *Modern Physical Organic Chemistry*, University Science Books, Sausalito, CA, **2006**.
[5] P. Ertl, *ChemRxiv 2021*, DOI 10.26434/Chemrxiv.14215964.V1, 2021
[6] E. Pretsch, P. Bühlmann, C. Affolter, in *Struct. Determ. Org. Compd. Tables Spectr. Data* (Eds.: E. Pretsch, P. Bühlmann, C. Affolter), Springer Berlin Heidelberg, Berlin, Heidelberg, 2000, pp. 161–243.

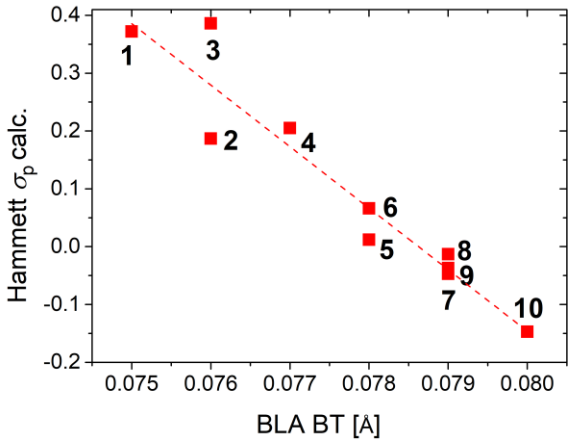

Figure S34. Correlation between BLA BT parameter and calculated Hammett σ_p constant.

2.2. Dipole moments

Table S2. Total dipole moments of the studied compounds and parent DTE molecule (Scheme S1) for comparison. All values are in Debye. Computational details are described in section 6.1 *Electric properties and photochemical study*.

Compound	Closed form C	Open form O	Ratio
DTE	4.08	4.41	0.9
1	7.63	6.78	1.1
2	7.32	6.54	1.1
3	6.02	5.05	1.2
4	5.57	4.68	1.2
5	5.92	4.39	1.3
6	4.53	3.70	1.2
7	6.21	4.67	1.3
8	6.51	3.74	1.7
9	5.76	3.93	1.5
10	7.98	5.85	1.4

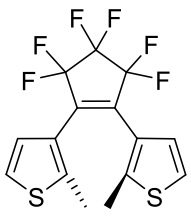

Scheme S1. Structure of parent DTE molecule.

2.3. Polarizability

Table S3. Isotropic polarizabilities of the studied compounds and parent DTE molecule (Scheme S1) for comparison. Computational details are described in section 6.1 *Electric properties and photochemical study*.

Isotropic polarizability [10^{-24} esu]	**Closed form C**	**Open form O**	**Ratio**
DTE	31.05	29.73	1.0
1	86.79	75.50	1.1
2	86.73	75.39	1.2
3	85.74	75.21	1.1
4	83.97	73.50	1.1
5	93.10	81.14	1.1
6	81.51	71.13	1.1
7	84.25	72.24	1.2
8	87.20	74.59	1.2
9	115.38	99.42	1.2
10	95.22	79.07	1.2

2.4. First hyperpolarizability

Table S4. Static first hyperpolarizability (β_{tot}) of the studied compounds and parent DTE molecule (Scheme S1) for comparison. Computational details are described in section 6.1 *Electric properties and photochemical study*.

β_{tot} [10^{-30} esu]	Closed form C	Open form O	Ratio
DTE	0.6	0.2	2.5
1	86.1	24.5	3.5
2	58.2	13.3	4.4
3	50.3	5.3	9.4
4	37.5	4.6	8.1
5	13.0	1.24	10.5
6	15.0	1.3	11.1
7	28.0	7.7	3.6
8	35.9	8.8	4.1
9	113.5	13.6	8.4
10	125.7	20.2	6.2

3. Photochemical Study

3.1. General Conditions

UV-Vis absorption spectra were measured on an Agilent 8453 diode array spectrophotometer (Hewlett Packard, USA) in toluene as a solvent (toluene, LiChrosolv®, Merck, Germany; DMSO, Acros Organics, UK; the solvent was used without further purification).

Photochemical measurements for determination of photoisomerization quantum yields (QYs) were performed at 25°C in the dark, with three 315 nm LED diodes (LED315W; Thorlabs) for determining photocyclization QY and four 520nm/624 nm LED diodes (LED520 OSG58A5111P; OptoSupply, or LED624 OS5RAA5111P; OptoSupply) for determining photocycloreversion QY.

Corresponding LED characteristics can be found at the following links:

1) https://www.thorlabs.com/thorproduct.cfm?partnumber=LED315W (accessed March 16, 2022)
2) https://www.gme.cz/data/attachments/dsh.518-089.1.pdf (accessed April 8, 2022)
3) https://www.gme.sk/data/attachments/dsh.518-090.1.pdf (accessed April 8, 2022)

The light sources were three 315 nm Thorlabs or four 520nm/624 nm LED diodes OptoSupply, with overall incident light intensity of I_0=1.69±0.10×10^{-6} mol s^{-1} dm^{-3}, I_0=2.00±0.20×10^{-5} mol s^{-1} dm^{-3} and I_0=2.15±0.14×10^{-5} mol s^{-1} dm^{-3}, respectively.

The incident light intensity I_0 at 315 nm ($I_{0\ 315}$) was determined by ferrioxalate (FE) actinometry as described in detail in our previous paper.[7] Contrary to irradiation with light of 315 nm wavelength, the incident light intensity I_0 at 520 nm ($I_{0\ 520}$) and 624 nm ($I_{0\ 624}$) was determined by sensitized singlet oxygen ($^1O_2$) mediated photooxidation of 1,3-diphenylisobenzofuran (DPIBF) as actinometer in methanol using Rose bengal (RB) or Methylene blue (MB) as a photosensitizer P, according to Eq. (S1) (no total absorption conditions):

$$I_{0\,\mathrm{X}} = \frac{I_{\mathrm{a,\,P\,X}}}{1-10^{-A_{\mathrm{P\,X}}}} \quad , \tag{S1}$$

where: $I_{\mathrm{a,P\,X}}$ is photosensitizer absorbed light intensity (in mol s^{-1} dm^{-3}) at the corresponding irradiation wavelength X and $A_{\mathrm{P\,X}}$ is photosensitizer absorbance of irradiation light beam (from LED sources) at corresponding irradiation wavelength X measured by the Thorlabs PM16-140 – USB Power Meter. The $I_{\mathrm{a,P\,X}}$ value was calculated from the slope of the following plot related to the DPIBF absorbance decrease in time at 410 nm due to its photooxygenation by photosensitizer generated $^1O_2$ (Fig. S35), according to Eq. (S2).[8]

$$A_{\mathrm{DPIBF}} + \varepsilon_{\mathrm{DPIBF}}\beta_{\mathrm{DPIBF}} \ln A_{\mathrm{DPIBF}} = A_{0\ \mathrm{DPIBF}} + \varepsilon_{\mathrm{DPIBF}}\beta_{\mathrm{DPIBF}} \ln A_{0\ \mathrm{DPIBF}} - \varepsilon_{\mathrm{DPIBF}} I_{\mathrm{a,\,P\,X}} \Phi_{^1O_2} t \quad , \tag{S2}$$

where: A_{DPIBF} is absorbance of DPIBF at 410 nm (measured perpendicular to $A_{\mathrm{P\ X}}$ by spectrophotometer Agilent 8453), $A_{0\ \mathrm{DPIBF}}$ is initial absorbance of DPIBF at 410 nm, $\varepsilon_{\mathrm{DPIBF}}$ is the corresponding molar absorption (extinction) coefficient of DPIBF at this wavelength ($\varepsilon_{\mathrm{DPIBF}}$ =

[7] B. Mravec, Š. Budzák, M. Medved', L. F. Pašteka, C. Slavov, T. Saßmannshausen, J. Wachtveitl, J. Kožíšek, L. Hegedüsová, J. Filo, M. Cigáň, *J. Org. Chem.* **2021**, *86*, 11633–11646.
[8] F. Amat-Guerri, M. M. C. López-González, R. Martínez-Utrilla, R. Sastre, *J. Photochem. Photobiol. A: Chem.* **1990**, *53*, 199–210.

23,000 M^{-1} cm^{-1} in MeOH), β_{DPIBF} is the reactivity index of DPIBF (the ratio between the rate constants of non-radiative unimolecular decay of DPIBF and oxidation of DPIBF by $^1O_2$; β_{DPIBF} = 1.1×10^{-4} mol dm^{-3} in MeOH[8]), Φ_{1O2} is the quantum yield of singlet oxygen production by the photosensitizer P ($\Phi_{1O2\ RB\ in\ MeOH}$ = 0.79; $\Phi_{1O2\ MB\ in\ MeOH}$ = 0.50)[9] and *t* is the irradiation time.

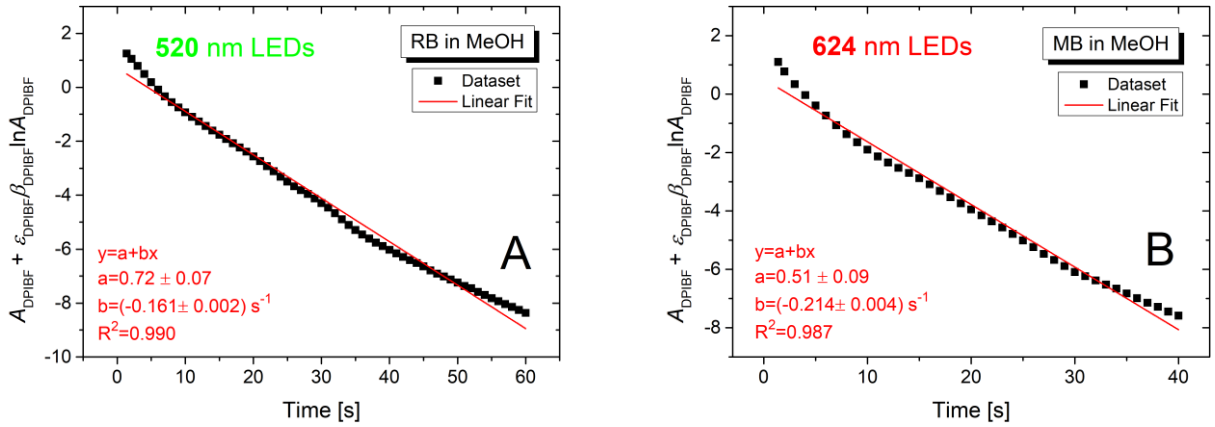

Figure S35. Decrease in absorbance of 1,3-diphenylisobenzofuran (DPIBF) as singlet oxygen actinometer at 410 nm in methanol during solution irradiation with light of 520 (A) and 624 (B) nm wavelength, respectively, using Rose Bengal (RB) and Methylene Blue (MB) as photosensitizer (four LED520 OSG58A5111P diodes; OptoSupply, or four LED624 OS5RAA5111P diodes; OptoSupply).

The photochemical measurements related to photocyclization/photocycloreversion quantum yield were performed in the dark using the modified apparatus described in Fig. 7 of reference[10]: without ultrasonic horn H and lens L1, and using a Thorlabs PM16-140 – USB Power Meter (Integrating Sphere Sensor, 350 – 1100 nm, 500 mW Max) or an Ocean Optics HR4000CG-UV-NIR spectrophotometer (for 315 nm LED source) for determination of initial and transmitted light intensity from LED light sources. The concentration change of the corresponding open or cyclic form in freshly prepared air-saturated solutions during irradiation in a 1 cm quartz fluorescence cuvette were measured spectrophotometrically (based on previously determined extinction coefficients of pure C forms) in right-angle arrangement (spectrophotometer Agilent 8453); no interference with the irradiation light beam from LED source was observed.

[9] R. W. Redmond, J. N. Gamlin, *Photochem. Photobiol.* **1999**, *70*, 391–475.
[10] A. Gáplovský, Š. Toma, J. Donovalová, *J. Photochem. Photobiol. A: Chem.* **2007**, *191*, 162–166.

3.2. Phocyclization/Photocycloreversion Quantum Yields

The photocycloreversion quantum yield (Φ_{CO}) of the studied DTEs **1**–**10** was determined by equation (S3) at photoconversion below 20%:[11]

$$\Phi_{CO} = \frac{\int_{c_0}^{c_t} dc_C}{\int_0^t I_a dt} = \frac{\Delta c_C}{\int_0^t I_a dt} = \frac{\frac{\Delta A_C}{\varepsilon_C}}{\int_0^t I_a dt} \quad \text{(S3)}$$

where: Δc_C is the concentration change of the initial closed form C, ΔA_C is the absorbance change of the initial closed form C in its absorption maximum, ε_C is the corresponding molar absorption (extinction) coefficient of the closed form C at its absorption maximum, I_a is light intensity absorbed by the closed isomer C at the irradiation wavelength λ_{irr} using a monochromatic light source, and t is the irradiation time. Because extinction coefficients of both forms were known and absorption maxima of both forms were sufficiently separated, the concentration change Δc_C of the form C can be easily determined spectrophotometrically as $\Delta A_C/\varepsilon_C$. Firstly, the synthesized (thermodynamically more stable) open O form were photochemically converted to the corresponding C form by irradiation at 315 nm. The extinction coefficients of C form were then calculated as $\varepsilon_C = A_C/(c_{iO} \times R)$, where c_{iO} is the initial concentration of the O form (the known value) and R is the O-to-C photoconversion factor in toluene (determined from ^{1}H NMR spectroscopy – see Figs. S40, S41 and S43; for all studied DTEs: $R \geq 0.95$).

The absorbed light intensity I_a during the mutual O and C form photoconversion at the corresponding irradiation wavelengths λ_{irr} was determined using a Thorlabs PM16-140 – USB Power Meter (Integrating Sphere Sensor, FC Fiber Adapter, Si, 350 – 1100 nm, 500 mW Max) or an Ocean Optics HR4000CG-UV-NIR spectrophotometer (for the wavelength of 315 nm) by Eq. (S4):

$$I_{a\lambda} = I_{0\lambda} - I_{T\lambda} \quad \text{(S4)}$$

Because the C form has significant absorption at the irradiation wavelength of 315 nm used for photocyclization of the O form (and the C form cannot be obtained directly from the synthesis), the corresponding photocyclization quantum yield (Φ_{CO}) was calculated at very low initial O-to-C photocyclization (below 10%) by Eq. (S5) analogous to Eq. (S3) at different irradiation wavelength:

$$\Phi_{OC} = \frac{\int_{c_0}^{c_t} dc_C}{\int_0^t I_a dt} = \frac{\Delta c_C}{\int_0^t I_a dt} = \frac{\frac{\Delta A_C}{\varepsilon_C}}{\int_0^t I_a dt} \quad \text{(S5)}$$

Due to the same shape of absorption spectra of both forms and reaction progress in both polar and nonpolar solvents, the extinction coefficient of the C form ε_{irrC} for molecules **9** and **10** with significantly reduced photocyclization efficiency in polar DMSO or MeCN was taken from photochemical experiments in toluene.

[11] Klán, P.; Wirz, J. *Photochemistry of Organic Compounds : From Concepts to Practice*; Wiley, 2009.

3.3. Photochromic Behavior

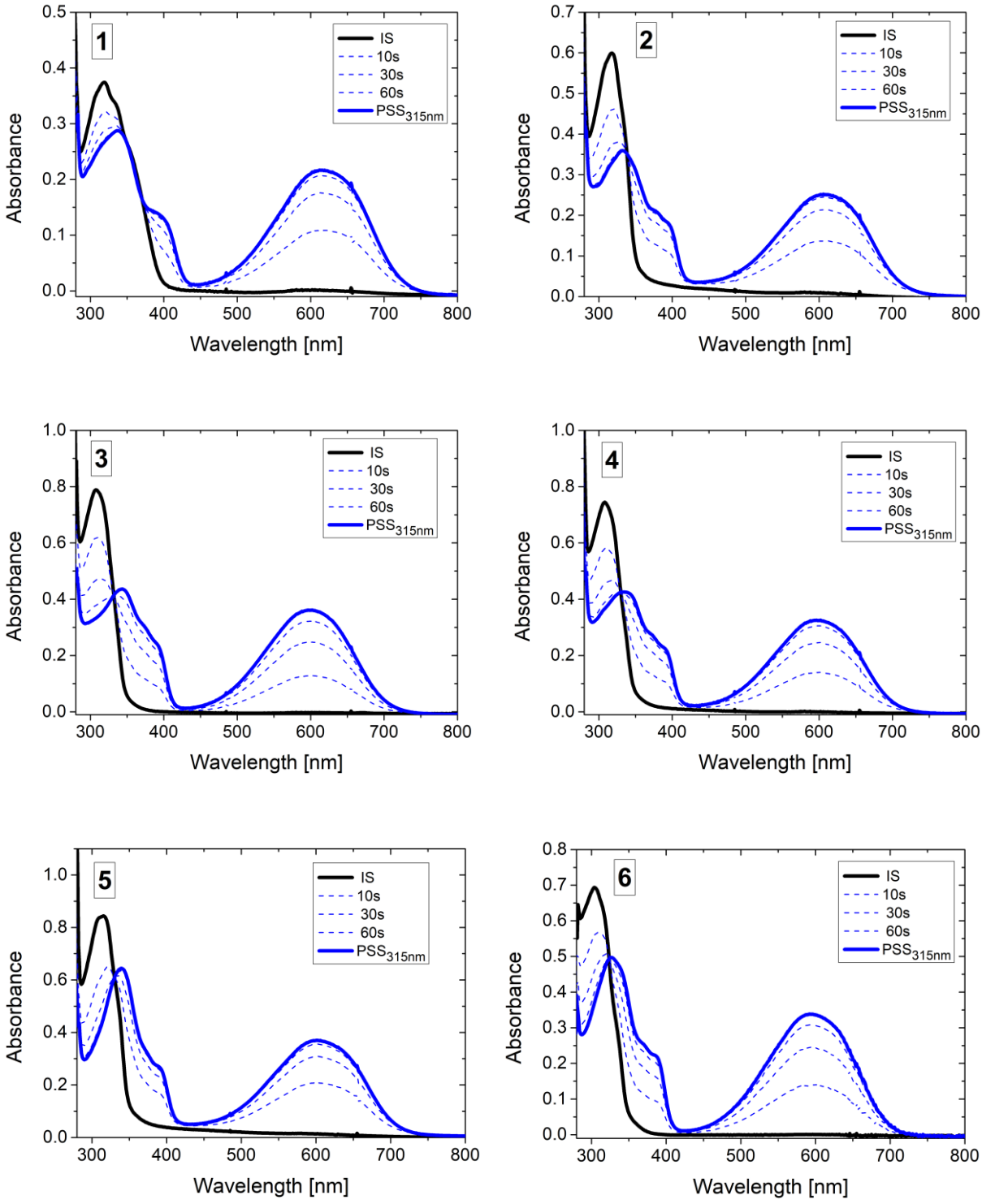

Figure S36. Evolution of UV-Vis spectra of studied DTEs **1**-**6** in toluene during irradiation of the open form O (λ_{irr} = 315 nm).

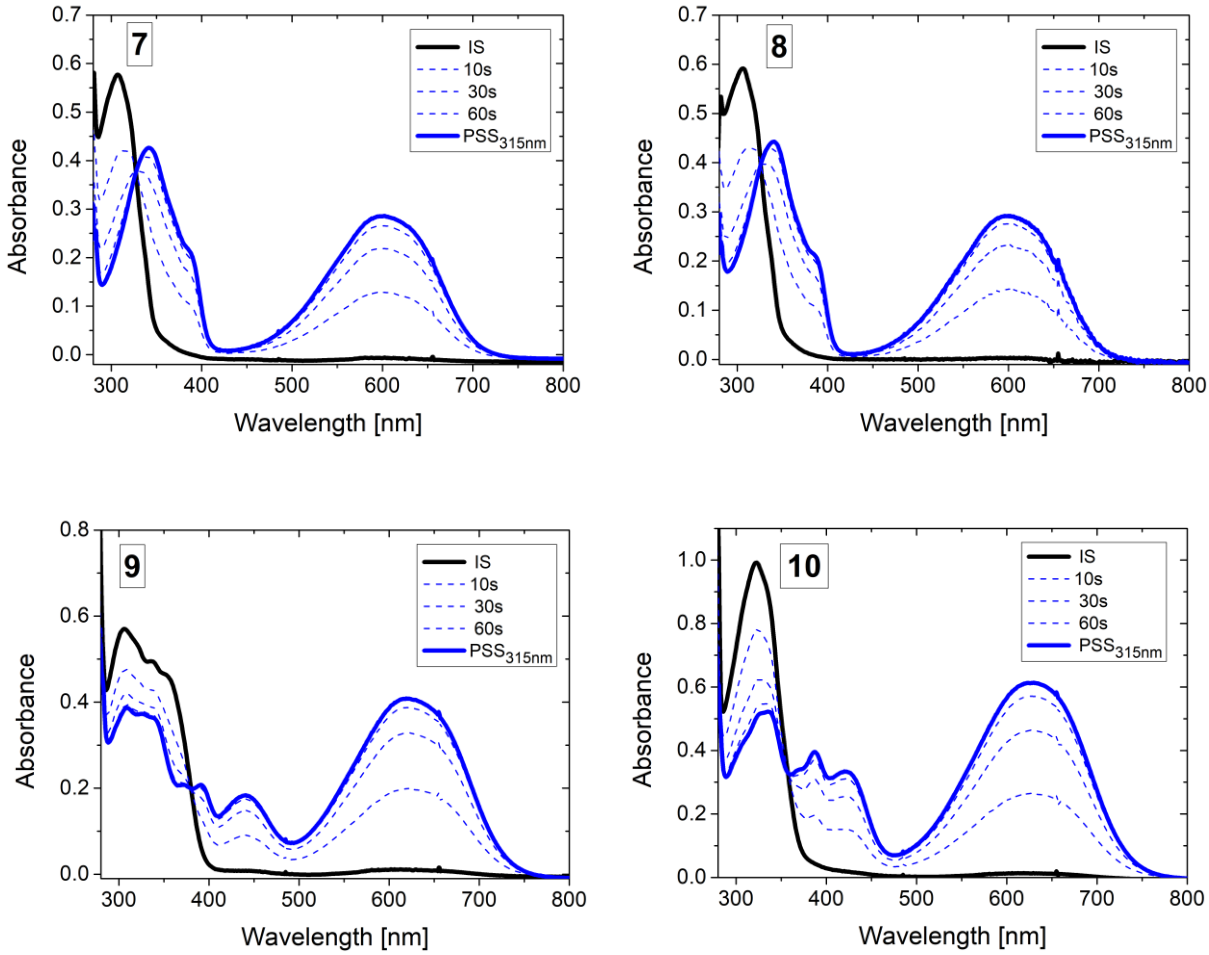

Figure S37. Evolution of UV-Vis spectra of studied DTEs **7**-**10** in toluene during irradiation of the open form O (λ_{irr} = 315nm).

As already demonstrated in previous papers[12,13], the change in π-conjugation of the C form due to the substituent effect reflects also in corresponding change of its absorption maximum position ($\lambda_{max\,C}$), as shown in the $\lambda_{max\,C}$ vs. BLA Full graph (Fig. S38). However, the meaningful correlation between the $\lambda_{max\,C}$ and the BLA BT parameter is not observed, because the BLA BT describes π-conjugation change only in a limited part of the overall π-conjugated chain.

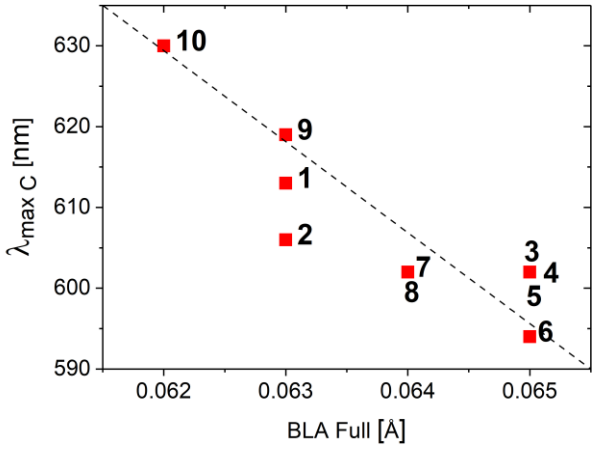

Figure S38. Correlation between BLA Full and λ_{max} of the form C.

[12] A. Perrier, F. Maurel, J. Aubard, *J. Photochem. Photobiol. Chem.* **2007**, *189*, 167–176.
[13] A. D. Laurent, J.-M. André, E. A. Perpète, D. Jacquemin, *J. Photochem. Photobiol. Chem.* **2007**, *192*, 211–219.

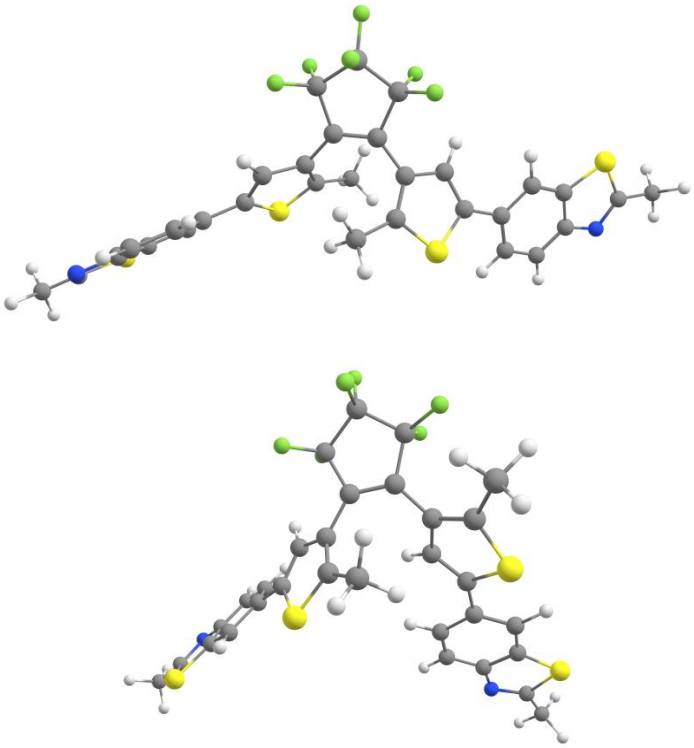

Figure S39. Optimized structures of antiparallel (top) and parallel (bottom) conformers of the molecule **5**. Computational details are described in section 6.1 *Electric properties and photochemical study*.

Table S5. Gibbs free energy difference ΔG between parallel and antiparallel conformers of the open form O calculated at the PBE0/6-311G(d,p) level of theory. Computational details are described in section 6.1 *Electric properties and photochemical study*.

Compound	**ΔG [kJ/mol]**
1	-5.9
2	-6.1
3	-5.7
4	-4.0
5	-5.2
6	-5.8
7	-6.0
8	-5.1
9	-6.4
10	-5.5 (-5.2 in DMSO)

Table S6. Excitation energies (ωB97XD/6-311++G(d,p), in eV) for S_1 and S_2 states of the open form O and S_1 of the closed form C. Oscillator strengths are given in parentheses. Computational details are described in section 6.1 *Electric properties and photochemical study*.

	Open form O		**Closed form C**
Compound/State	**S_1**	**S_2**	**S_1**
1	318.85 (1.1005)	308.04 (0.0155)	592.76 (0.6412)
2	300.99 (0.1754)	298.75 (1.4460)	585.42 (0.6362)
3	299.85 (0.1254)	288.11 (1.6068)	576.31 (0.5800)
4	300.67 (0.1227)	288.77 (1.7104)	574.89 (0.5847)
5	303.42 (0.0733)	291.76 (1.9500)	576.87 (0.6588)
6	302.77 (0.1279)	288.66 (1.2948)	569.45 (0.5783)
7	306.53 (0.0965)	289.25 (1.4110)	575.29 (0.6410)
7 (DMSO)	307.48 (0.1105)	289.84 (1.4072)	
8	306.96 (0.0970)	289.19 (1.4968)	576.73 (0.6567)
8 (DMSO)	307.63 (0.1130)	290.05 (1.4812)	
9	323.74 (1.2570)	308.97 (0.1393)	591.35 (0.8417)
9 (DMSO)	324.41 (1.2897)	310.08 (0.1309)	
10	318.10 (0.0512)	301.05 (1.5607)	591.30 (0.8030)
10 (DMSO)	320.04 (0.0469)	303.96 (1.5368)	

Table S7. Excitation energies (CAM-B3LYP/6-311++G(d,p), in eV) for S_1 and S_2 states of the open form O and S_1 of the closed form C. Oscillator strengths are given in parentheses. Computational details are described in section 6.1 *Electric properties and photochemical study*.

	Open form O		**Closed form C**
Compound/State	**S_1**	**S_2**	**S_1**
1	327.52 (1.0380)	307.97 (0.0056)	600.35 (0.6662)
2	306.14 (0.1294)	302.74 (1.4113)	590.30 (0.6562)
3	304.98 (0.0987)	291.66 (1.5818)	581.52 (0.6016)
4	305.63 (0.0989)	292.32 (1.6635)	580.03 (0.6061)
5	308.76 (0.0619)	295.39 (1.8484)	581.09 (0.6801)
6	307.70 (0.1055)	292.34 (1.2441)	574.08 (0.5989)
7	312.16 (0.0765)	292.66 (1.3002)	581.85 (0.6825)
8	312.97 (0.0769)	292.91 (1.3868)	597.81 (0.8878)
9	330.69 (1.1592)	317.80 (0.1519)	600.35 (0.6662)
10	328.88 (0.0413)	305.67 (1.4594)	597.94 (0.8415)

3.4. PSS composition (*Ex Situ* Irradiation NMR spectroscopy)

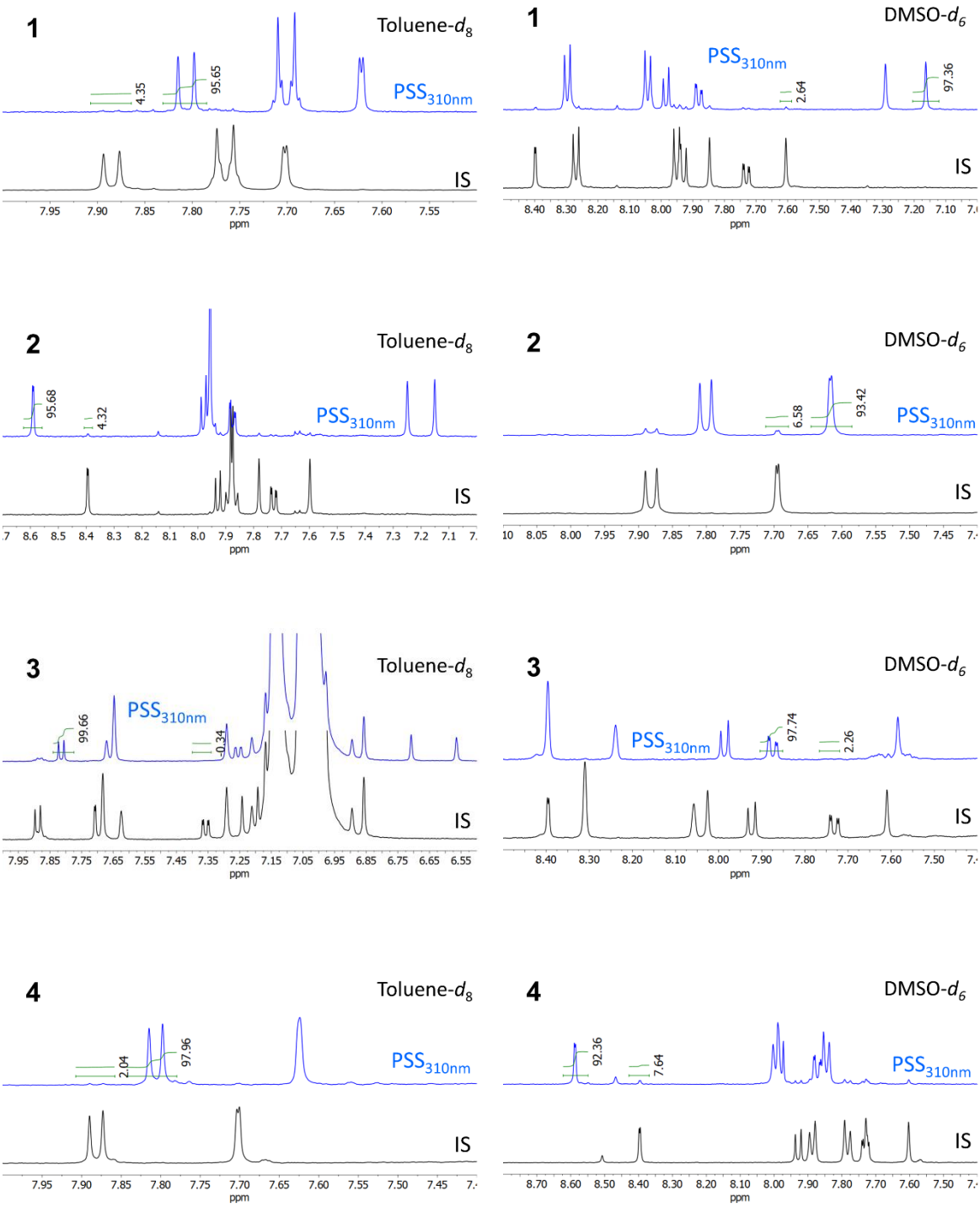

Figure S40. ^{1}H NMR spectra of **1**–**4** measured in toluene-d_8 (left column) and in DMSO-d_6 (right column) prior to (black) and after irradiation by UV light (310 nm, blue) into photostationary state (PSS; cyclic form C/open form O ratio; IS - Initial State, e.g. pure open form O).

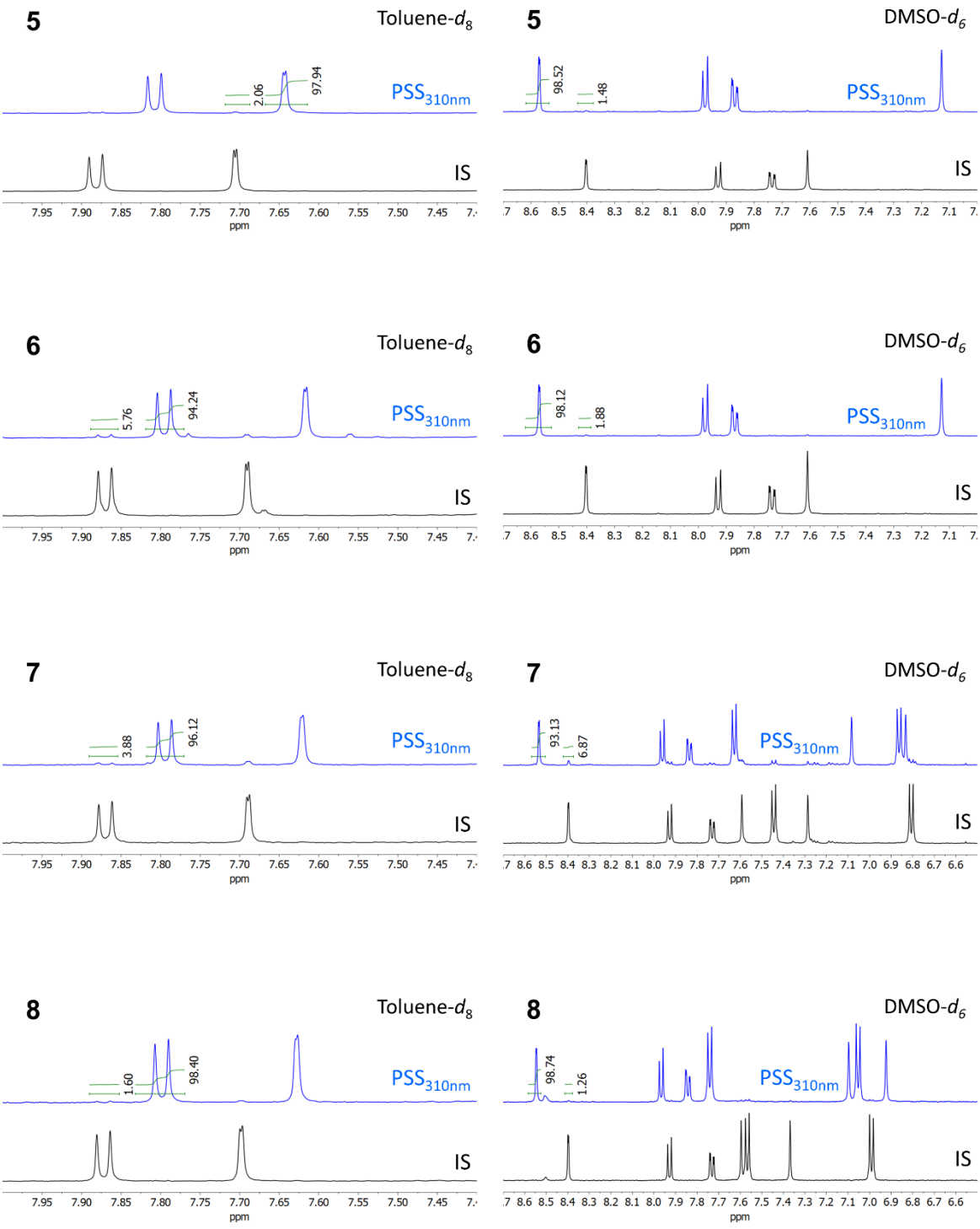

Figure S41. ^{1}H NMR spectra of **5**–**8** measured in toluene-d_8 (left column) and in DMSO-d_6 (right column) prior to (black) and after irradiation by UV light (310 nm, blue) into photostationary state (PSS; cyclic form C/open form O ratio; IS - Initial State, e.g. pure open form O).

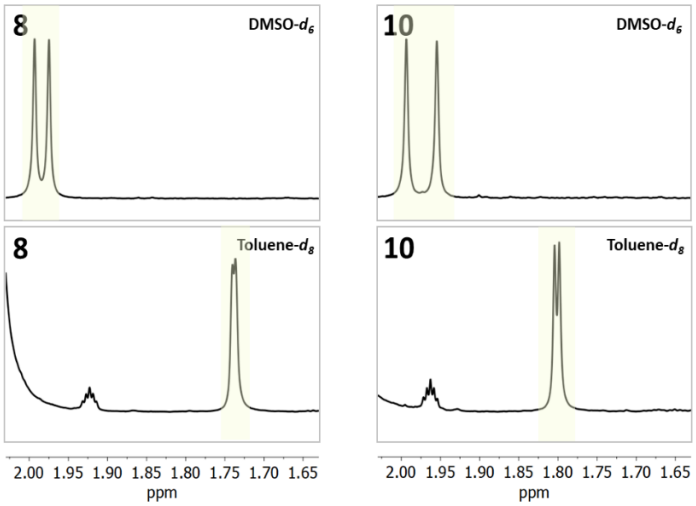

Figure S42. ^{1}H NMR spectra of pure open form O of studied DTEs **8** and **10** measured in toluene-d_8 and in DMSO-d_6 prior to irradiation.

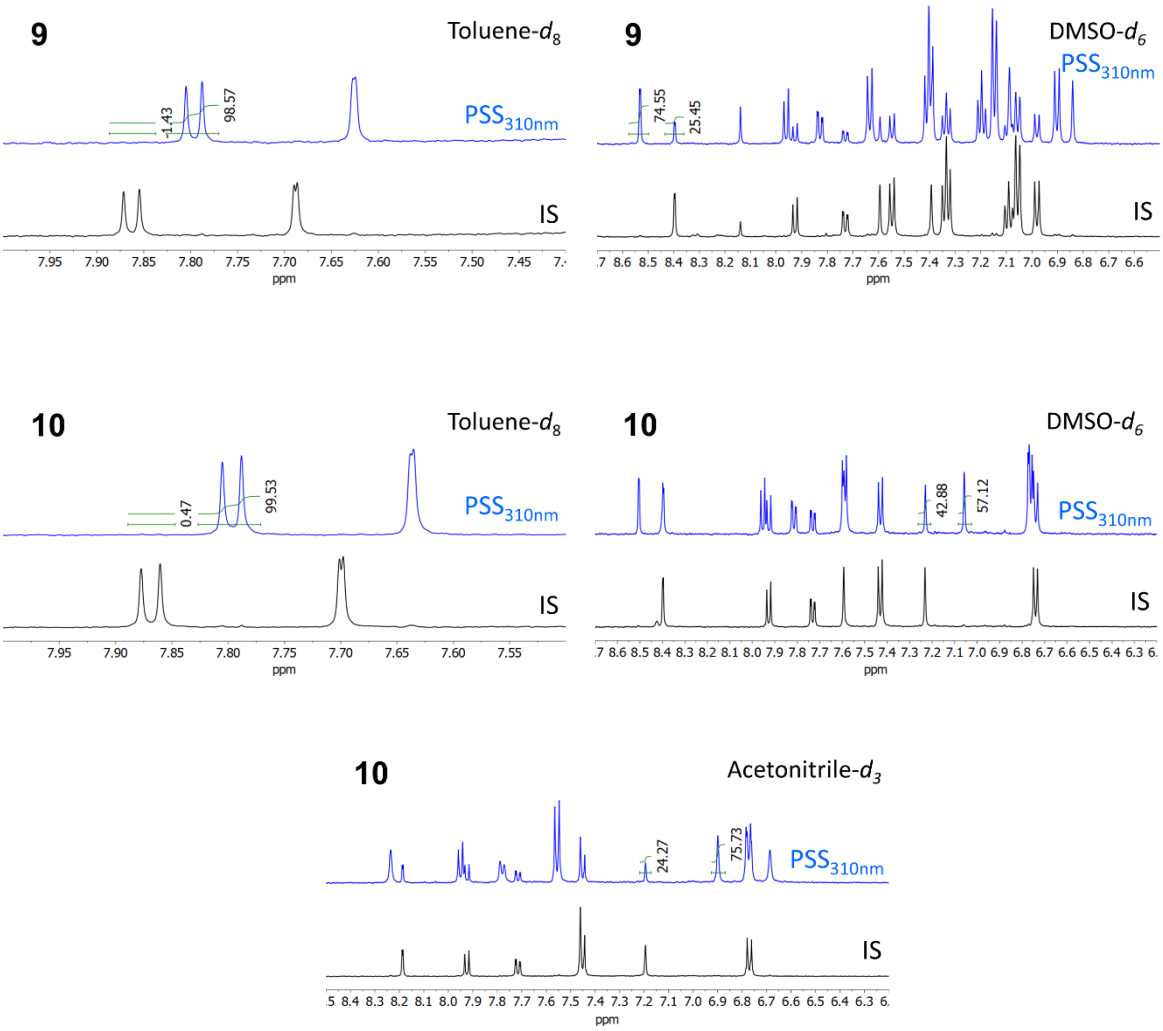

Figure S43. ^{1}H NMR spectra of **9**–**10** measured in toluene-d_8 (left column) and in DMSO-d_6 (right column) prior to (black) and after irradiation by UV light (310 nm, blue) into photostationary state (PSS; cyclic form C/open form O ratio; IS - Initial State, e.g. pure open form O).

3.5. Emission Spectroscopy and Nanosecond Flash Photolysis

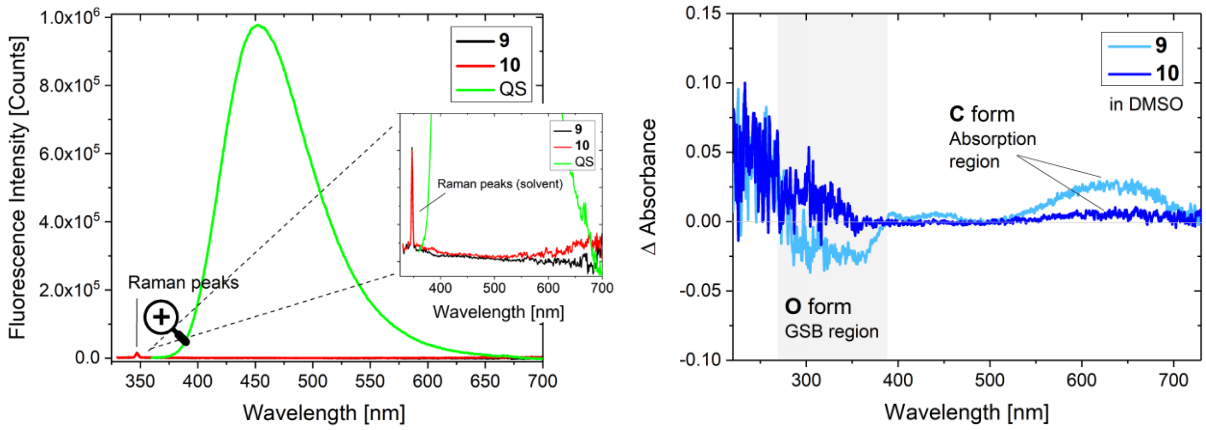

Figure S44. (A) Fluorescence of open form O of studied DTEs **9** and **10** in DMSO (measured on FLS1000 Photoluminescence Spectrometer, Edinburgh Instruments; λ_{EX} = 315 nm, ExBW = 1 nm, EmBW = 1 nm; QS – Quinine Sulphate in 0.5M H_2SO_4, fluorescent QY = 0.55)[14] and (B) Transient absorption spectra of open form O of studied DTEs **9** and **10** in DMSO at 355 nm excitation, measured by ns flash photolysis (measured on LP980 Transient Absorption Spectrometer, Edinburgh Instruments).

As shown in Figs. S44A and S45, studied DTE derivatives exhibit only poor fluorescence (in both open O and closed C forms) with fluorescent quantum yields below 1% in both polar and nonpolar solvents (fluorescence was slightly enhanced in polar solvents, but still below 1% as shown in Fig. S44A). Transient absorption spectra of studied open forms DTE derivatives **9** and **10** in DMSO indicate only photocyclization process with no sign of triplet-triplet absorption due to intersystem crossing (Fig. S44B).

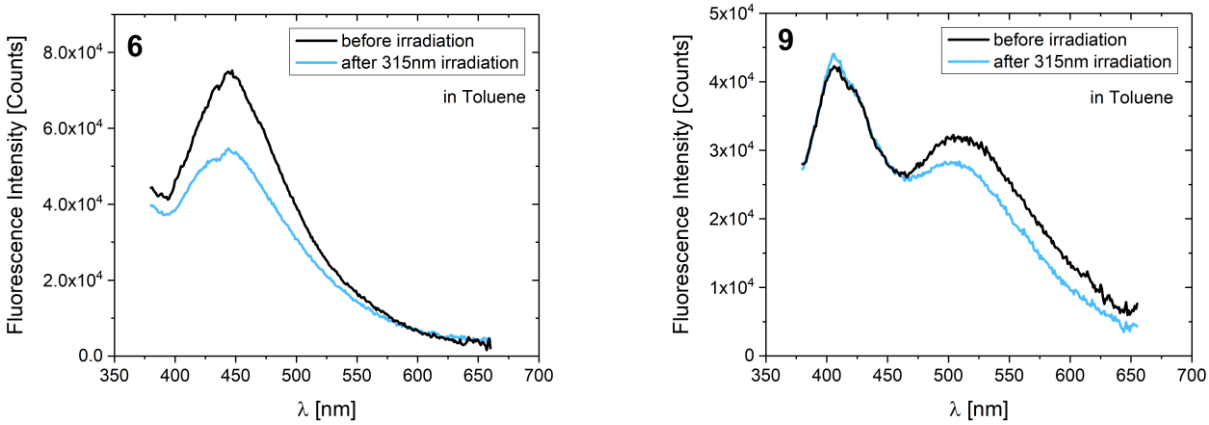

Figure S45. Fluorescence of studied DTEs **6** (left) and **10** (right) in toluene prior to (black) and after irradiation by UV light (315 nm, blue) into photostationary state (measured on FLS1000 Photoluminescence Spectrometer, Edinburgh Instruments; λ_{EX} = 315 nm, ExBW = 9 nm, EmBW = 1 nm).

[14] D.F Eaton, *Pure Appl. Chem.* **1988**, *60*, 1107-1114.

3.6. Photoswitching Cycles

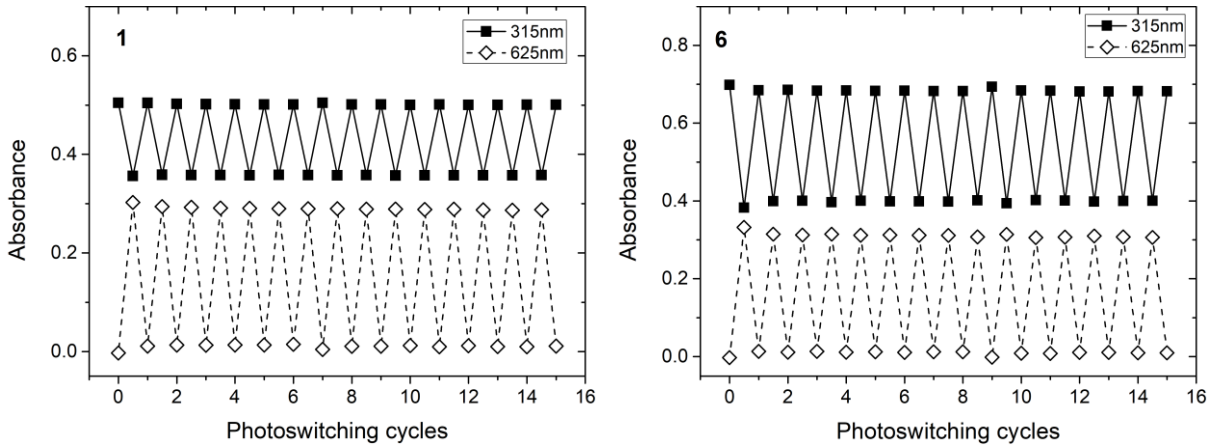

Figure S46. Photoswitching cycles of studied DTEs **1** and **6** in toluene.

3.7. Electron density differences (EDD) for the S_1 state

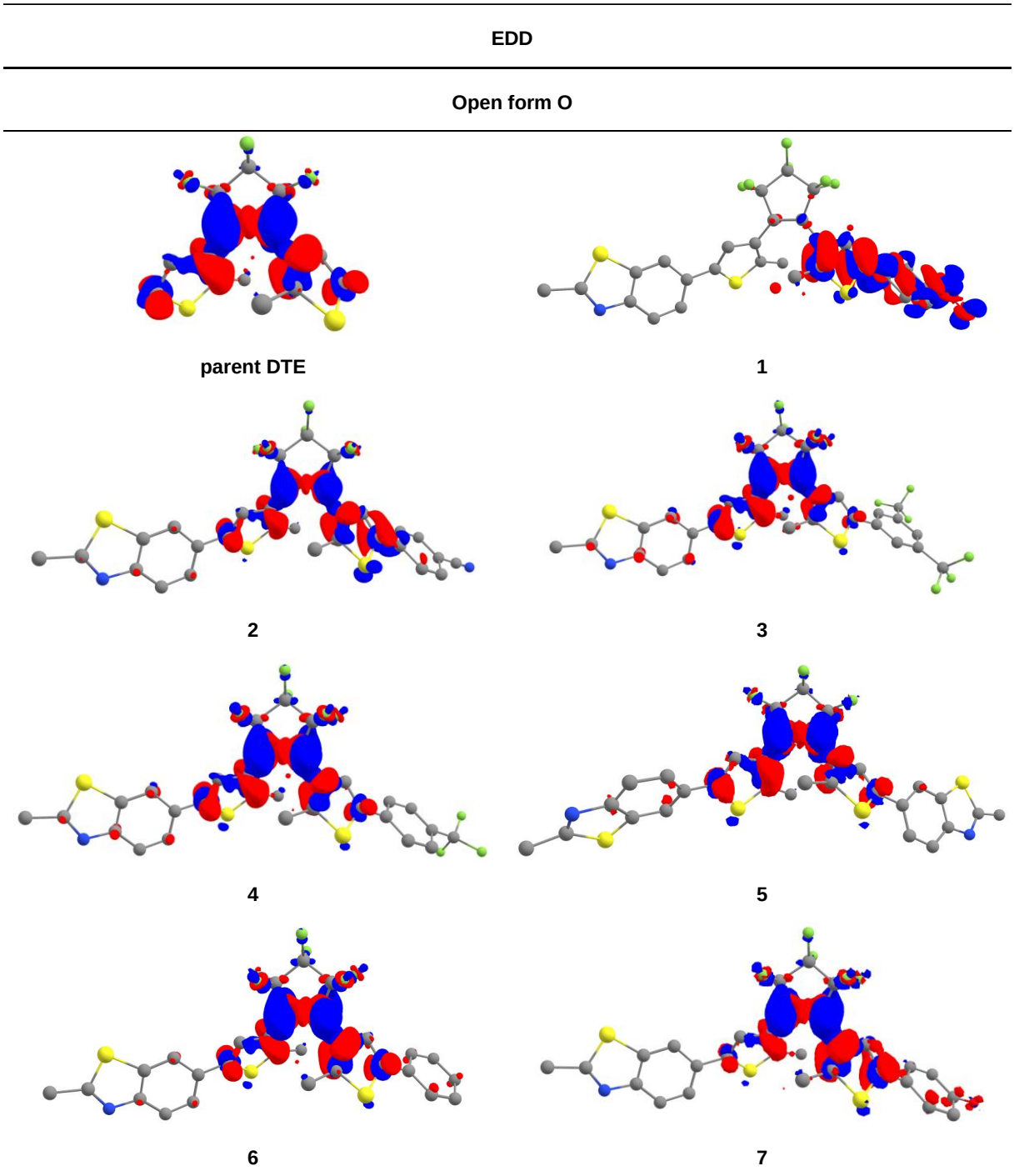

Figure S47. Electron density differences (EDD) for the S_1 state of studied compounds. Red/blue lobes show increase/decrease of the electron density upon the excitation, isovalue of 0.002 was used. Hydrogen atoms are omitted in the graphic for clarity.

EDD
Open form O
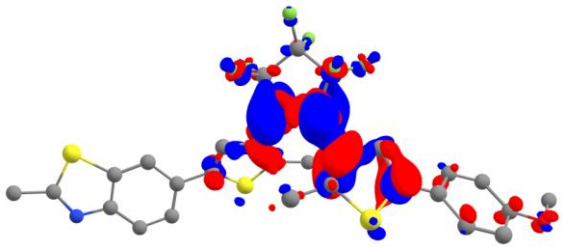 **8**
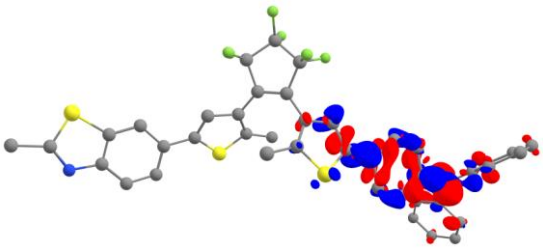 **9**
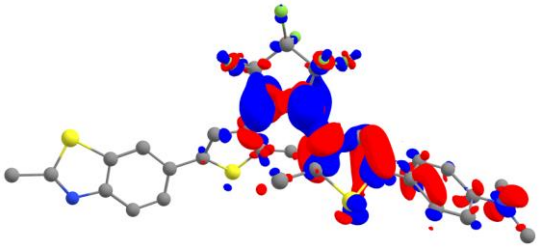 **10**
Closed form C
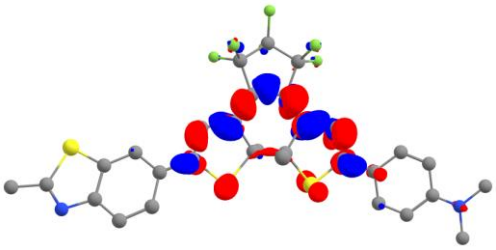 **10**

Figure S47 cont. Electron density differences (EDD) for the S_1 state of studied compounds. Red/blue lobes show increase/decrease of the electron density upon the excitation, isovalue of 0.002 was used. Hydrogen atoms are omitted in the graphic for clarity. Last row shows S_1 of the closed form of **10** for comparison.

4. Vibrational spectroscopy

4.1. Raman Spectroscopy

The Raman spectra were collected with a BWTek portable Polimi Raman spectrometer equipped with a 785 nm laser.

4.2. Raman Normal Modes

Density functional theory (DFT) calculations were carried out on both open and closed forms for the evaluation of the equilibrium geometry, the normal modes of vibration and the Raman spectrum. Additionally, the thermal transition state of the derivatives under consideration was calculated. We employed the B3LYP/6-31G(d,p) method for the open and close form, while employed the UB3LYP/6-31G(d,p) for the transition state. In both cases the quantum chemistry code utilized was Gaussian 09.

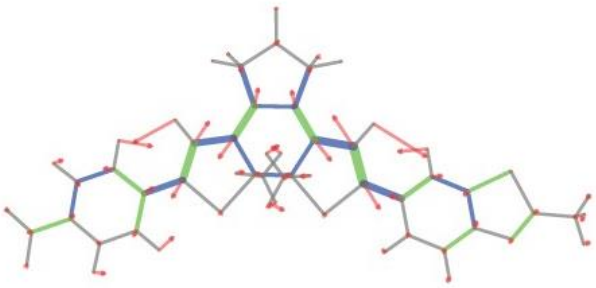

Figure S48. Raman normal mode corresponding to the CC skeletal vibration of **1** (1541 cm^{-1}; 531 km/mol; 134855 A^4/amu).

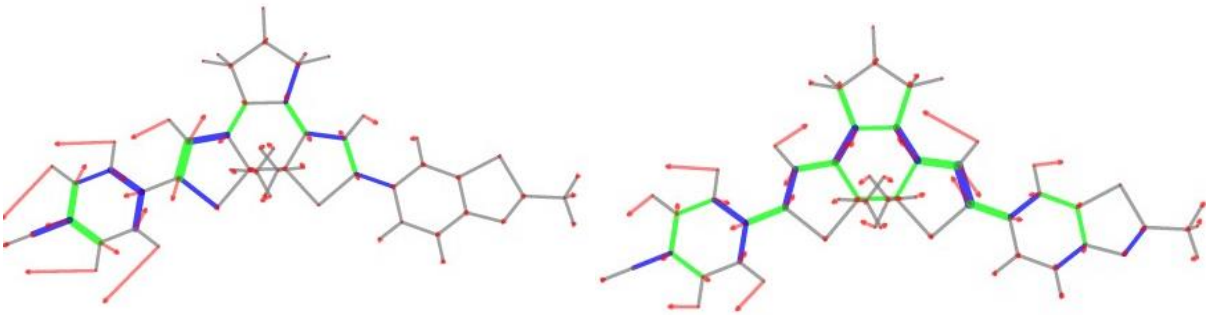

Figure S49. Raman normal mode corresponding to the CC skeletal vibration of **2** (left: 1541 cm^{-1}; 37 km/mol; 18585 A^4/amu; right: 1544 cm^{-1}; 433 km/mol; 105554 A^4/amu).

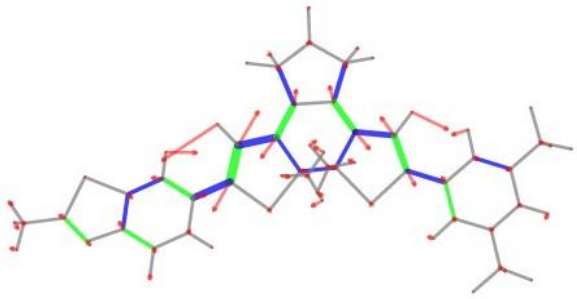

Figure S50. Raman normal mode corresponding to the CC skeletal vibration of **3** (1549 cm^{-1}; 387 km/mol; 90317 A^4/amu).

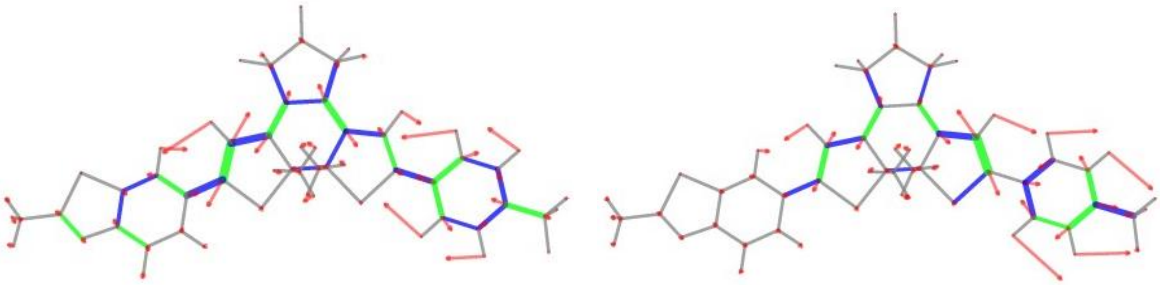

Figure S51. Raman normal mode corresponding to the CC skeletal vibration of **4** (left: 1550 cm^{-1}; 227 km/mol; 68237 A^4/amu; right: 1548 cm^{-1}; 53 km/mol; 27990 A^4/amu).

Figure S52. Raman normal mode corresponding to the CC skeletal vibration of **5** (1549 cm^{-1}; 119 km/mol; 133111 A^4/amu).

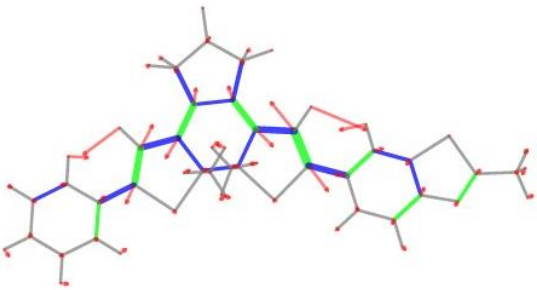

Figure S53. Raman normal mode corresponding to the CC skeletal vibration of **6** (1553 cm^{-1}; 139 km/mol; 84413 A^4/amu).

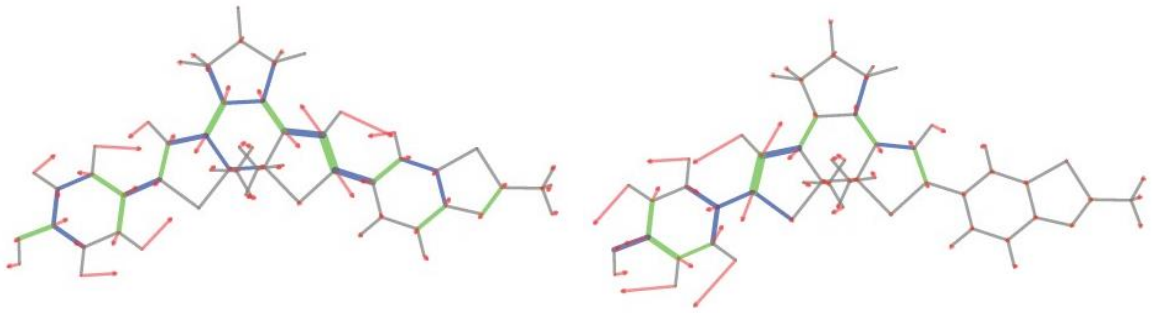

Figure S54. Raman normal mode corresponding to the CC skeletal vibration of **7** (left: 1554 cm^{-1}; 118 km/mol; 76313 A^4/amu; right: 1545 cm^{-1}; 601 km/mol; 21958 A^4/amu).

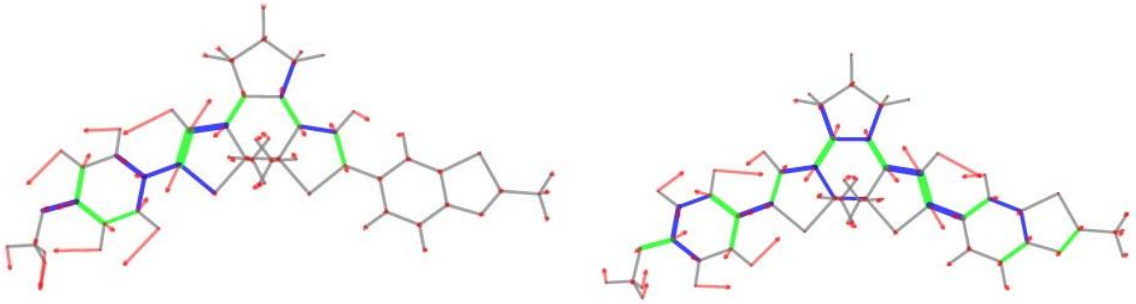

Figure S55. Raman normal mode corresponding to the CC skeletal vibration of **8** (left: 1546 cm^{-1}; 618 km/mol; 31147 A^4/amu; right: 1554 cm^{-1}; 101 km/mol; 74499 A^4/amu).

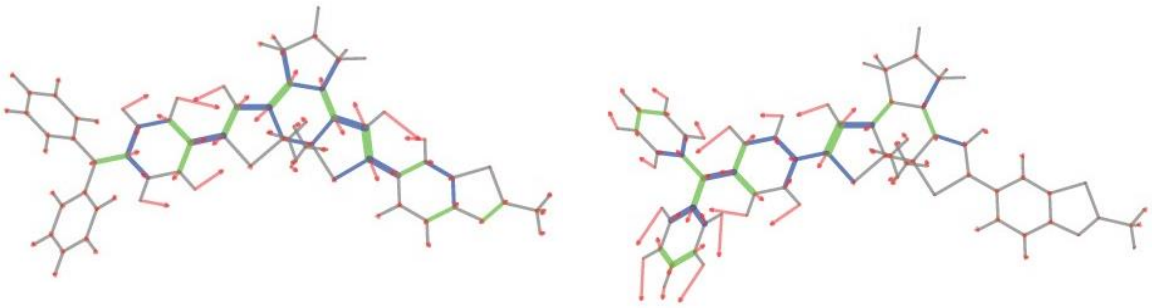

Figure S56. Raman normal mode corresponding to the CC skeletal vibration of **9** (left: 1551 cm^{-1}; 78 km/mol; 170369 A^4/amu; right: 1531 cm^{-1}; 1130 km/mol; 21532 A^4/amu).

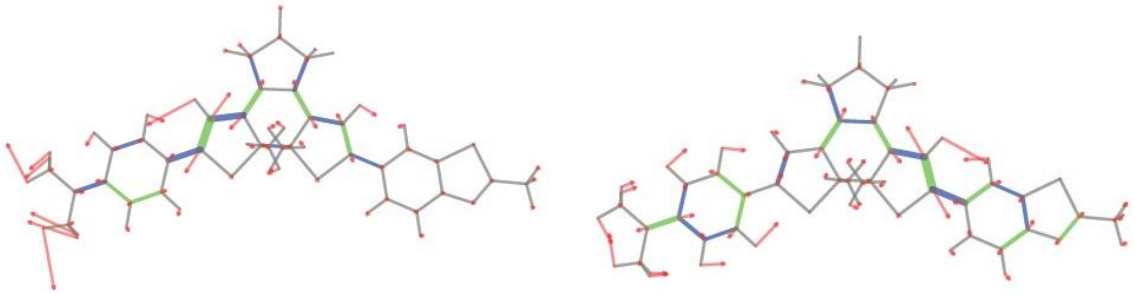

Figure S57. Raman normal mode corresponding to the CC skeletal vibration of **10** (left: 1541 cm^{-1}; 1364 km/mol; 68818 A^4/amu; right: 1559 cm^{-1}; 301 km/mol; 56689 A^4/amu).

4.3. IR Spectroscopy

IR spectra were collected on KBr pellets using a Jasco FT/IR 6600 with a resolution of 2 cm^{-1}. The IR spectra of all studied DTE derivatives under investigation in open O and closed C form are shown below (Fig. S55).

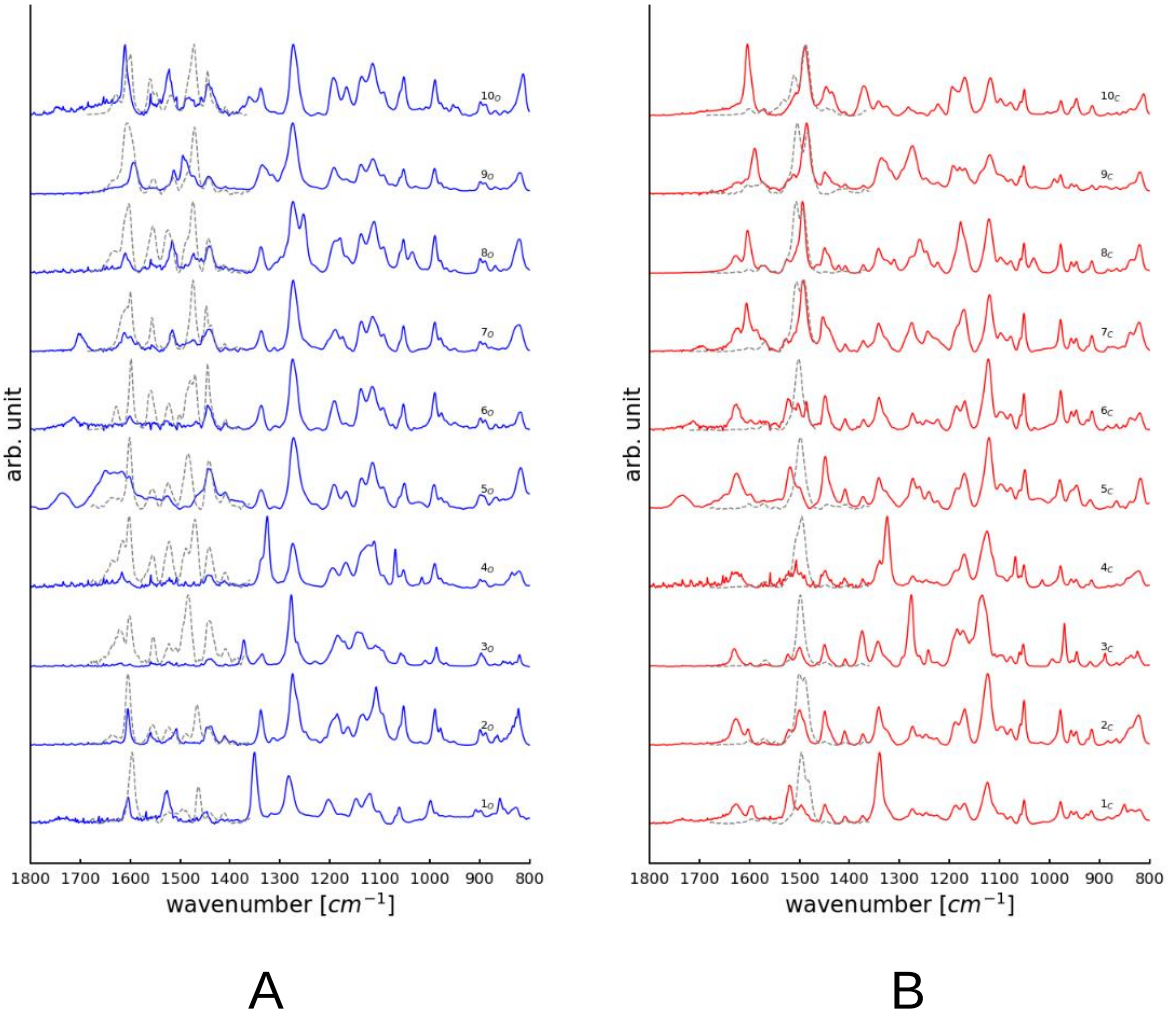

Figure S58. IR spectra and section of Raman spectra (dashed grey with range from 1670 to 1370 cm^{-1}) of the (A) open and (B) closed form of the complete series of dithienylethene derivatives. Each spectrum is identified by the label of the compound.

5. Thermal Kinetics Study

5.1. General conditions

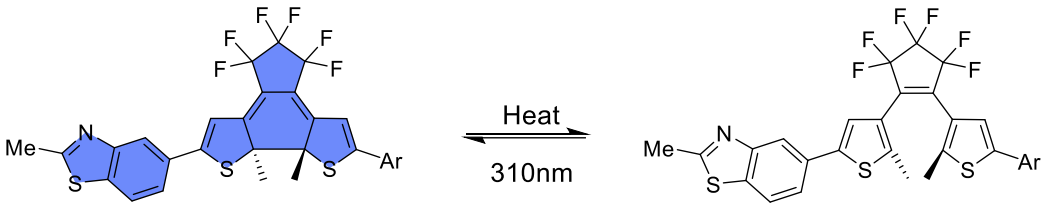

Thermal relaxation (ring-opening) of compounds **1**–**10** was monitored by ^{1}H NMR spectroscopy. NMR spectra were recorded on a Bruker Avance III spectrometer with a broad-band cryo-probe probe with ATM module (5 mm CPBBO BB-^{1}H/^{19}F/^{15}N/D Z/GRD) operating at 500 MHz for ^{1}H and 125 MHz for ^{13}C.

At first, the closed forms of **1**–**10** were generated photochemically (310 nm) in our home-made photoreactor consisting of eight LEDs from TME Electronics, Czech Republic (https://www.tme.eu/cz/details/rf-c37d0-utp-ar/diody-led-uv/refond/) with 8 mW each. Solutions of **1**–**10** (0.5 mg/mL) in toluene-d_8, DMSO-d_6 and **1**, **6**, **10** (0.5 mg/mL) in acetonitrile-d_8 were irradiated in a quartz cuvette (0.7 mL) until reaching photostationary state (usually 10–15 minutes), which was checked by NMR spectroscopy. The NMR tubes were then sealed in order to keep constant concentration. Thermal relaxation was monitored at elevated temperature, at 110 °C in case of DMSO and toluene samples and 70 °C in acetonitrile (MeCN).

Rate constants for thermally initiated C-to-O cycloreversion (k_{CO}) were determined from mono-exponential fit of relative concentration decay of the closed form C (Fig. 13 and Fig. S82). In the case of **1** in MeCN, due to incomplete conversion (Fig. S82 right), the rate constant k_{CO} was determined from non-linear fitting of equilibrium kinetics between the corresponding two forms (closed form C and open form O), according to Eq. (S6)[15]:

$$\mathrm{C} \underset{k_{\mathrm{O\text{-}C}}}{\overset{k_{\mathrm{C\text{-}O}}}{\leftrightharpoons}} \mathrm{O}$$

$$S = \left(S_0/(k_{\mathrm{CO}} + k_{\mathrm{OC}})\right)\left(k_{\mathrm{OC}} + k_{\mathrm{CO}} \exp[-(k_{\mathrm{CO}} + k_{\mathrm{OC}})t]\right) \qquad \text{(S6)}$$

where: S_0 is the percentage of the closed form C and t is time.

Gibbs free energy of transition state ($\Delta G^{\neq}$) for the thermal cycloreversion process was determined from the Eyring-Polanyi equation[16] and the corresponding half-life of the closed C form at room temperature ($t_{1/2}$; T = 298.15 K) in toluene (toluene-d_8) was estimated from Eq. (S7) assuming constant $\Delta G^{\neq}$ value over the whole temperature range:

$$t_{1/2} = {\ln 2}/{k_{\mathrm{CO\ (298.15\ K)}}} \qquad \text{(S7)}$$

[15] Atkins, P.; de Paula, J. *Atkins' Physical Chemistry, 10th ed.*; Oxford University Press: Oxford, 2014.

[16] Eyring, H., Polanyi, M. *Zeitschrift fur Physikalische Chemie* **2013**, *227*, 1221–1245.

where

$$k_{\mathrm{CO\ (298.15\ K)}} = (k_{\mathrm{B}}T/h)\exp(-\Delta G^{\neq}/RT) \quad \text{(S8)}$$

and k_{B} is the Boltzmann constant (1.38×10^{-23} J K^{-1}), h is the Planck constant (6.63×10^{-34} J s^{-1}) and R is the universal gas constant (8.314 J K^{-1} mol^{-1}).

5.2. Kinetic ^{1}H NMR experiments

Interestingly, except the closed forms of derivatives **1**,**2**,**4**,**6** and **8**, the temperature increase to 383.15 K in polar aprotic DMSO leads to unexpected competitive oxidation of their benzothiazole methyl group to the corresponding aldehyde (Figs. S65, S69, S74 and S78). Moreover, the formation of other unidentified product in DMSO was observed in the case of derivatives **5**, **7** and **10** (Fig. S69, S74 and S80). Surprisingly, the aldehyde formation was not observed after heating solutions of the open forms. The oxidation proceeds probably through radical mechanism using O_2/DMSO as oxidants[17,18] and could be useful intermediate step in the subsequent synthesis of dicyanovinyl analogues with increased NLO response for both O and C forms (Table S8 and Scheme S2). However, further deeper insight into the reaction mechanism is needed.

Significant role of a solvation in the thermal cycloreversion reaction further reflects in opposite sign of the slope of the $\Delta G^{\neq}$ vs. BLA BT graph in MeCN, as other polar aprotic solvent, in which the thermal stability of the closed form decreases below 10 years at room temperature (Figs. S82 and S83).

[17] H. Sterckx, J. De Houwer, C. Mensch, W. Herrebout, K. A. Tehrani, B. U. W. Maes, *Beilstein J. Org. Chem.* **2016**, *12*, 144–153.
[18] Y.-F. Wang, F.-L. Zhang, S. Chiba, *ChemInform* **2012**, *43*.

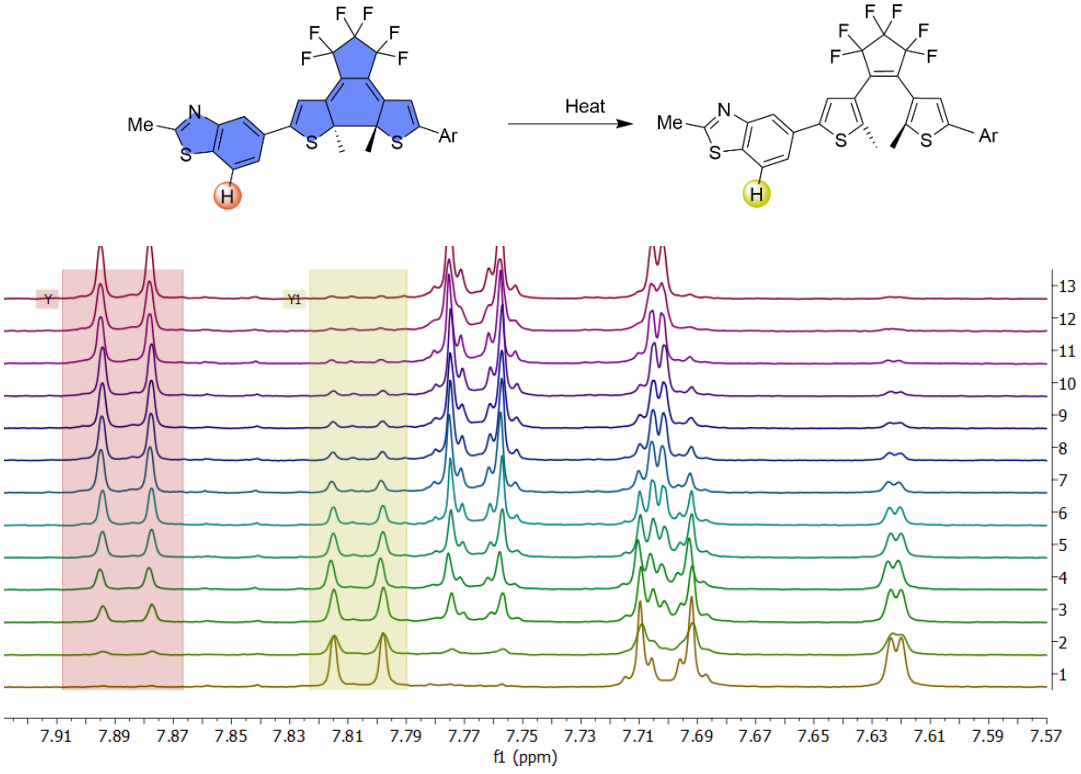

Figure S59. Array of ^{1}H NMR spectra of **1** in toluene-d_8 (from 1 to 13) during thermal ring opening of the cyclic form C. Highlighted signals were used for calculation of relative concentration of both forms.

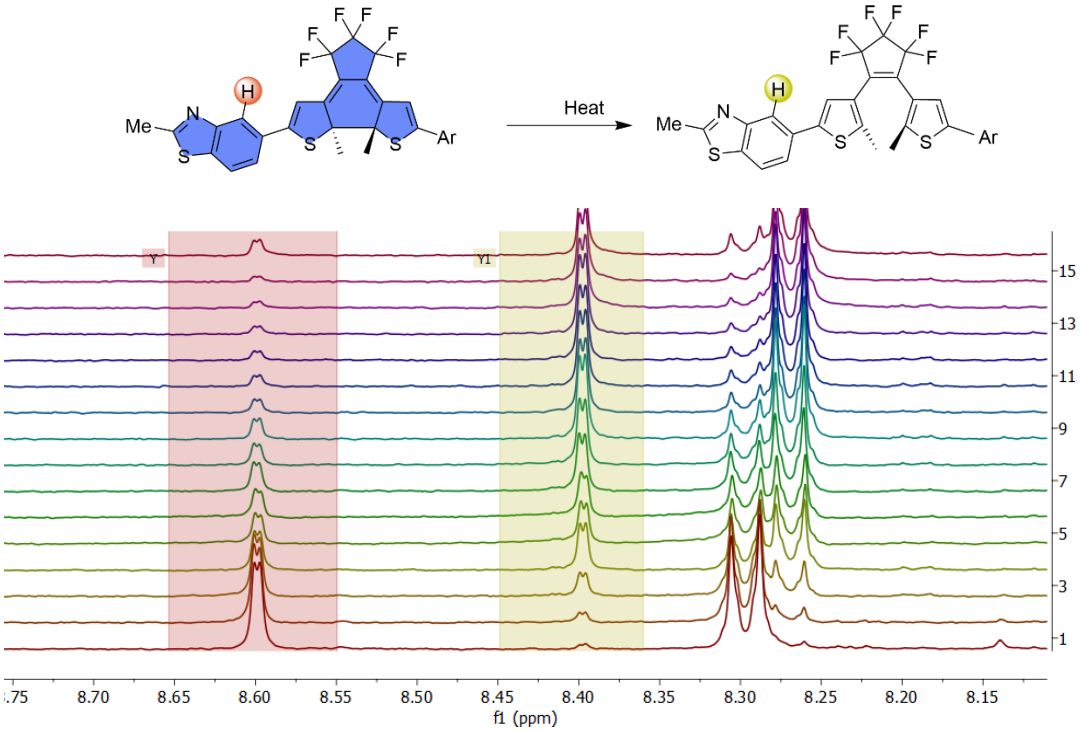

Figure S60. Array of ^{1}H NMR spectra of **1** in DMSO-d_6 (from 1 to 15) during thermal ring opening of the cyclic form C. Highlighted signals were used for calculation of relative concentration of both forms.

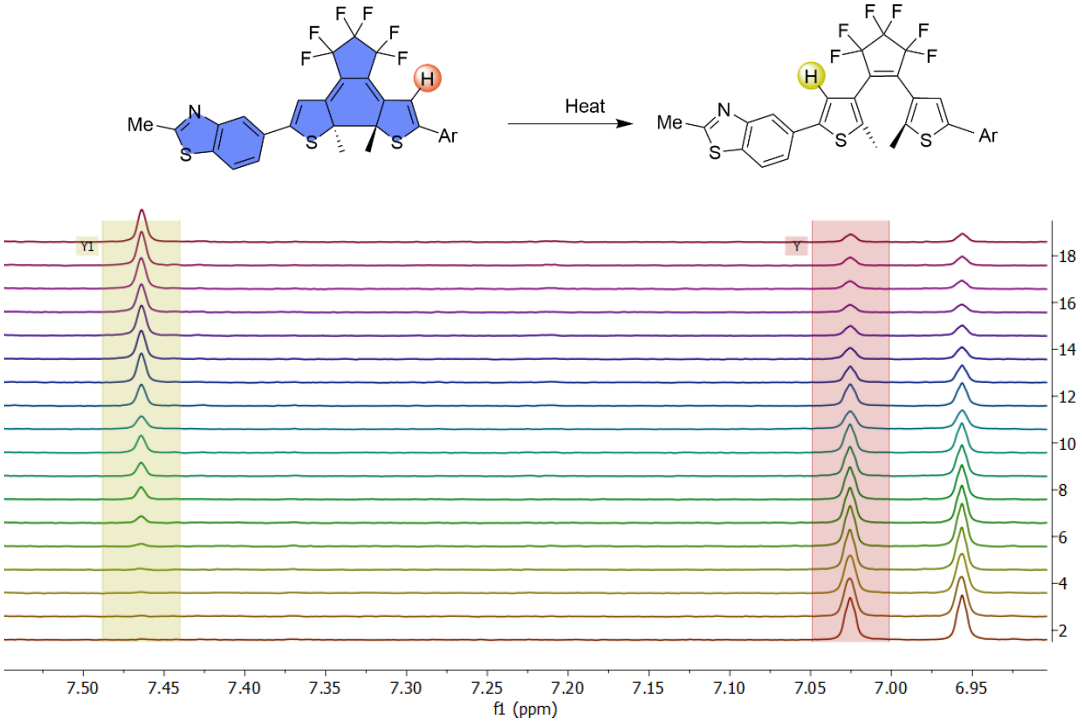

Figure S61. Array of ^{1}H NMR spectra of **1** in acetonitrile-d_3 (from 2 to 18) during thermal ring opening of the cyclic form C. Highlighted signals were used for calculation of relative concentration of both forms.

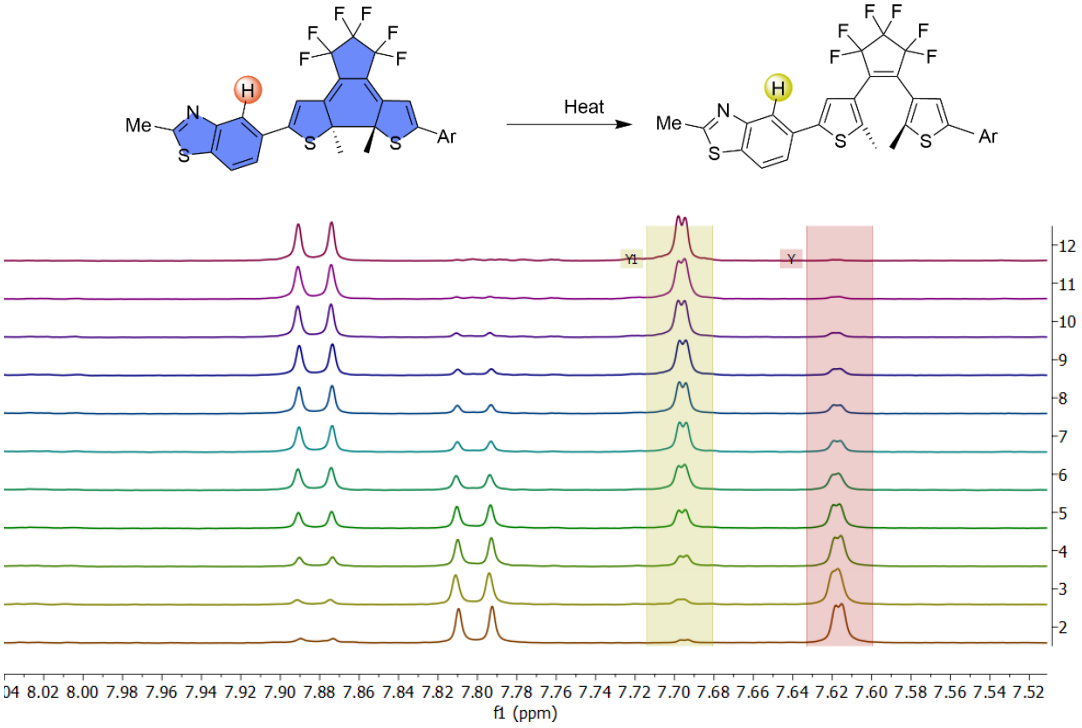

Figure S62. Array of ^{1}H NMR spectra of **2** in toluene-d_8 (from 2 to 12) during thermal ring opening of the cyclic form C. Highlighted signals were used for calculation of relative concentration of both forms.

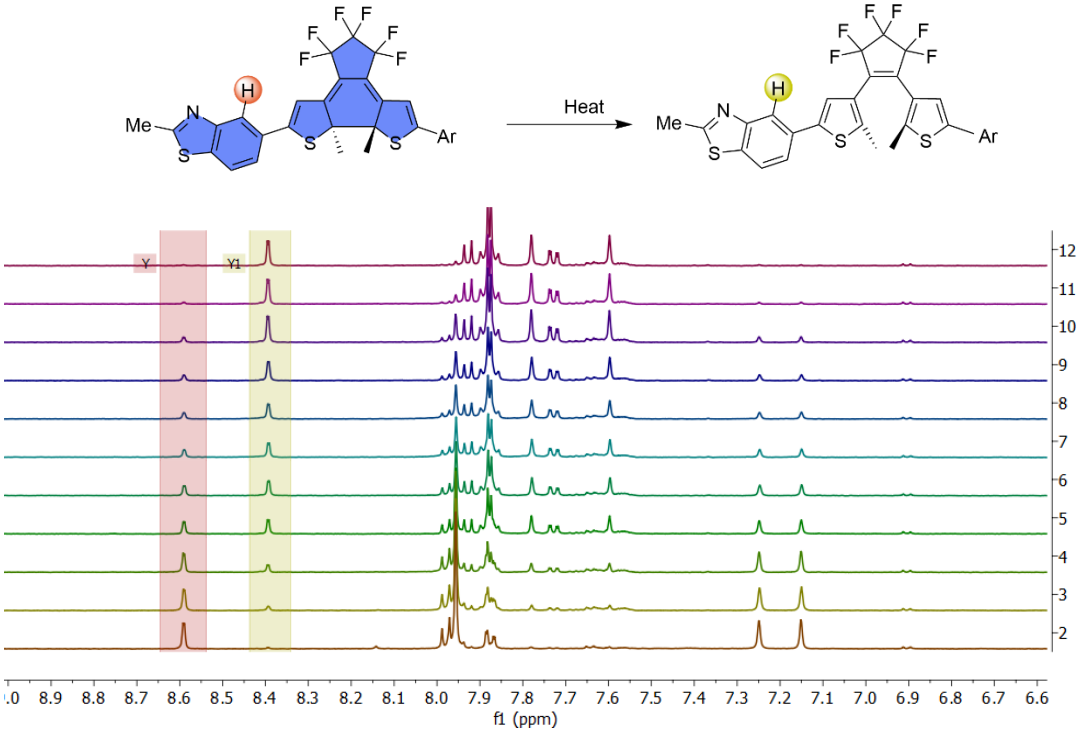

Figure S63. Array of ^{1}H NMR spectra of **2** in DMSO-d_6 (from 2 to 12) during thermal ring opening of the cyclic form C. Highlighted signals were used for calculation of relative concentration of both forms.

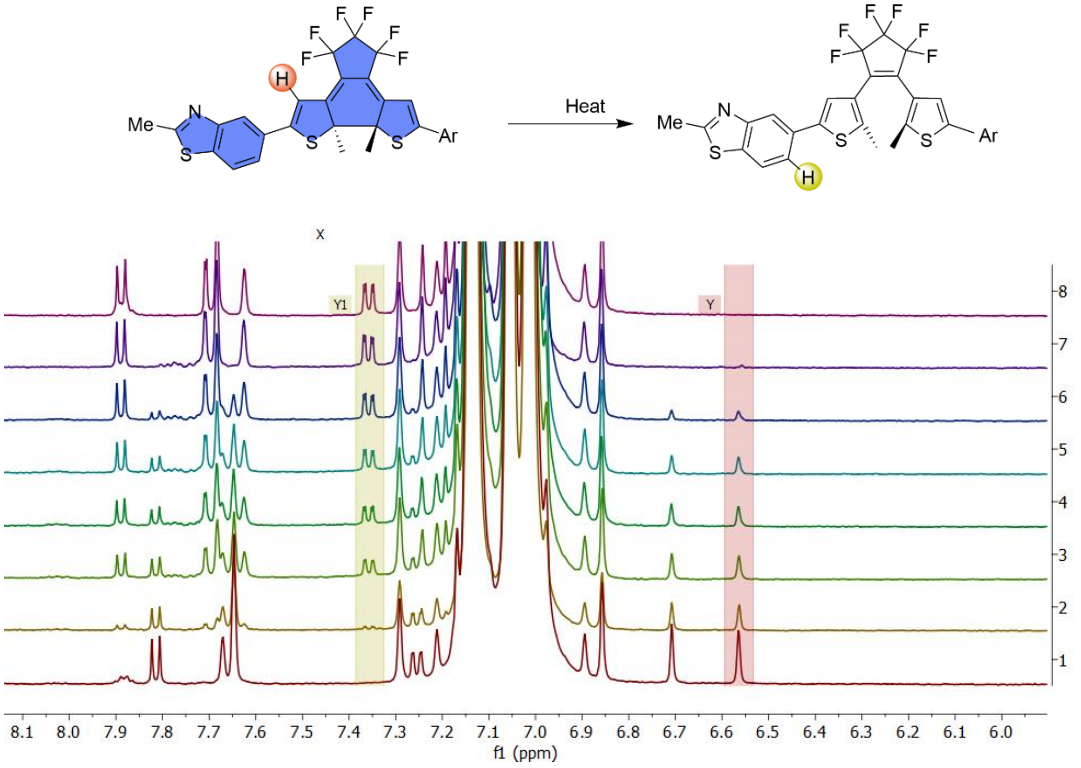

Figure S64. Array of ^{1}H NMR spectra of **3** in toluene-d_8 (from 1 to 8) during thermal ring opening of the cyclic form C. Highlighted signals were used for calculation of relative concentration of both forms.

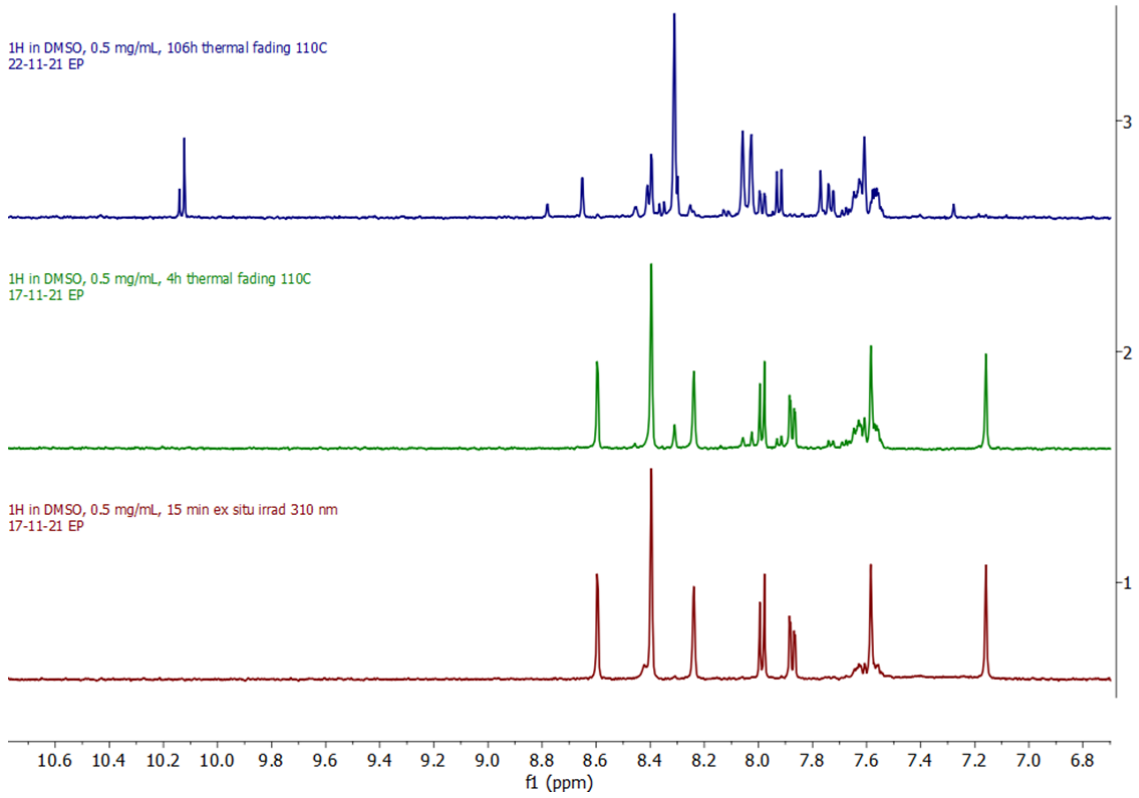

Figure S65. Array of ^{1}H NMR spectra of **3** in DMSO-d_6 (from 1 to 3) during thermal ring opening of the cyclic form C. Oxidation to aldehyde is observed by formation of new signal around 10.2 ppm.

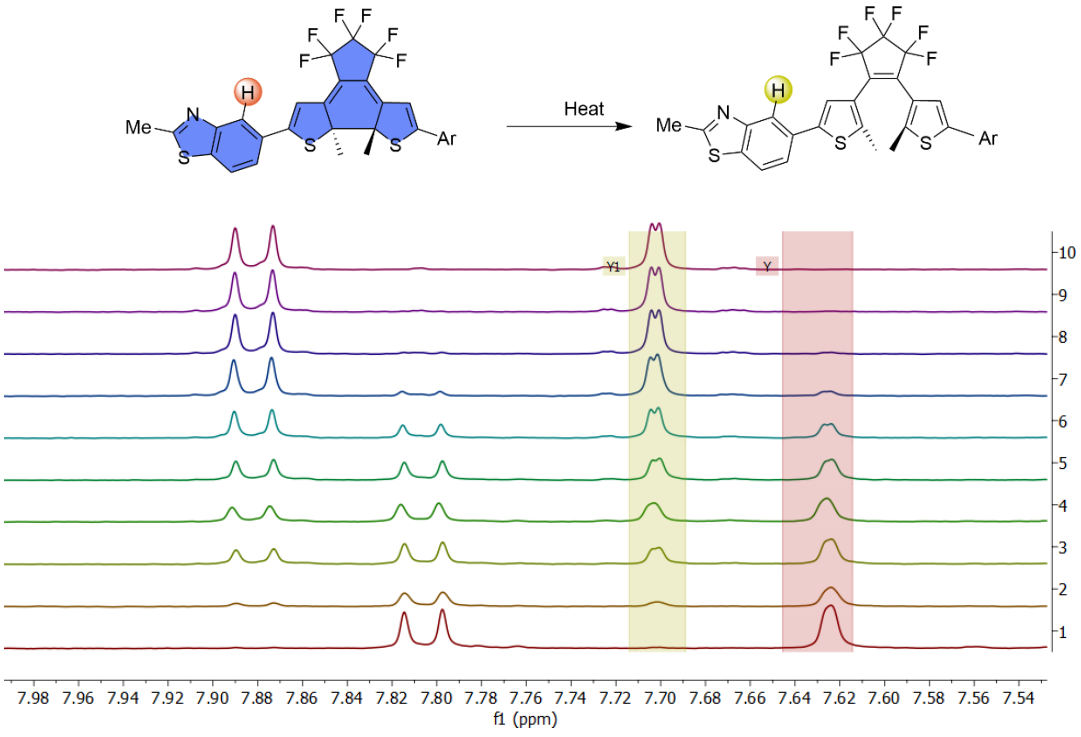

Figure S66. Array of ^{1}H NMR spectra of **4** in toluene-d_8 (from 1 to 10) during thermal ring opening of the cyclic form C. Highlighted signals were used for calculation of relative concentration of both forms.

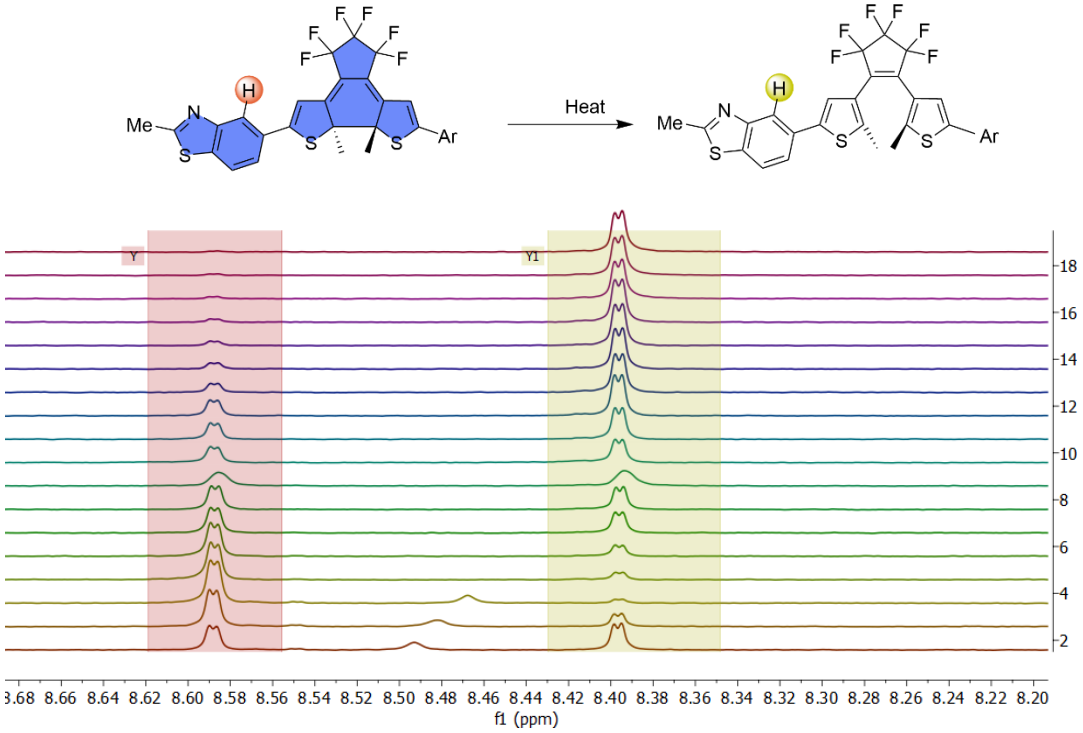

Figure S67. Array of ^{1}H NMR spectra of **4** in DMSO-d_6 (from 2 to 18) during thermal ring opening of the cyclic form C. Highlighted signals were used for calculation of relative concentration of both forms.

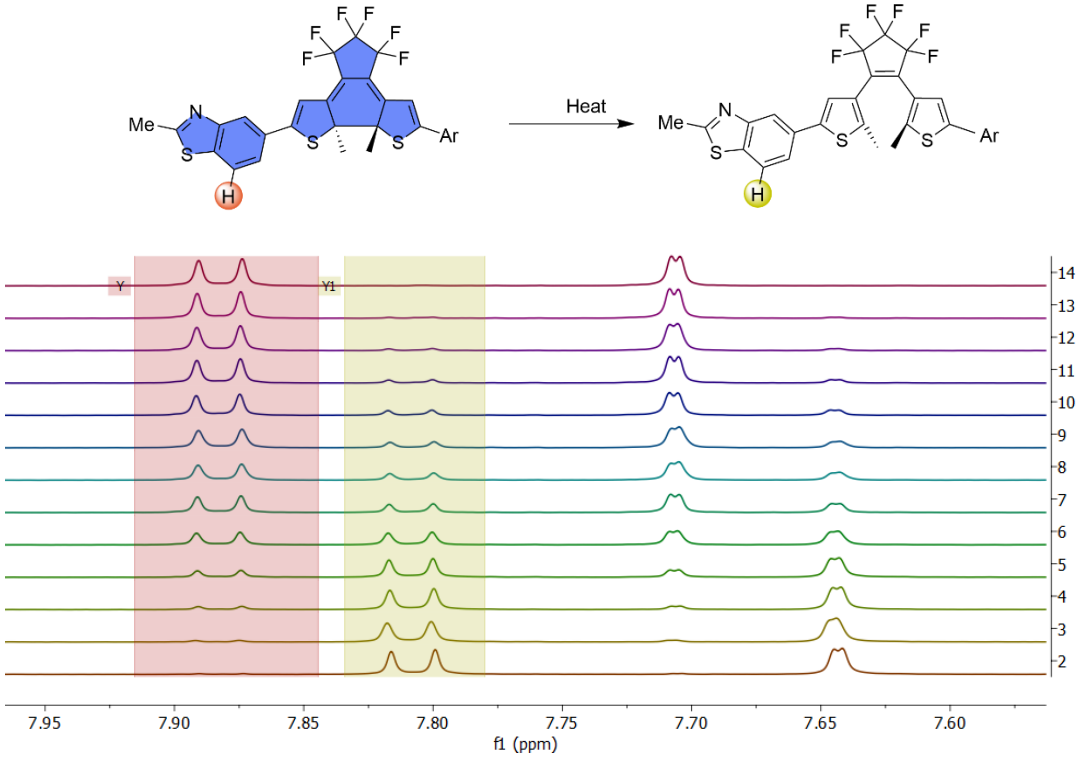

Figure S68. Array of ^{1}H NMR spectra of **5** in toluene-d_8 (from 2 to 14) during thermal ring opening of the cyclic form C. Highlighted signals were used for calculation of relative concentration of both forms.

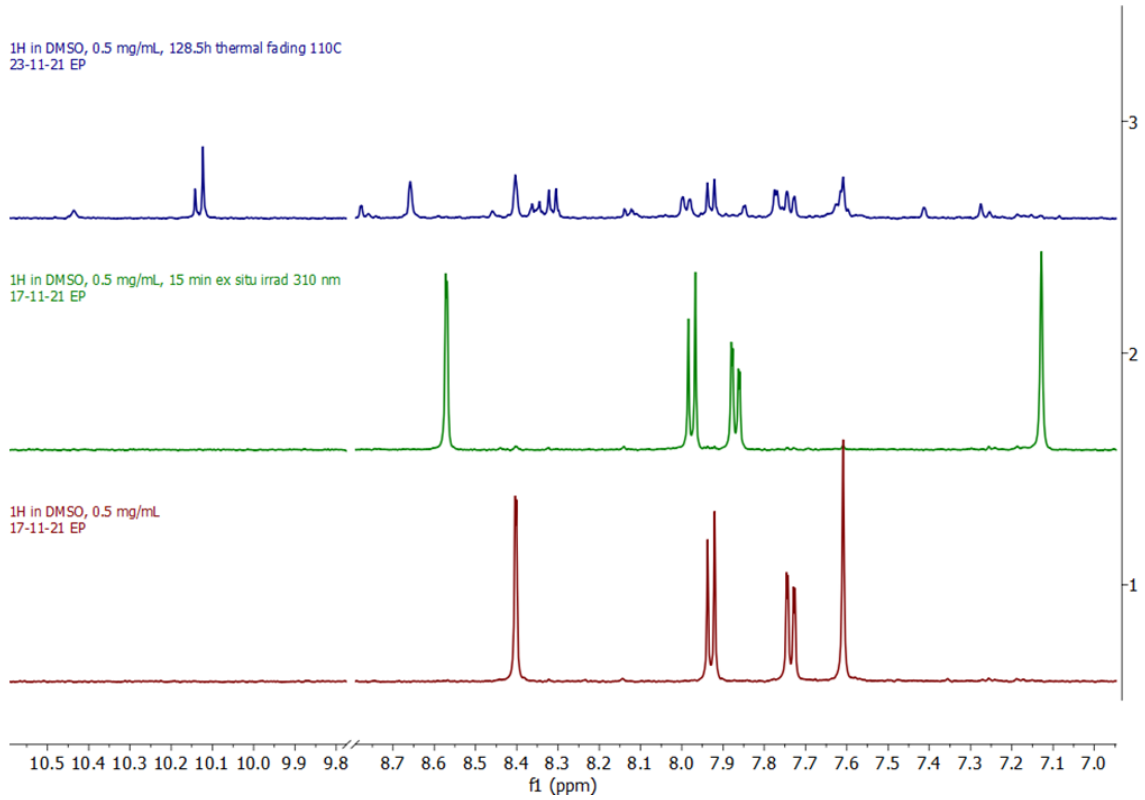

Figure S69. Array of ^{1}H NMR spectra of **5** in DMSO-d_6 (from 1 to 3) during thermal ring opening of the cyclic form C. Oxidation to aldehyde is observed by formation of new signal around 10.2 ppm.

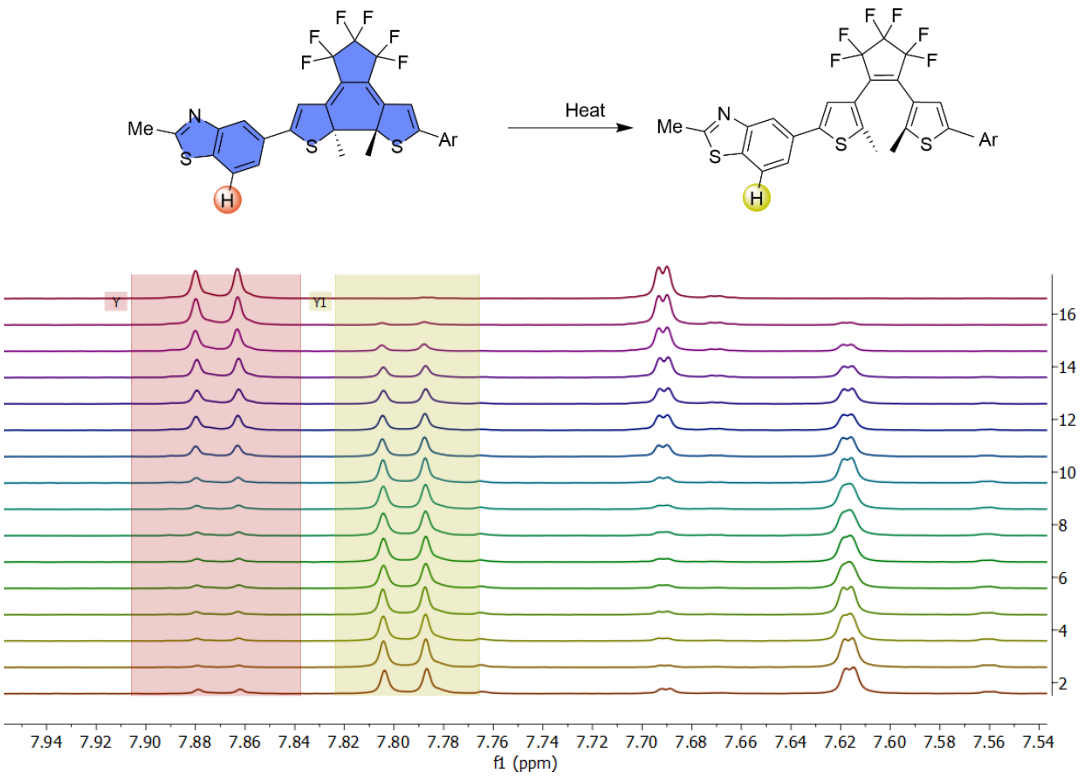

Figure S70. Array of ^{1}H NMR spectra of **6** in toluene-d_8 (from 2 to 16) during thermal ring opening of the cyclic form C. Highlighted signals were used for calculation of relative concentration of both forms.

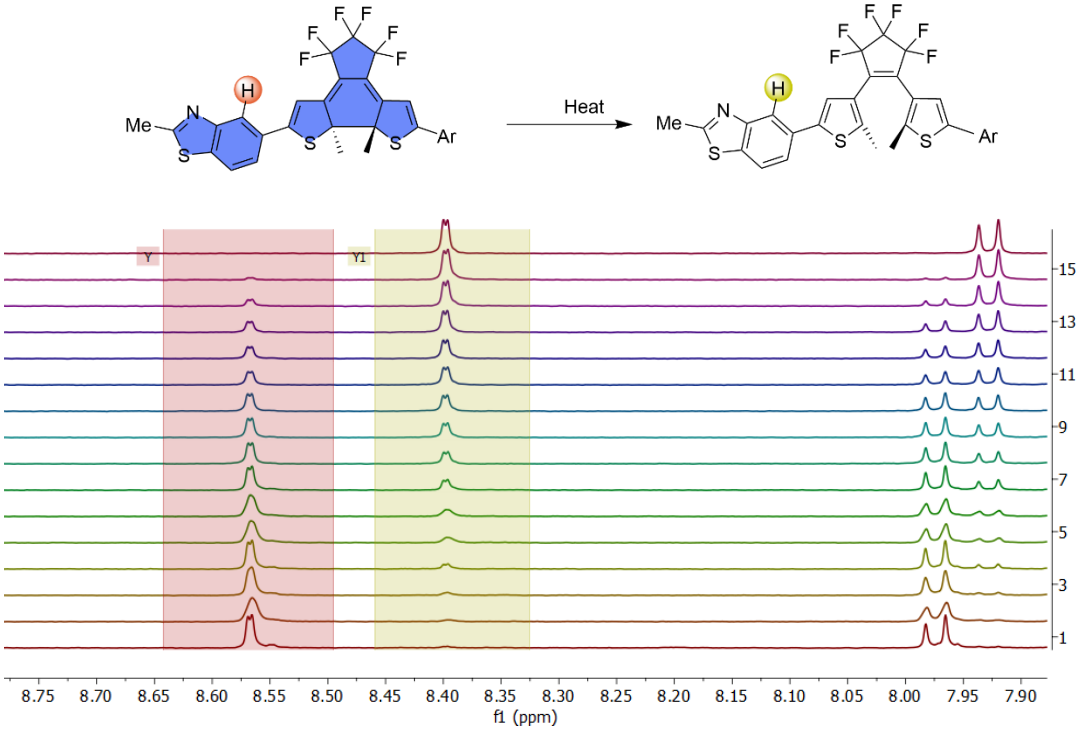

Figure S71. Array of ^{1}H NMR spectra of **6** in DMSO-d_6 (from 1 to 15) during thermal ring opening of the cyclic form C. Highlighted signals were used for calculation of relative concentration of both forms.

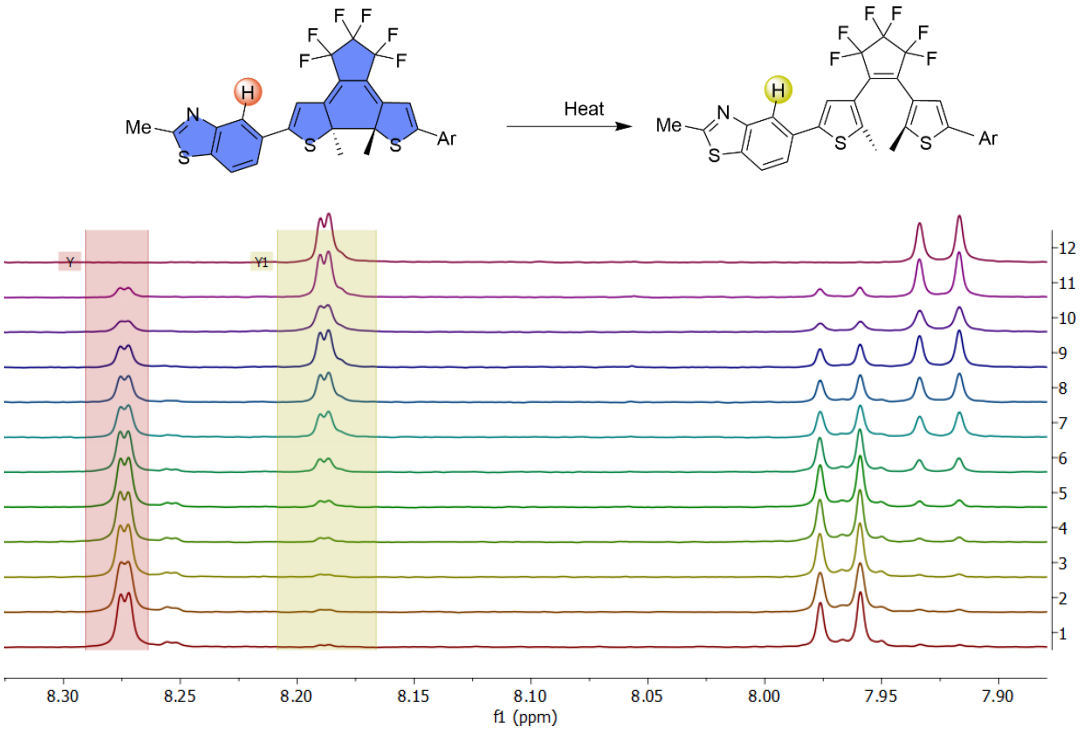

Figure S72. Array of ^{1}H NMR spectra of **6** in acetonitrile-d_3 (from 1 to 12) during thermal ring opening of the cyclic form C. Highlighted signals were used for calculation of relative concentration of both forms.

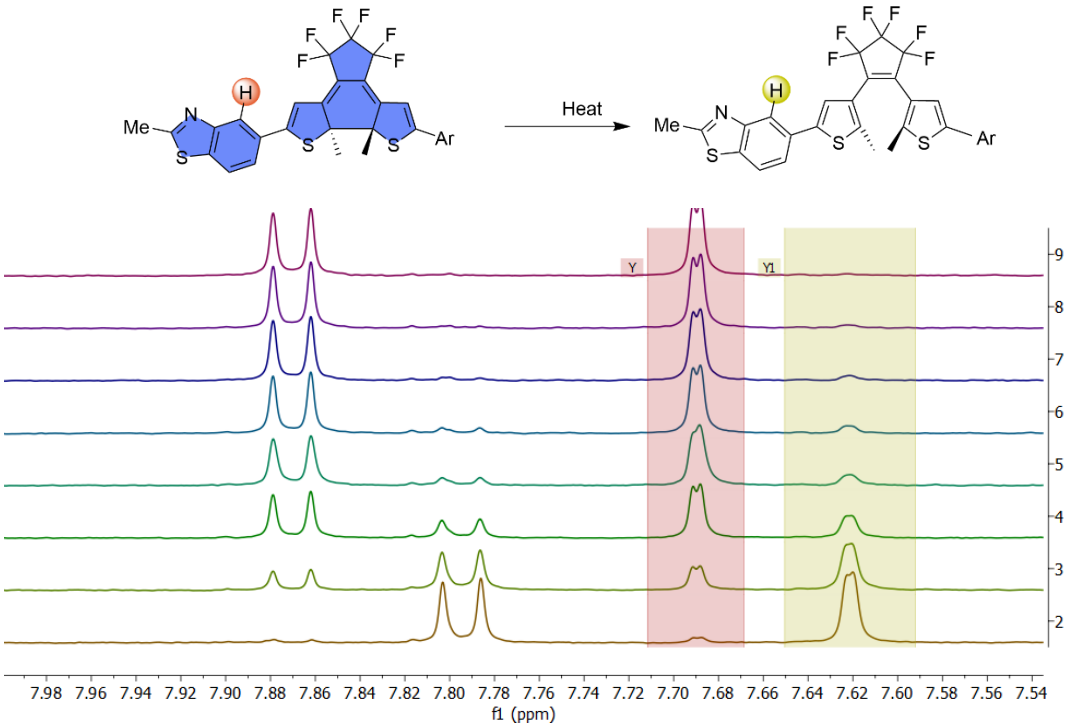

Figure S73. Array of ^{1}H NMR spectra of **7** in toluene-d_8 (from 2 to 9) during thermal ring opening of the cyclic form C. Highlighted signals were used for calculation of relative concentration of both forms.

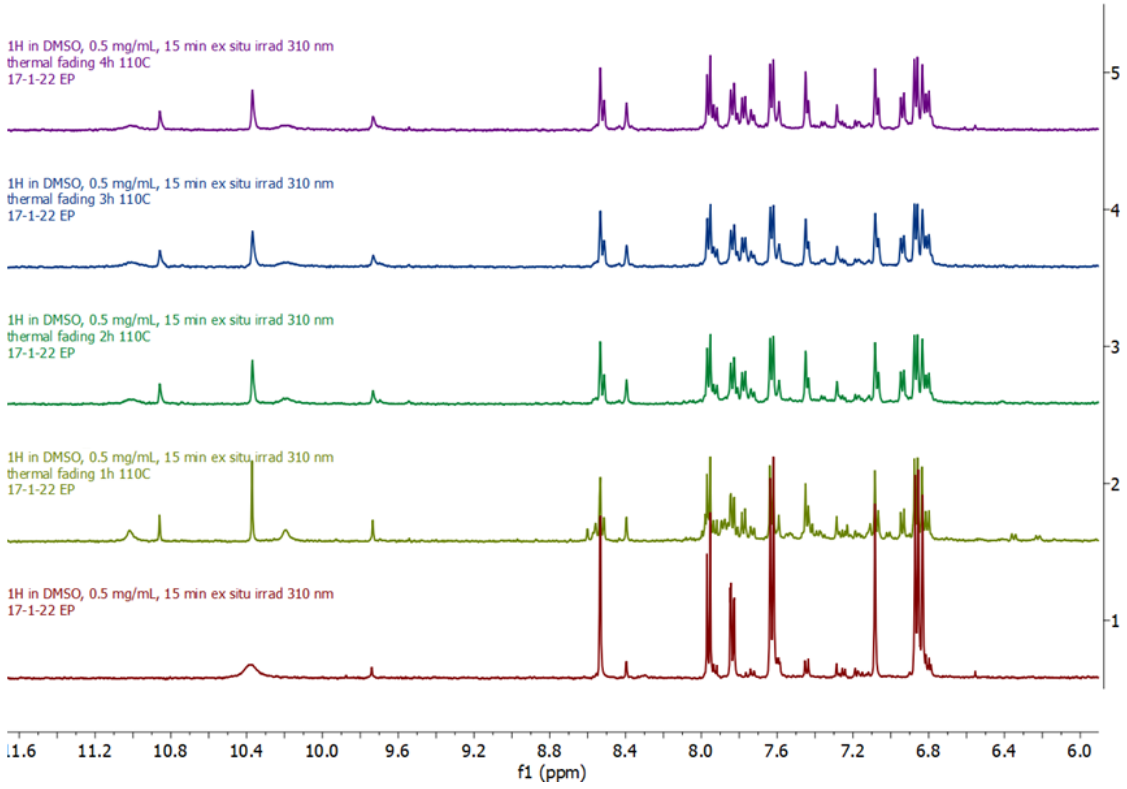

Figure S74. Array of ^{1}H NMR spectra of **7** in DMSO-d_6 (from 1 to 5) during thermal ring opening of the cyclic form C. Oxidation to aldehyde is observed by formation of new signal around 10.2 ppm. Signs of sideproducts/degradation are also present.

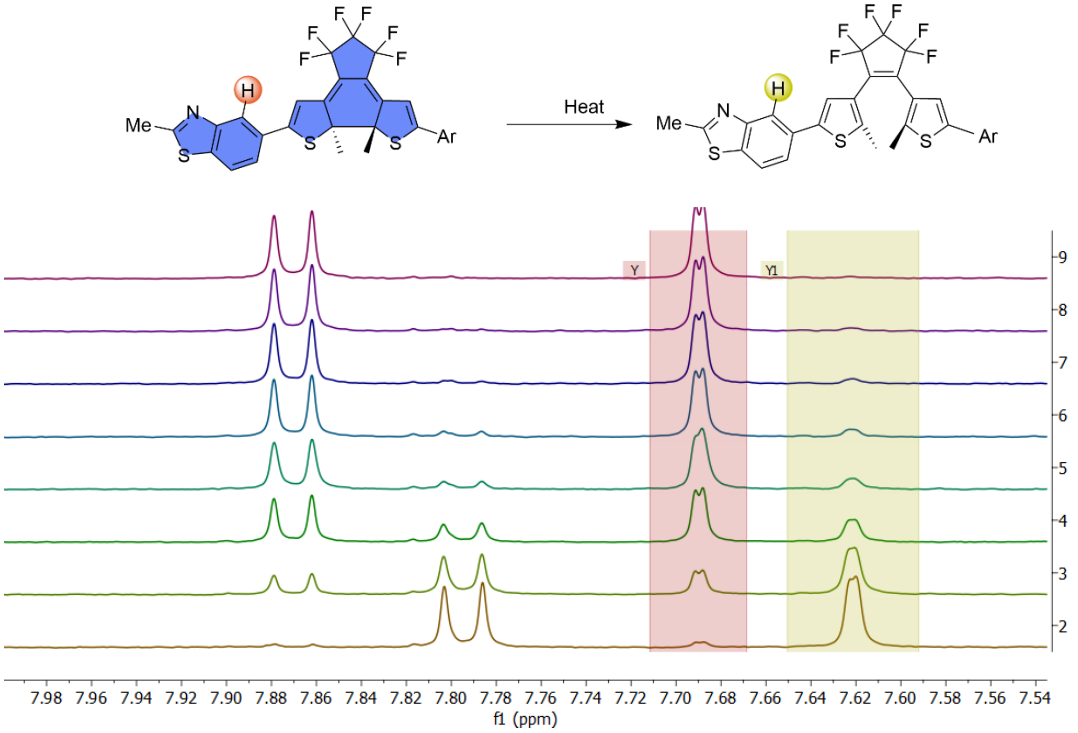

Figure S75. Array of ^{1}H NMR spectra of **8** in toluene-d_8 (from 2 to 9) during thermal ring opening of the cyclic form C. Highlighted signals were used for calculation of relative concentration of both forms.

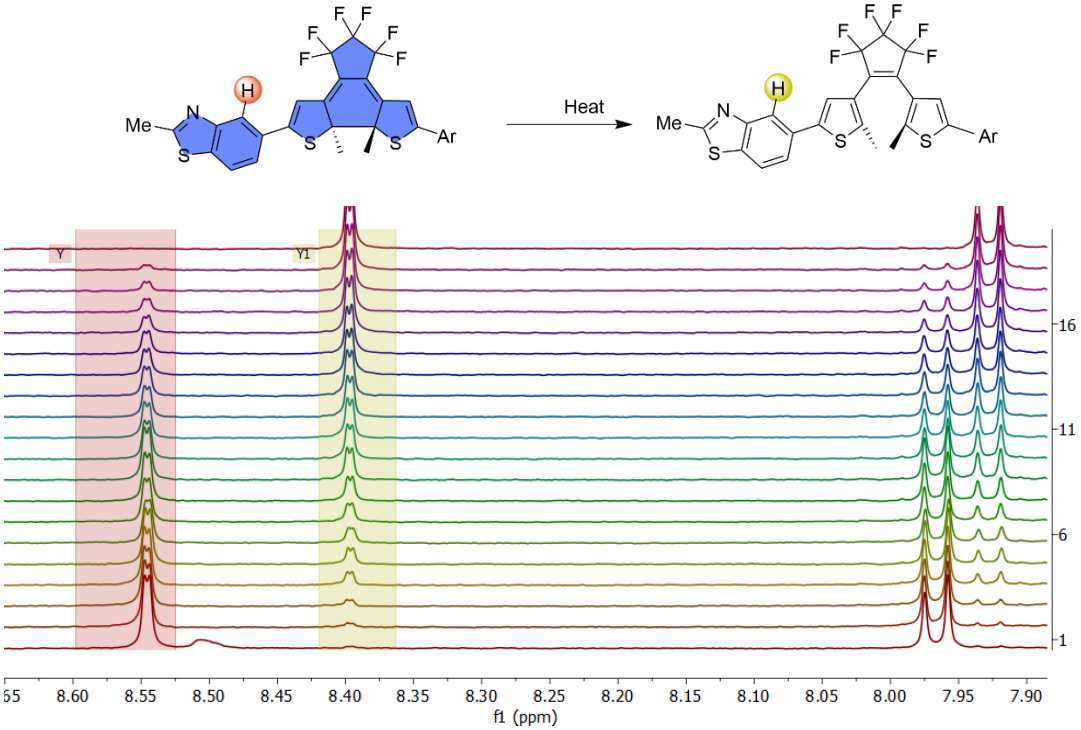

Figure S76. Array of ^{1}H NMR spectra of **8** in DMSO-d_6 (from 1 to 20) during thermal ring opening of the cyclic form C. Highlighted signals were used for calculation of relative concentration of both forms.

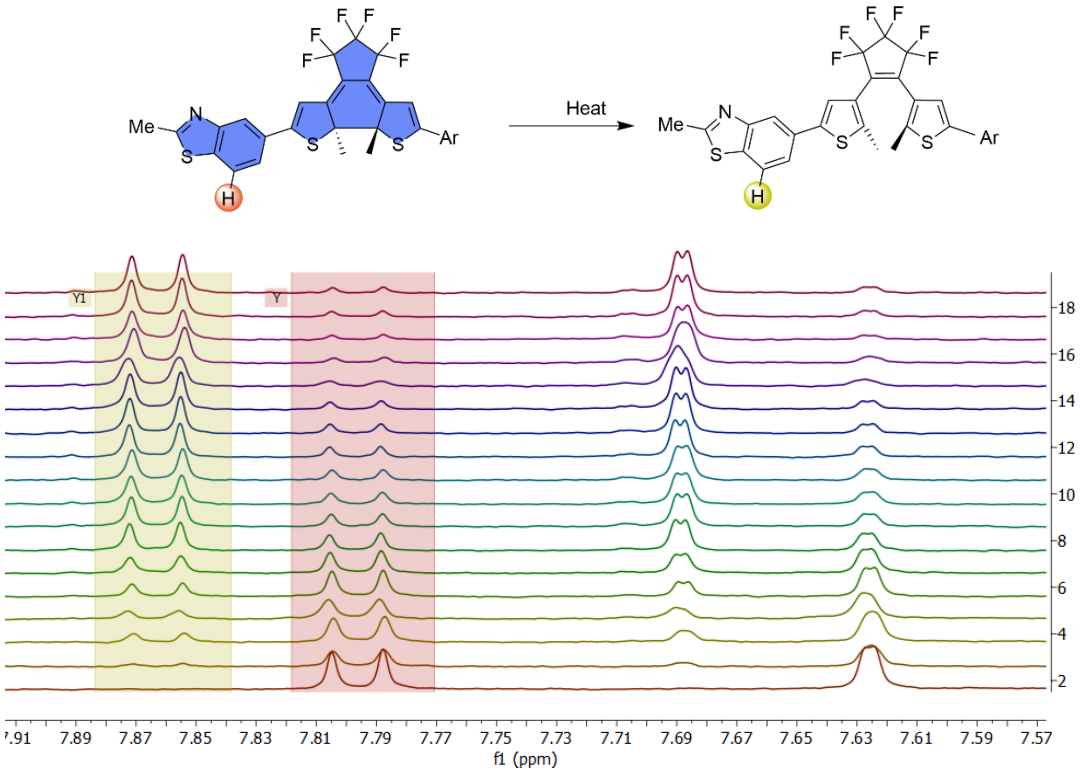

Figure S77. Array of ^{1}H NMR spectra of **9** in toluene-d_8 (from 2 to 18) during thermal ring opening of the cyclic form C. Highlighted signals were used for calculation of relative concentration of both forms.

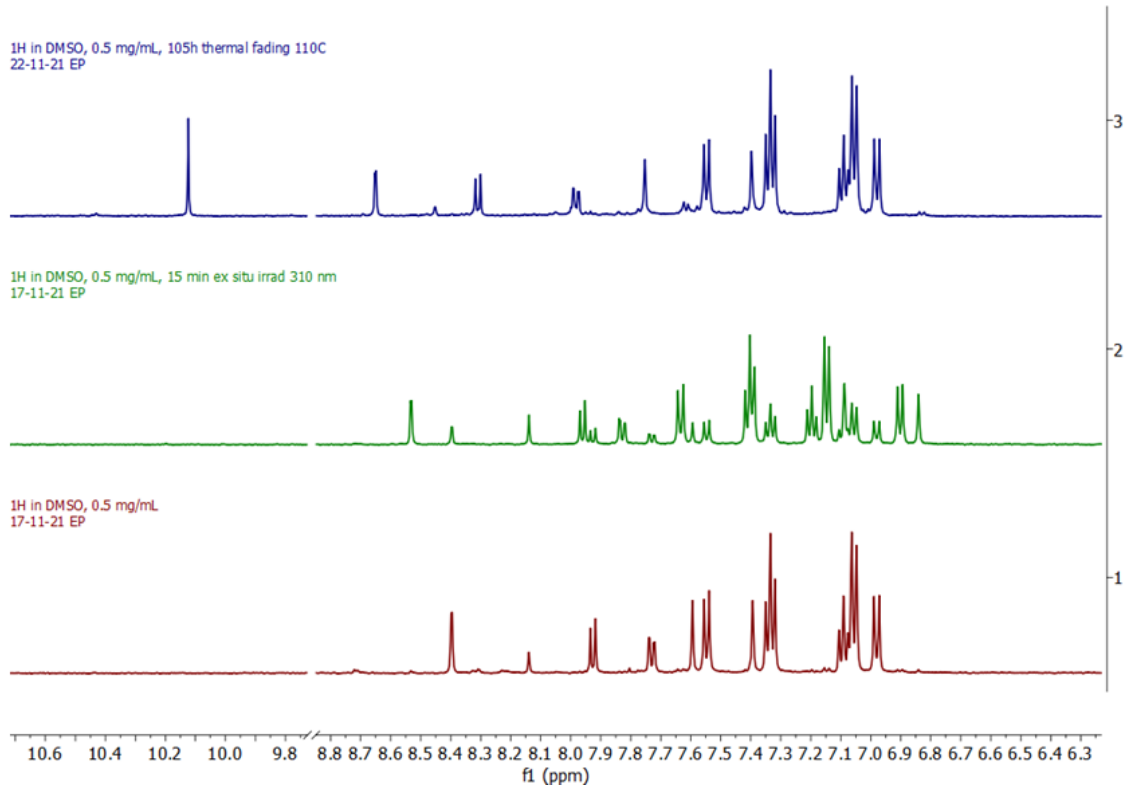

Figure S78. Array of ^{1}H NMR spectra of **9** in DMSO-d_6 (from 1 to 3) during thermal ring opening of the cyclic form C. Oxidation to aldehyde is observed by formation of new signal around 10.2 ppm.

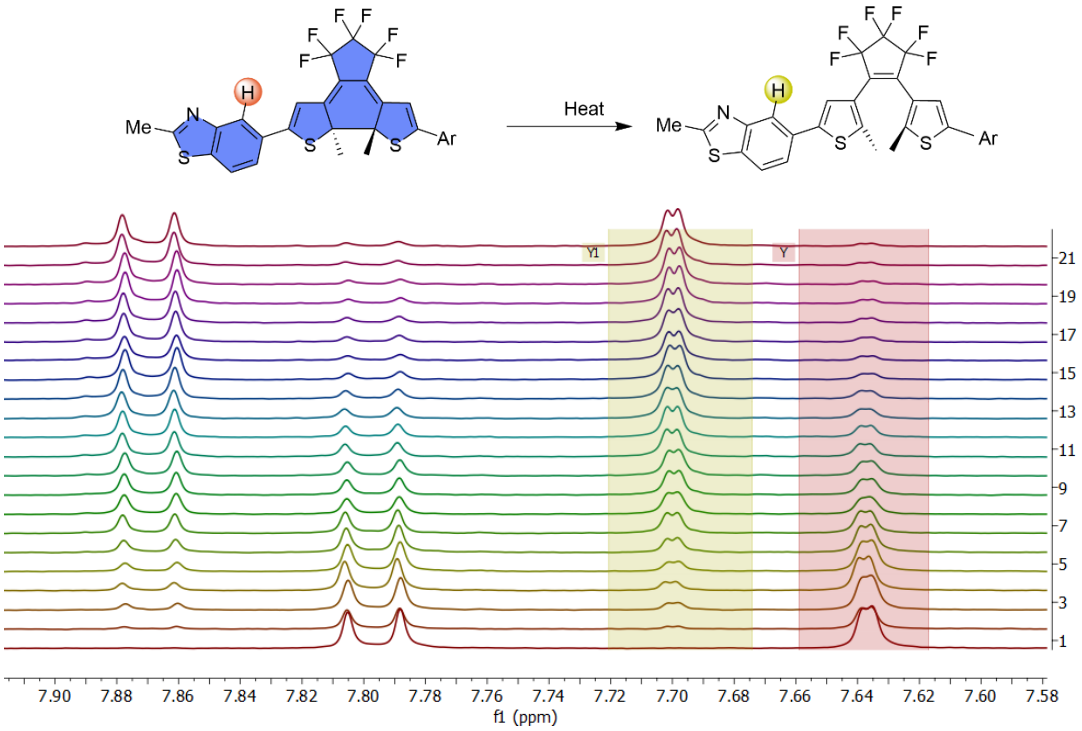

Figure S79. Array of ^{1}H NMR spectra of **10** in toluene-d_8 (from 1 to 21) during thermal ring opening of the cyclic form C. Highlighted signals were used for calculation of relative concentration of both forms.

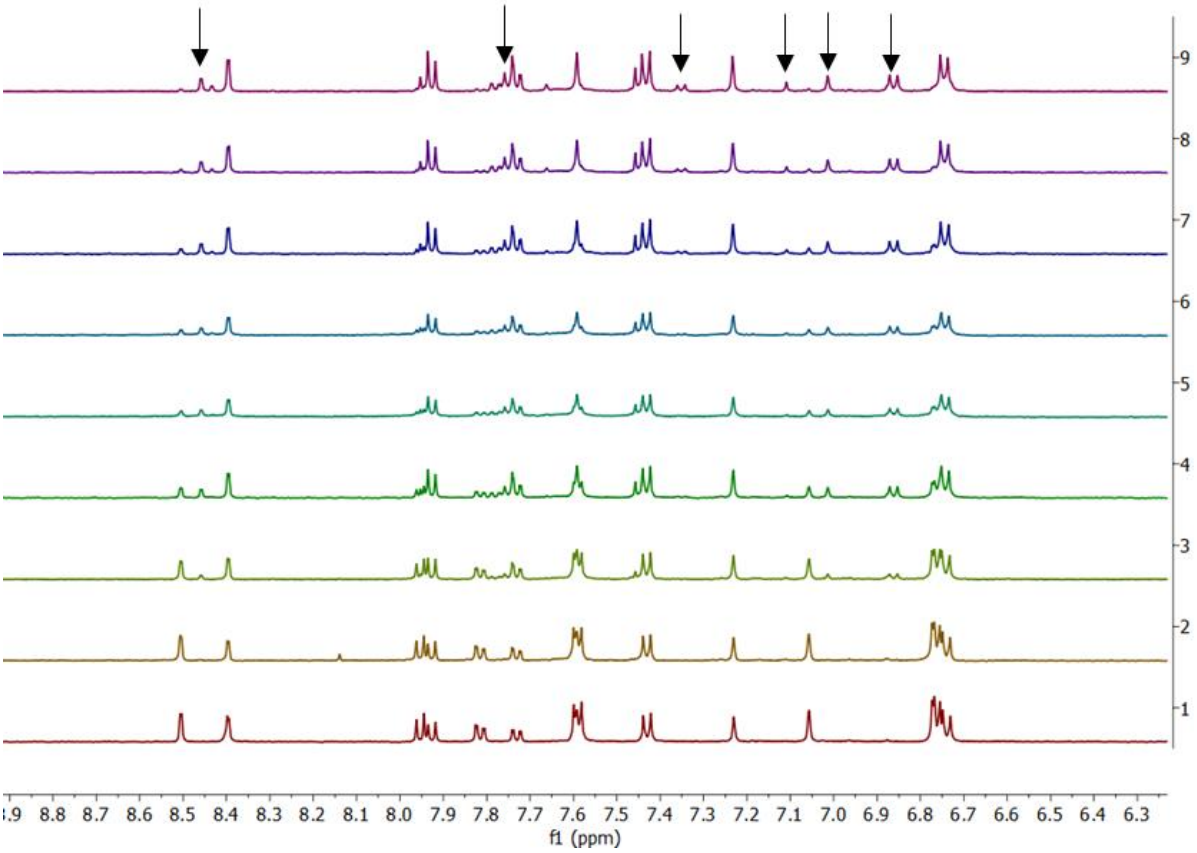

Figure S80. Array of ^{1}H NMR spectra of **10** in DMSO-d_6 (from 1 to 9) during thermal ring opening of the cyclic form C. Signs of degradation/side reactions are clearly present in NMR spectra (black arrows).

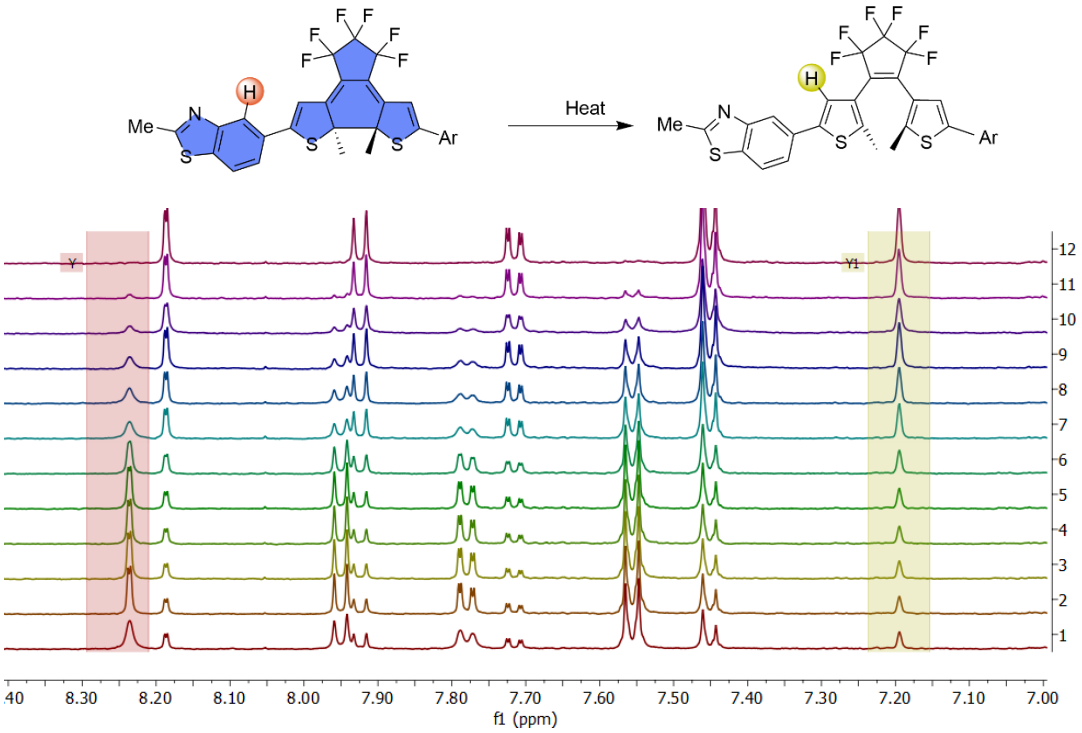

Figure S81. Array of ^{1}H NMR spectra of **10** in acetonitrile-d_3 (from 1 to 12) during thermal ring opening of the cyclic form C. Highlighted signals were used for calculation of relative concentration of both forms.

5.3. NLO response of oxidation product and its dicyanovinyl analogues

Table S8. Electric properties of benzothiazole derivatives prepared by oxidation of the benzothiazole methyl group in studied DTEs **8** and **10** followed by nucleophilic addition-elimination reaction (Ad_N-E) with malononitrile (C – closed form, O – open form). Structures of compounds can be found in Scheme S2. Computational details are described in section 6.1 *Electric properties and photochemical study*.

Property	μ_{tot} [D]			α_{iso} [10^{-24} esu]			β_{tot} [10^{-30} esu]		
Cpd	**C**	**O**	**Ratio**	**C**	**O**	**Ratio**	**C**	**O**	**Ratio**
10-aldehyde	12.65	10.49	1.2	98.65	81.17	1.2	218.50	49.57	4.4
10-DCNE	16.13	13.91	1.2	114.48	93.81	1.2	384.00	109.33	3.5
8-aldehyde	9.66	7.94	1.2	89.77	76.63	1.2	101.00	36.99	2.7
8-DCNE	12.55	11.30	1.1	104.18	89.16	1.2	209.56	93.74	2.2

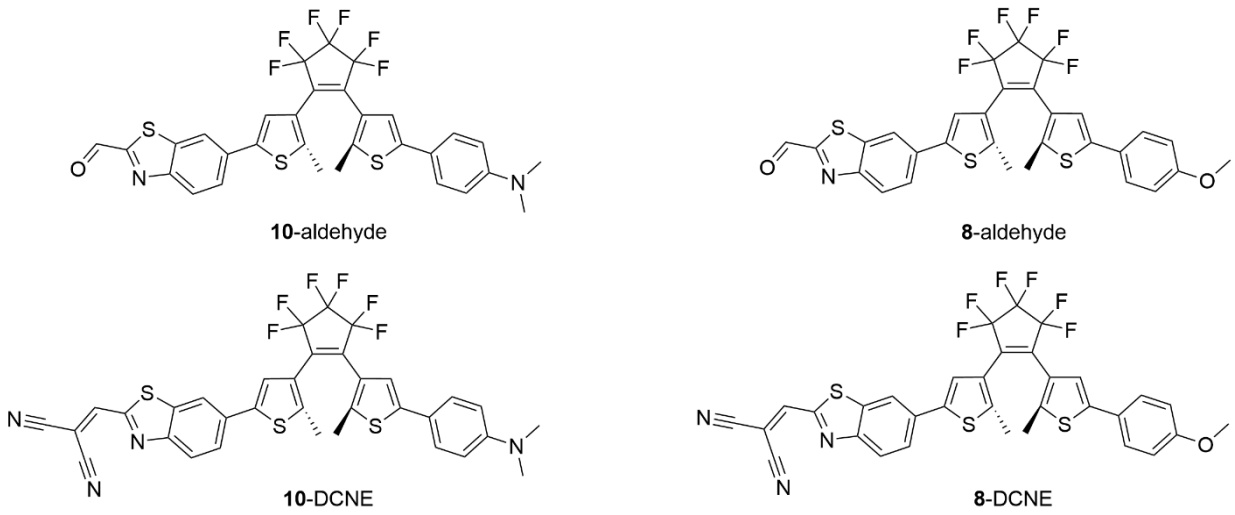

Scheme S2. Molecular structure of benzothiazole derivatives described in Table S8**.**

5.4. Thermal stability in polar solvents

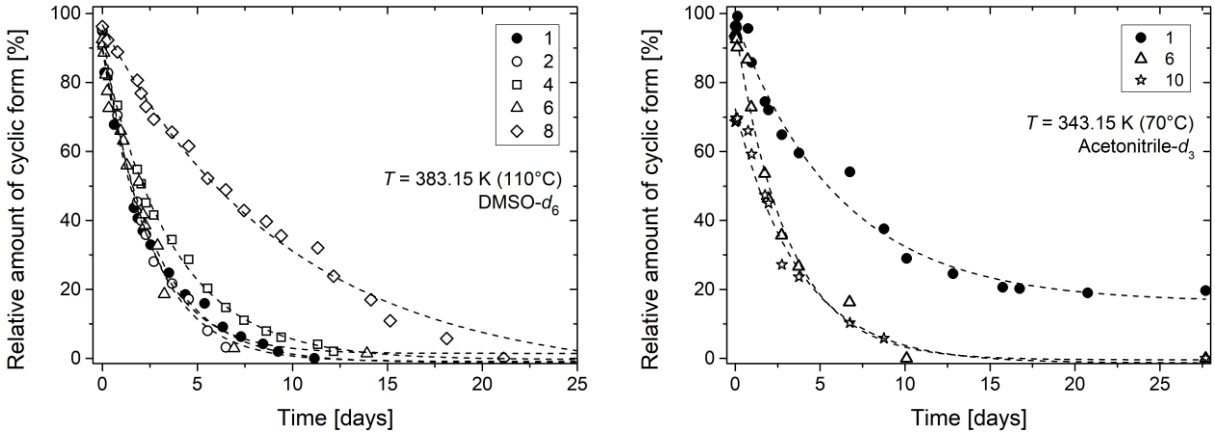

Figure S82. Thermal cycloreversion reaction of closed C form of studied benzothiazole DTEs in DMSO-d_6 (left) at 383.15 K and MeCN-d_3 (right) at 343.15 K. The plots show the decreasing relative amount of the cyclic form as a function of time.

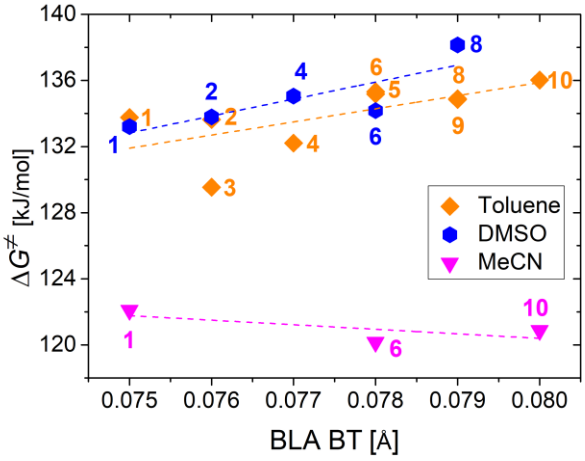

Figure S83. Correlation between experimentally determined transition state Gibbs free energy ($\Delta G^{\neq}$) of the thermal cycloreversion (ring opening) process of studied benzothiazole DTEs and the BLA BT parameter (see Section *Molecular structure* in the main text) describing electronic effect of the Ar ring (Scheme 1 in the main text) in three solvents.

Table S9. Experimentally determined rate constant (k_{CO}), transition state Gibbs free energy ($\Delta G^{\neq}$) and corresponding room-temperature half-life ($t_{1/2}$) for thermal cycloreversion (ring openenig) process in studied DTEs in polar solvents.

DMSO-d_6				
cpd number	k_{CO} at 383.15 K [s^{-1}]	$\Delta G^{\neq}$ [kcal/mol]	$\Delta G^{\neq}$ [kJ/mol]	Half-life $t_{1/2}$ at 298.15K [years]
1	5.59E-06	31.8	133.2	812
2	4.61E-06	32.0	133.8	961
4	3.13E-06	32.3	135.1	1594
6	4.11E-06	32.1	134.2	1118
8	1.18E-06	33.0	138.2	5559
MeCN-d_3				
	k_{CO} at 343.15 K [s^{-1}]	$\Delta G^{\neq}$ [kcal/mol]	$\Delta G^{\neq}$ [kJ/mol]	Half-life $t_{1/2}$ at 298.15K [years]
1	1.88E-06	29.2	122.1	8.7
6	3.65E-06	28.7	120.2	4.0
10	2.85E-06	28.9	120.9	5.3

5.5. Structure-property relationships

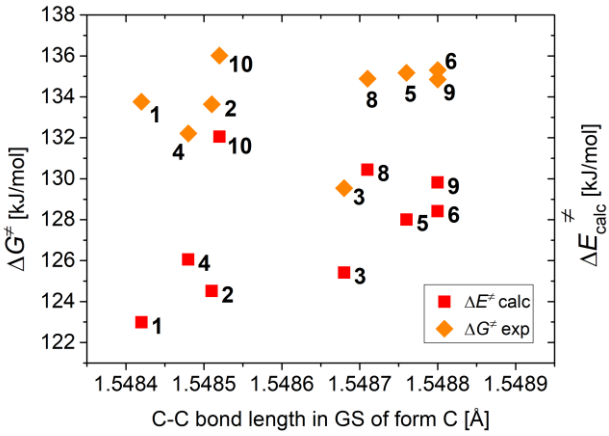

Figure S84. Correlation between calculated ZP (zero point energy) corrected (B3LYP/6-31G(d,p) in vacuum)[19] activation barrier ($\Delta E_{calc}^{\neq}$) for the thermal cycloreversion (ring opening) process of studied benzothiazole DTEs, corresponding experimentally determined transition state Gibbs free energy ($\Delta G^{\neq}$) of this process and the central C-C bond in minimum of ground state of the cyclic form C.

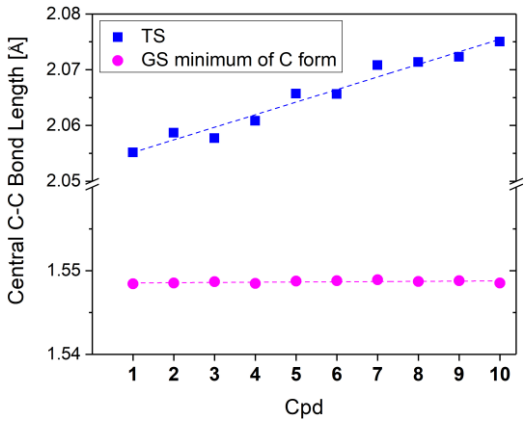

Figure S85. Evolution of central C-C bond length in the minimum of ground state (GS) and in the transition state (TS) with the increasing electron-donating character of the Ar ring (Scheme 1 in the main text).

[19] P. D. Patel, A. E. Masunov, *J. Phys. Chem. C* **2011**, *115*, 10292–10297

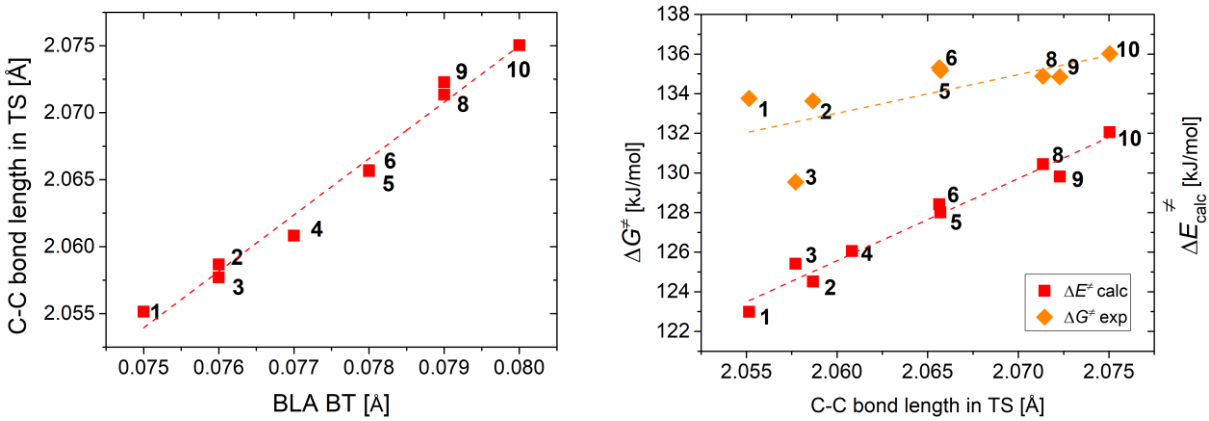

Figure S86. (left) Correlation between (calculated) central C-C bond length in transition state (TS) and the BLA BT parameter describing electronic effect of the Ar ring (Scheme 1 in the main text);
(right) Correlation between calculated ZP (zero point energy) corrected (B3LYP/6-31G(d,p) in vacuum)[19] activation barrier ($\Delta E_{calc}^{\neq}$) for the thermal cycloreversion (ring opening) process of studied benzothiazole DTEs, corresponding experimentally determined transition state Gibbs free energy ($\Delta G^{\neq}$) of this process and the central C-C bond in TS of the cyclic form C.

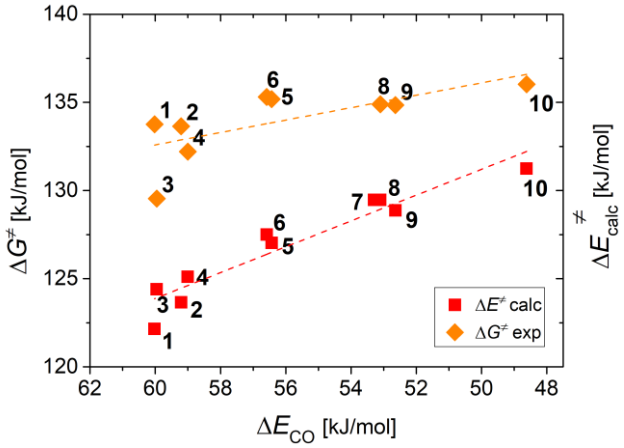

Figure S87. Correlation between calculated ZP (zero point energy) corrected (B3LYP/6-31G(d,p) in vacuum)[19] activation barrier ($\Delta E_{calc}^{\neq}$) for the thermal cycloreversion (ring opening) process of studied benzothiazole DTEs, corresponding experimentally determined transition state Gibbs free energy ($\Delta G^{\neq}$) of this process and the ground state energy difference between O and C form (ΔE_{CO}).

6. Quantum chemical-calculations

6.1. Electric properties and photochemical study

Electric properties can be significantly influenced by opening/closing the DTE photochrome. Our methodology is closely following work of Chen et al.[20] who studied a large set of DTE-based photochromes, allowing to directly compare obtained values with previous results.

Molecular geometry was optimized using the hybrid PBE0 functional[21], 6-311G(d,p) atomic basis set utilizing ultrafine integration grid. Local minima character was confirmed by frequency analysis. In all cases, no imaginary frequencies were found. Next, electric properties, dipole moment, static polarizability and static first hyperpolarizability, were calculated using analytical differentiation, employing larger atomic basis set 6-311++G(d,p) and long range corrected ωB97X functional[22], both being important factors for obtaining converged values of the electric properties.

First ten excited states were obtained in the framework of time-dependent density functional theory (TD-DFT) approach using ωB97XD[23] functional and 6-311++G(d,p) basis set as a single point calculations on top of the above-described geometries. Since our hypothesis on the quantum yields analysed excited states ordering, we preformed TD-CAM-B3LYP/6-311++G(d,p)[24] calculations to estimate influence of the functional, but found no change compared to ωB97XD approach. Excited state optimizations were performed with smaller 6-31G(d) basis set. For the structures near the conical intersection, spin-flip TD-DFT[25] was used instead with BHHLYP functional. Minimal energy conical intersection search was performed using branching plane updating method[26].

[20] K. J. Chen, A. D. Laurent, D. Jacquemin, *J. Phys. Chem. C* **2014**, *118*, 4334–4345.
[21] C. Adamo, V. Barone, *The Journal of Chemical Physics* **1999**, *110*, 6158–6170.
[22] J. da Chai, M. Head-Gordon, *J. Chem. Phys.* **2008**, *128*, 084106.
[23] J. da Chai, M. Head-Gordon, *Phys. Chem. Chem. Phys.* **2008**, *10*, 6615–6620.
[24] T. Yanai, D. P. Tew, N. C. Handy, *Chemical Physics Letters* **2004**, *393*, 51–57.
[25] Y. Shao, M. Head-Gordon, A. I. Krylov, *J. Chem. Phys.* **2003**, *118*, 4807.
[26] S. Maeda, K. Ohno, K. Morokuma, *J. Chem. Theor. Comput.* **2010**, *6*, 1538–1545.

In all DFT and TD-DFT calculations, IEF-PCM[27] continuum solvation model was applied, with toluene and DMSO as a solvent. Minimal energy conical intersection was optimized in the gas phase, while single point SF-TD-DFT calculations in toluene were performed afterwards.

All DFT and TD-DFT calculation were performed in Gaussian 16 software[28], while spin-flip calculations utilized Gamess 2020 R2 software[29].

6.1.1. Alternative relaxation pathways for molecules **9** and **10** in DMSO

Significant drop in QY was experimentally observed for the photochemical closing of DTEs **9** and **10** in DMSO. To explain this behaviour, we firstly optimized geometry of the ground state (GS) in DMSO and calculated excited states (ESs) using above-described methods. The relaxation of the ES was leading to the vicinity of the conical intersection (CI), comparable to situation in toluene. Other question is how the solvent changes branching ratio of the CI, i.e. how is the total population of open isomer split after moving to the GS surface. Dipole moment value of the open (O) isomer **10** in the productive ES is 16.1 D, significantly larger compared to closed (C) isomer ES with the dipole moment value of 9.9 D. Thus, the O form ES becomes more stabilized in polar solvents, decreasing slope of the pathway to CI. Comparison shows that the ES difference is much smaller for molecules without drop of the QY, e.g. 8.7 D for the O and 7.2 D for the C isomer of molecule **8**. Molecule **1** has larger dipole moment in ES of the C isomer than in O isomer, and for this molecule we observed small increase in QY with increased solvent polarity. Although this hypothesis seems plausible, our calculation also shows that optimization of the productive ES for all molecules ends in CI.

Twisted intramolecular charge transfer (TICT) mechanism presumes that rotation of the amino group changes ordering of the ESs opening deactivation pathway in originally higher ES. We optimized dimethylamino group in perpendicular position to the phenyl ring, but the ordering of states remained unchanged compared to global minimum. Photoelectron transfer (PET) is occasionally suggested and found as a mechanism changing ES behaviour. Our

[27] J. Tomasi, B. Mennucci, R. Cammi, *Chem. Rev.* **2005**, *105*, 2999–3094.

[28] M. J. Frisch, G. W. Trucks, H. B. Schlegel, G. E. Scuseria, M. A. Robb, J. R. Cheeseman, G. Scalmani, V. Barone, G. A. Petersson, H. Nakatsuji, X. Li, M. Caricato, A. v. Marenich, J. Bloino, B. G. Janesko, R. Gomperts, B. Mennucci, H. P. Hratchian, J. v. Ortiz, A. F. Izmaylov, J. L. Sonnenberg, D. Williams-Young, F. Ding, F. Lipparini, F. Egidi, J. Goings, B. Peng, A. Petrone, T. Henderson, D. Ranasinghe, V. G. Zakrzewski, J. Gao, N. Rega, G. Zheng, W. Liang, M. Hada, M. Ehara, K. Toyota, R. Fukuda, J. Hasegawa, M. Ishida, T. Nakajima, Y. Honda, O. Kitao, H. Nakai, T. Vreven, K. Throssell, J. A. J. Montgomery, J. E. Peralta, F. Ogliaro, M. J. Bearpark, J. J. Heyd, E. N. Brothers, K. N. Kudin, V. N. Staroverov, T. A. Keith, R. Kobayashi, J. Normand, K. Raghavachari, A. P. Rendell, J. C. Burant, S. S. Iyengar, J. Tomasi, M. Cossi, J. M. Millam, M. Henderson, D. Ranasinghe, V. G. Zakrzewski, J. Gao, N. Rega, G. Zheng, W. Liang, M. Hada, M. Ehara, K. Toyota, R. Fukuda, J. Hasegawa, M. Ishida, T. Nakajima, Y. Honda, O. Kitao, H. Nakai, T. Vreven, K. Throssell, J. A. J. Montgomery, J. E. Peralta, F. Ogliaro, M. J. Bearpark, J. J. Heyd, E. N. Brothers, K. N. Kudin, V. N. Staroverov, T. A. Keith, R. Kobayashi, J. Normand, K. Raghavachari, A. P. Rendell, J. C. Burant, S. S. Iyengar, J. Tomasi, M. Cossi, J. M. Millam, M. Klene, C. Adamo, R. Cammi, J. W. Ochterski, R. L. Martin, K. Morokuma, O. Farkas, J. B. Foresman, D. J. G. Fox, **2016**.

[29] G. M. J. Barca, C. Bertoni, L. Carrington, D. Datta, N. de Silva, J. E. Deustua, D. G. Fedorov, J. R. Gour, A. O. Gunina, E. Guidez, T. Harville, S. Irle, J. Ivanic, K. Kowalski, S. S. Leang, H. Li, W. Li, J. J. Lutz, I. Magoulas, J. Mato, V. Mironov, H. Nakata, B. Q. Pham, P. Piecuch, D. Poole, S. R. Pruitt, A. P. Rendell, L. B. Roskop, K. Ruedenberg, T. Sattasathuchana, M. W. Schmidt, J. Shen, L. Slipchenko, M. Sosonkina, V. Sundriyal, A. Tiwari, J. L. Galvez Vallejo, B. Westheimer, M. Włoch, P. Xu, F. Zahariev, M. S. Gordon, *J. Chem. Phys.* **2020**, *152*, 154102.

approach by ESs for the whole molecule would hint for electron transfer from local to some long-range charge transfer state, which is the main concept of PET. No signs of PET behaviour, e.g. some low lying charge transfer states in DMSO, were found. These results are based on the static calculations, nonadiabatic molecular dynamics of excited states could hint more on the dynamical behaviour of the DTEs after excitation in different solvents.

6.2. Transition State calculations

In addition to geometry optimizations of the studied diarylethens (described in section 4.2) we performed transition state (TS) search. This computation required a multistep approach consisting in an initial relaxed scan of the starting derivative, to locate the critical distance between the 2 reactive carbons.

Successively, starting from this configuration, it was possible to calculate, following a rigid input structure (reported below) the effective transition state geometry of each derivative. Closed and open isomers were calculated at the same level.

%chk=ts-search_Phenyl.chk
#P UB3LYP/6-31G(d,p) scf(conver=9) integral(superfinegrid) guess(mix,always) opt(modredundant,vtight)

(1) TS guess at the fixed critical bond length obtained from relaxed energy scan

0 1
xyz coordinates

bond to fix F

--Link1--
%chk=ts-search_Phenyl.chk
#P UB3LYP/6-31G(d,p) geom=check guess(mix, always) scf(conver=9) integral(superfinegrid) freq(NoRaman)

(2) frequency calculation on the TS guess

0 1

--Link1--
%chk=ts-search_Phenyl.chk
#P UB3LYP/6-31G(d,p) geom=check guess(mix, always) scf(conver=9) integral(superfinegrid) opt(TS,ReadFC,MaxStep=5,NoFreeze)

(3) TS optimization using the previous Hessian (WARNING: use NoFreeze to allow optimization of the critical bond length)

0 1

--Link1--
%chk=ts-search_Phenyl.chk
#P UB3LYP/6-31G(d,p) geom=check guess(mix, always) scf(conver=9) integral(superfinegrid) freq(NoRaman)

(4) frequency calculation on the TS

0 1

Some TS calculations were performed using the below input procedure, starting once more, from the reasonable TS configuration found in the previous step.

%chk=ts_VO_15_anionic_Simon_solvent.chk
#P UB3LYP/6-31G(d,p) guess(mix,always) scf(conver=9) integral(superfinegrid) opt(TS,CalcFC,NoEigenTest,vtight) Freq SCRF(PCM,solvent=Toluene) geom=check

(1) TS guess at the fixed critical bond length obtained from relaxed energy scan

0 1
xyz coordinate